



MSU Graduate Theses

Summer 2019


The Effect of Metal Composition and Particle Size on Nanostructure-Toxicity in Plants

Natalie Lynn Smith

Missouri State University, Venette658@live.missouristate.edu

As with any intellectual project, the content and views expressed in this thesis may be considered objectionable by some readers. However, this student-scholar's work has been judged to have academic value by the student's thesis committee members trained in the discipline. The content and views expressed in this thesis are those of the student-scholar and are not endorsed by Missouri State University, its Graduate College, or its employees.

Follow this and additional works at: <https://bearworks.missouristate.edu/theses>

 Part of the [Biology Commons](#), and the [Genetics and Genomics Commons](#)

Recommended Citation

Smith, Natalie Lynn, "The Effect of Metal Composition and Particle Size on Nanostructure-Toxicity in Plants" (2019). *MSU Graduate Theses*. 3429.

<https://bearworks.missouristate.edu/theses/3429>

This article or document was made available through BearWorks, the institutional repository of Missouri State University. The work contained in it may be protected by copyright and require permission of the copyright holder for reuse or redistribution.

For more information, please contact [BearWorks@library.missouristate.edu](mailto: BearWorks@library.missouristate.edu).

**THE EFFECT OF METAL COMPOSITION AND PARTICLE SIZE ON
NANOSTRUCTURE-TOXICITY IN PLANTS**

A Master's Thesis

Presented to

The Graduate College of

Missouri State University

In Partial Fulfillment

Of the Requirements for the Degree

Master of Science, Biology

By

Natalie Lynn Smith

August 2019

Copyright 2019 by Natalie Lynn Smith

THE EFFECT OF METAL COMPOSITION AND PARTICLE SIZE ON NANOSTRUCTURE-TOXICITY IN PLANTS

Biology

Missouri State University, August 2019

Master of Science

Natalie Lynn Smith

ABSTRACT

Silver nanoparticles (AgNPs) have consistently been shown to have a detrimental effect on bacteria, fungi, and plants. The interaction of AgNPs with plants has received considerable scientific attention, because it is potentially through plants that these structures can enter the food chain and bioaccumulate in humans and animals. To determine the effects of AgNPs on plants, *Arabidopsis thaliana* seedlings were chronically exposed to sublethal levels of AgNPs using a standardized method. To gain insight on mechanism of phytotoxicity, the seedlings were exposed to low concentrations of Ag⁺ (in the form of silver nitrate), AgNPs, or gold nanoparticles (AuNPs). To test if NP size influenced the response by the plant, AgNPs and AuNPs were tested at both 20 nm and 80 nm sizes. Exposure to AgNO₃ altered the expression of several genes, but exposure to AuNPs did not cause any measurable changes in the *Arabidopsis* transcriptome. Exposure of plants with 20 nm and 80 nm AgNPs, on the other hand, caused the differential expression of 226 and 212 genes, respectively, indicative of cell wall reorganization and response to oxidative and biotic stress. The size of the AgNPs had little influence on gene expression patterns. Root length measurements were taken to quantify phytotoxicity of various NPs. While AgNO₃ increased root elongation, the NPs, irrespective of metal composition and size, did not cause significant differences in root length. Taken together, my data suggest that the chemical nature of the metal core is the major determinant of AgNP phytotoxicity in chronically exposed plants.

KEYWORDS: phytotoxicity, nanotoxicology, engineered nanoparticles, silver nanoparticles, *Arabidopsis thaliana*, RNA-seq, gene expression

**THE EFFECT OF METAL COMPOSITION AND PARTICLE SIZE ON
NANOSTRUCTURE-TOXICITY IN PLANTS**

By

Natalie Lynn Smith

A Master's Thesis
Submitted to the Graduate College
Of Missouri State University
In Partial Fulfillment of the Requirements
For the Degree of Master of Science, Biology

August 2019

Approved:

Laszlo Kovacs, Ph.D., Thesis Committee Chair

Kyoungtae Kim, Ph.D., Committee Member

Alexander Wait, Ph.D., Committee Member

Julie Masterson, Ph.D., Dean of the Graduate College

In the interest of academic freedom and the principle of free speech, approval of this thesis indicates the format is acceptable and meets the academic criteria for the discipline as determined by the faculty that constitute the thesis committee. The content and views expressed in this thesis are those of the student-scholar and are not endorsed by Missouri State University, its Graduate College, or its employees.

ACKNOWLEDGEMENTS

I would like to thank the following people for their support during the course of my graduate studies: the Missouri State Graduate College, the Missouri State Department of Biology and Jordan Valley Innovation Center. I would like to extend a thanks to my thesis committee: Laszlo Kovacs, Kyoungtae Kim and Alexander Wait. I would like to extend a special thanks to Rishi Patel, and all of the undergraduates who have helped with this project: Cory Hanson, Basant Hens, Anita Ma, and Jennifer Probst. Thanks to all of my family for always believing in me and providing unconditional support during this time. This thesis and project was funded by the U.S. Army Engineer Research and Development Center – Environmental Laboratory through the Environmental Quality and Technology Program; Contract No. W912HZ-15-2-0032 P00002.

I dedicate this thesis to my loving and supportive husband, Mitchell Smith.

TABLE OF CONTENTS

Overview	Page 1
Engineered Nanomaterials	Page 1
The Experimental System of Silver Nanoparticles and <i>Arabidopsis thaliana</i>	Page 2
Silver quantum dot-induced gene-expression signature in <i>Arabidopsis</i> : toward a standardized method to study the phytotoxicity of engineered nanoparticles	Page 5
1. Introduction	Page 5
2. Methods	Page 6
3. Results	Page 12
4. Discussion	Page 14
References	Page 21
Particle size does not influence gene expression in silver and gold nanoparticle-exposed <i>Arabidopsis</i>	Page 31
1. Introduction	Page 31
2. Methods	Page 33
3. Results	Page 39
4. Discussion	Page 42
References	Page 49
Summary	Page 64
Additional References	Page 66
Appendices	Page 68
Appendix A	Page 68
Appendix B	Page 69
Appendix C	Page 70
Appendix D	Page 74
Appendix E	Page 75
Appendix F	Page 76
Appendix G	Page 77
Appendix H	Page 91

LIST OF FIGURES

Figure 1. Schematic structure of non-ionic silver nanoparticles.	Page 4
Figure 2. RT-qPCR validation of eight DEGs in response to chronic AgNP exposure.	Page 25
Figure 3. Hierarchical clustering of the expression data of DEGs in response to chronic AgNP exposure.	Page 26
Figure 4. Enrichment of DEGs in various biological processes in AgNP-exposed <i>A. thaliana</i> seedlings.	Page 27
Figure 5. Sample mean root length in millimeters for AgNP and AgNO ₃ .	Page 28
Figure 6. RT-qPCR validation of eight biomarker genes in response to AgNP treatment in an independent experiment.	Page 29
Figure 7. RT-qPCR validation of eight biomarker genes in response to AgNO ₃ treatment.	Page 30
Figure 8. The translucent green phenotype.	Page 53
Figure 9. Hierarchical clustering of rate of expression change of DEGs in response to chronic nanoparticle exposure.	Page 54
Figure 10. Number of differentially expressed genes responsive to AgNPs at only 20 nm, at only 80 nm particle size and at both sizes.	Page 55
Figure 11. Fold-change of the 158 genes differentially expressed in response to AgNP at both 20 nm and 80 nm sizes.	Page 56
Figure 12. qPCR validation of three genes in response to AgNP at 20 nm treatment.	Page 57
Figure 13. qPCR validation of three genes in response to AgNP at 80 nm treatment.	Page 58
Figure 14. Enrichment of DEGs in various ontologies in AgNP at 20 nm-exposed <i>A. thaliana</i> seedlings.	Page 59
Figure 15. Visualization of the relatedness between GO terms in response to AgNP at 20 nm.	Page 60
Figure 16. Enrichment of DEGs in various ontologies in AgNP at 80 nm-exposed <i>A. thaliana</i> seedlings.	Page 61
Figure 17. Visualization of the relatedness between GO terms in response to AgNP at 80 nm.	Page 62

OVERVIEW

Engineered Nanomaterials

Engineered nanomaterials (ENMs) are artificial ultrafine particles that are between 1-100 nm in at least a single dimension. Over the last 15 years, the usage of ENMs in consumer products has increased exponentially despite ongoing research into the environmental and human health risks associated with ENM exposure. The Nanotechnology Consumer Products Inventory (CPI) was created in 2005 to track consumer products containing one or more ENM, with 54 products originally listed. Today, more than 1,800 products are listed on the CPI's database including food packaging, clothes, sunscreens, cosmetics, dietary supplements and electronics (Vance et al., 2015). The most commonly used ENMs for consumer products include metal-, metal oxide- and carbon-based nanomaterials, with silver nanomaterial-containing products consumed in largest quantities and advertised with greatest intensity (Vance et al., 2015).

ENMs are considered potentially hazardous chemical substances by the EPA and are highly regulated when used in consumer products by the Federal Food, Drug, and Cosmetic Act (FFDCA). This is concerning since embedded ENMs are known to “leak” from their respective products into the air or waste water and can become harmful to the environment or human health (Colman et al., 2013). Waste water effluent from waste water treatment plants in Illinois already contain measurable amounts of silver, zinc-oxide, and titanium-dioxide nanomaterials (Liu et al., 2018), making these specific ENMs of environmental concern.

Scientific research over the past decade on the effect of ENMs on microbes, plants and mammals have yielded highly variable results, with the variability attributed primarily to the size and concentration of ENMs (reviewed in Aken, 2015). While the impact of ENMs on microbes

and mammalian cells have attracted considerable scientific attention, the effect of ENMs on plants has just recently been the focus of experimental research. The interaction of these materials with plants, nonetheless is an important question because of the possibility that ENMs are taken up by plants and thereby enter the food chain and accumulate in higher organisms.

The Experimental System of Silver Nanoparticles and *Arabidopsis thaliana*

To study the impact of ENMs on plants, I have chosen the experimental system based on the chronic exposure of *Arabidopsis thaliana* plants to silver nanoparticles (AgNPs). *A. thaliana* is a small flowering dicotyledonous plant which belongs to the mustard (Brassicaceae) family having a natural distribution across the Northern Hemisphere. It has become the most widely used model organism for plant physiology and genetics. While many natural ecotypes are available for experimental studies, the most commonly used ecotype is Columbia (Col-0). While *Arabidopsis* is not an agriculturally significant species, its genomic and phenotypic features make it an ideal model species for plant molecular biology.

In terms of quantities produced, silver-based nanomaterials are at the third place behind zinc-oxide and titanium-dioxide nanomaterials, but in terms of amounts incorporated into consumer products, silver-based ENMs rank as number one (Vance et al., 2015). In 2014, the annual global production of silver ENMs amounted to 550 metric tons (Massarsky et al., 2014). At present, 25% of all nanotechnology-enhanced products contain nanosilver. To a great extent, this is due to the antimicrobial and anti-inflammatory properties of silver, which are useful in the medical, food and clothing industries. Consumer products containing nanosilver include food packaging, hygiene products, clothing and bedding materials, medical instruments, and various non-medical equipment (Buzea et al., 2007; Liu et al., 2010). In certain applications, silver

nanomaterials are used in combination with other ENMs. In certain cosmetics, for example, they are combined with titanium-dioxide (Vance et al., 2015). The most common form of silver nanomaterial is a quasi-spherical silver neutral core surrounded by an organic buffer to create a shell around the particle (Figure 1).

While the mass production of silver nanomaterials is expected to level off, accumulation of silver nanomaterials in landfills and soil/sediment is expected to climb over 500 metric tons in the EU by 2030 (Sun et al., 2017). The effects of AgNPs on plant systems have been studied over the years, and while there is a consensus on toxicity in plants (reviewed in Yan and Chen, 2019), the specific effects of AgNPs vary widely. Reports on phytotoxic impact range from reduced germination rates (Yin et al., 2012; Geisler-Lee et al., 2014; Thuesombat et al., 2014) to lower biomass (Nair and Chung, 2014a; Vishwakarma et al., 2017), growth inhibition (Geisler-Lee et al., 2014; Thuesombat et al., 2014), stunted elongation and/or root hair development (Geisler-Lee et al., 2013; Nair and Chung, 2014a; García-Sánchez et al., 2015), reduced chlorophyll content and photosynthesis (Jiang et al., 2014; Nair and Chung, 2014b), oxidative stress (Nair and Chung, 2014a; Nair and Chung, 2014b; Geisler-Lee et al., 2013), cellular damage (Geisler-Lee et al., 2013; Nair and Chung, 2014a), and cell death (Panda et al., 2011; Bagherzadeh and Ehsanpour, 2016). Transcriptomic studies on AgNPs of multiple sizes show an overall upregulation of oxidative stress-related gene expression (Kaveh et al., 2013; García-Sánchez et al., 2015).

The purpose of this study was to determine the effect of metal composition and particle size in silver nanomaterial phytotoxicity in plants by comparing the phenotypic traits and transcriptomic impact of AgNPs to silver ions (Ag^+) and to gold nanoparticles (AuNPs) at various particle sizes using a standardized bioassay.

Silver Nanostructure Core-Shell Model

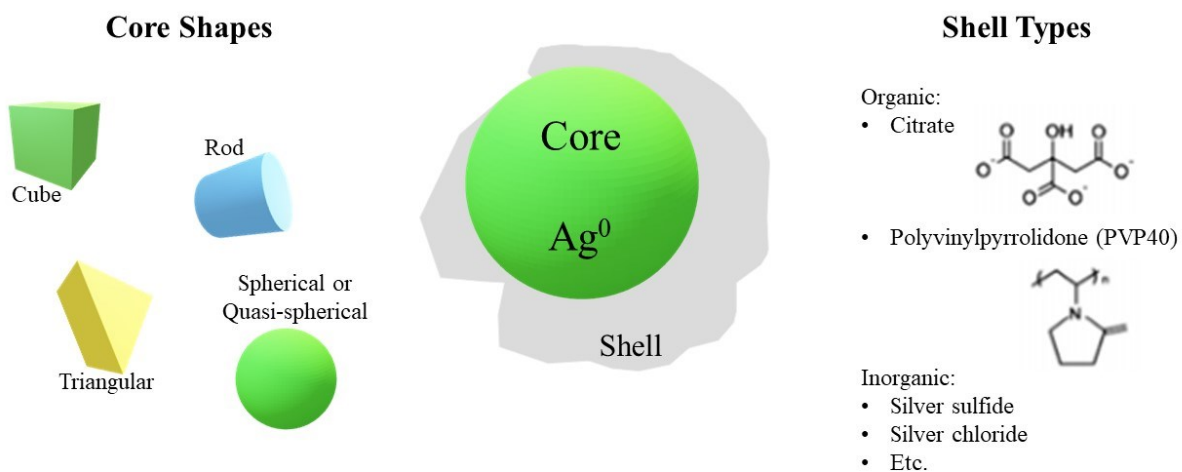


Figure 1. Schematic structure of non-ionic silver nanoparticles. The core and the shell can be of various shapes and chemical composition, respectively, as shown. The shell-like structure around the core is created as result of the interaction between the core and the resuspension buffer. Adapted from Sharma et. al. (2014).

SILVER NANOPARTICLE-INDUCED GENE-EXPRESSION SIGNATURE IN *ARABIDOPSIS*: TOWARD A STANDARDIZED METHOD TO STUDY THE PHYTOTOXICITY OF ENGINEERED NANOPARTICLES

1. Introduction

Engineered nanomaterials (ENMs) have been manufactured in large quantities and used in consumer products including food packaging, clothes, sunscreens, cosmetics, dietary supplements and electronics (Vance et al., 2015). From post-consumer waste of nanotechnology-enhanced products, ENMs can leak from their respective products and enter the air, soil, and water, and become environmental contaminants. In the state of Illinois, for example, ENMs can already be detected in re-usable waste water effluent (Liu et al., 2018). While past scientific research on the effects of ENMs on living organisms have mainly focused on microbes and mammals, current efforts have begun to examine how ENMs impact plants. A major concern that drives these studies is the possibility that ENMs are taken up by plants, through which they enter the food chain and ultimately accumulate in higher organisms.

Studies on the effects of ENMs on plants have produced highly variable results that are primarily dependent on nanomaterial type, size and concentration. In plants, responses are also dependent on exposure type (*in vitro*, hydroponic or soil), exposure length (chronic vs. short-term), and growth conditions. Metal- and metal oxide-nanomaterials have been reported to have both enhancing and deleterious effects on root growth, biomass, and physiological and biochemical activities (Mohamed and Kumar, 2016). For example, zinc-oxide nanoparticles (ZnO) have been shown to increase the growth and biomass in alfalfa, tomato and cucumber plants at low concentrations (20 mg/mL) (de la Rosa et al., 2013; Panwar et al., 2012), and small

doses of ZnO in wheat increased seed germination (Ramesh et al., 2014). However, Wang et. al. (2015) showed that ZnO inhibited plant growth, caused reduced biomass, and induced strong oxidative stress in *Arabidopsis thaliana*.

Various carbonaceous nanomaterials have been shown to have an even wider range of physiological effects in plants including reduced or increased biomass, reduced or enhanced elongation in root length, inhibited or activated seed germination, and reduced or enhanced fruit yield (reviewed in Zuverza-Mena et. al., 2017). The contrasting physiological changes depend on the plant species and the type of nanomaterial, though results on most studies are in agreement that carbon-based nanomaterials increase ROS production and affect gene expression (reviewed in Zuverza-Mena et. al., 2017).

The goal of this study was to create a standard bioassay to test the impact of a broad range of nanomaterials on plants using *A. thaliana* as a model organism. Due to the variation in methodology for ENM-based research, comparisons between different ENMs, or different species, is illogical. A standardized methodology in comparing different types of ENMs is necessary to directly compare toxicity-levels. This bioassay was created by testing the effects of chronic silver nanoparticle (AgNP) exposure from germination through 14 days of growth. The effects of AgNPs on plants have been studied previously with consistent results of deleterious effects (Zuverza-Mena et. al., 2016; Verma et. al., 2018; Yan and Chen, 2019), making this ENM well suited for the development of a standardized bioassay.

2. Methods

2.1 Nanoparticles. The AgNPs used in this study were 20 nm-diameter quasi-spherical neutral silver core particles surrounded by a citrate shell. They were purchased as a colloidal

preparation in sodium citrate at 2 mM concentration (PELCO® NanoXact™ particles) from Ted Pella, Inc. (Redding, California). Upon arrival, the AgNPs were stored at 4°C in the dark. In natural light, this preparation had a yellow color, whereas AgNPs of other particle-size differed in color. This indicated that the material had electromagnetic properties which were different from that of bulk silver, and therefore the particles used in this study are considered to be quantum dots.

2.2 Plant Material and Culture Conditions. This study was performed using *A. thaliana* Col-0 ecotype. Seeds were sterilized for three hours in chlorine gas generated by mixing 3 mL of concentrated HCl with 100 mL of 6 % NaOCl (Clorox bleach). The sterile seeds were then sprinkled on the surface of the agar-solidified plant culture media (see below) in Petri plates under axenic conditions. The plates were then wrapped with Parafilm, and the seeds were stratified at 4°C in the dark for 3 days. Following stratification, the Parafilm seal was removed, the plates were placed in a sandwich-sized plastic bags and transferred to a Conviron Adaptis A1000-AR Growth Chamber for 14 days. Plants were grown at 21°C, in a 10-hour light/14-hour dark diurnal cycle. During the entire 14-day growth period, the plates were randomly rearranged once a day within the growth chamber to eliminate positional effect.

2.3 Plant Culture Media. Complete plant culture media was prepared using half-strength Murashige and Skoog nutrients with Gamborg's vitamins supplemented with 2.5% MOPS buffer and 0.8% agar. The final pH was adjusted to 7.0 using 100 mM KOH. Neutral pH was necessary to prevent nanoparticle aggregation. Media was sterilized in an autoclave at 121°C for 20 minutes. Once cooled to 55°C, the media was supplemented with sterilized water (control) or aqueous AgNP suspension or AgNO₃ solution for a final concentration of 4 µg/mL and

sonicated for 2 minutes to prevent particle aggregation. Carbenicillin and Amphotericin B were added to the media during sonication to ensure axenic growth conditions.

2.4 Experimental Design. For each treatment, plants were grown in blocked environments with three technical replicates for each of the three biological repeats. For both gene expression and phenotyping experiments, methods were performed on each replicate individually. For RNA-seq, replicates were pooled before library construction after RNA extraction and quantification.

2.5 RNA Extraction, RNA-seq Library Construction and Sequencing. Total RNA was extracted from 14-day old plants using the Trizol reagent (Invitrogen, Carlsbad, California). In all experiments, RNA extraction was performed 3 hours after the start of the light period to mitigate the effect of the diurnal cycle on gene expression. Homogenization of plant tissue in liquid nitrogen using mortar and pestle was performed before addition of Trizol. RNA purification was performed using the RNeasy RNA-Extraction Kit by Qiagen (Hilden, Germany) following the manufacturer's guidelines. Total RNA was eluted in 50 μ L of DEPC-treated water, quantified using a NanoDrop 2000 UV/Vis spectrometer (ThermoFisher Scientific, Waltham, Massachusetts) and stored at -80°C.

mRNA purification and RNA-seq library construction were performed using TruSeq Stranded mRNA Sample Preparation Kit by Illumina Corporation (San Diego, California) following the low sample-size protocol. In brief, poly(A) mRNA was selected from 1 μ g of total RNA using poly(T) beads. The selected mRNA was fragmented, purified and reverse-transcribed into cDNA. The cDNA underwent library construction which consisted of end repair, adapter ligation and strand selection. Illumina adapters contain priming sites and a nucleotide sequence barcode which facilitate annealing to sequencing primers and assigns reads to a given library,

respectively. The cDNA underwent strand selection, so that only the forward strand was used for sequencing, making the cDNA library a “stranded” library. The stranded cDNA library was purified and amplified for a total of six libraries corresponding to the three biological repeats for control and AgNP treatment.

Library single-end sequencing of 100 bp reads was performed on an Illumina HiSeq 2500 Sequencing System at the Genome Sequencing Facility of the University of Kansas Medical Center on two flow cells.

2.6 RNA-seq Analysis. RNA-seq analysis for differential gene expression was performed in the bioinformatics software CLC Genomics Workbench 9.5.1. and 7.0.4. Raw read files were downloaded from the server of the sequencing center using a SSH file transfer protocol in zipped FASTQ files, which were subsequently uploaded into CLC Genomics Workbench as unzipped Illumina files. Reads were filtered based on length (between 15 and 1,000 nt) and quality (limit 0.05) using default parameters, and 15 nucleotides were deleted from the 5’ end of all reads to remove any remaining adapter sequences. Reads were mapped to the *A. thaliana* TAIR10 reference genome sequence, downloaded from the ENSEMBL database (Hunt et al., 2018) using default parameters in the forward direction. Expression data from mapped reads were normalized as the number of reads per kilobase per million reads mapped (RPKM). Differentially expressed genes (DEGs) were identified through pairwise comparison of control and AgNP treatment libraries using the statistical tool “empirical analysis of differential gene expression” (EDGE), which uses the “Exact Test” algorithm created by Robinson and Smyth (2008). False discovery rate (FDR)- and Bonferroni-correction of DEGs were performed to remove any false-positives. Genes that were differentially expressed at 2-fold or higher up or down-regulation and had an FDR-corrected *p*-value of less than 0.05 were used for subsequent data analysis.

2.7 RT-qPCR Analysis. Gene expression analysis was performed for eight selected genes using real-time quantitative PCR (RT-qPCR) using both the RNA samples that were basis of the RNA-seq analysis and RNA samples from an independently repeated experiment. The reference gene used was *AT3G18780* or *AT4G02080* to normalize expression. cDNA synthesis was performed using the SuperScript® II Reverse Transcriptase kit from Invitrogen, Inc, following the First-Strand cDNA Synthesis protocol with the following deviations: The starting amount of RNA was 1 µg; instead oligo-dTs, random primers were used at 100 ng/µL concentration; and finally, the RNA, primer and dNTP mix were incubated at 70°C instead of 65°C for 5 min. Following the addition of the reverse transcription buffer, DTT and RNaseOUT, the mixture was incubated at 25°C for 10 min, followed by the addition of the reverse transcriptase and incubations at 25°C for 10 min, at 42°C for 50 minutes and at 70°C for 15 min. cDNA concentrations were measured with a Qubit 4.0 fluorimeter using ssDNA kit reagents (ThermoFisher Scientific, Waltham, Massachusetts).

Primer pairs were designed using the Primer-BLAST platform on the NCBI website (Ye et al., 2012) from sequence data obtained from The *Arabidopsis* Information Resource (TAIR) website (Berardini et al., 2015), and synthesized by Integrated DNA Technologies, Inc (Appendix A). qPCR experiments were performed on a MxPro 3005P instrument (Agilent Technologies, Santa Clara, California) using the GoTaq qPCR Master Mix (Promega Corp., Madison, Wisconsin). qPCR reaction mixtures were assembled and thermal cycling was performed following the manufacturer's guidelines with the following modifications: the reactions were performed using 20 µL instead of 50 µL volume. At the completion of the qPCR cycles, the following final dissociation thermal cycle segment was added: 95°C for 1 minute,

50°C for 30 seconds, and 95°C for 30 seconds. Cycle threshold (C_t) of 0.200 dRn fluorescence was used for primer efficiency calculations and differential expression analysis.

Primer efficiency for each primer pair was determined on a series of five-time cDNA dilutions in quadruplicates. The efficiency values for each replicate was accepted if the standard curve had an $r^2 > 0.985$ and efficiency was between 70% and 110%. qPCR analysis of differential expression for each gene was performed in three biological repeats in two technical replicates each, and with the inclusion of a no-template control. The average C_t value for each gene was used for differential expression analysis using the Pfaffl equation (Pfaffl, 2001). Statistical analysis of differential expression was determined by finding the difference in C_t values between target genes and the reference gene for both control and treatment. A one-way ANOVA was performed in Minitab 17 for each primer pair and considered significant at p -value < 0.05 .

2.8 Root Length Phenotyping. Root length measurements were performed on 14-day old plants 3 hours after the light period has started. High-quality images of 15 plant roots were taken per replicate. Root length in millimeters was determined using the Image-J software using the free-hand line tool. The effect of treatment on root length was assessed using a multi-factor ANOVA. Treatment was treated as a fixed-effects factor, while biological repeat and replicate was treated as a random-effects factor. Replicate was nested under treatment and biological repeat; otherwise, factors were crossed. All conclusions are based on a type-I error rate of 0.05. The analysis was performed using the general linear model (GLM) procedure of Minitab 17.

3. Results

3.1 Differential Expression of Genes in Response to Chronic AgNP Exposure.

Illumina sequencing of the RNA-seq libraries generated an average of 31 million reads per library with an average of 91% of reads mapping to the TAIR10 reference genome sequence of *A. thaliana* (Appendix B). Out of the 33,603 genes of the *Arabidopsis* genome, the number of DEGs (p -value < 0.05 , fold change rate 2-fold or greater) was 439 before correction, and 76 and 35 after FDR- or Bonferroni-correction, respectively. Only DEGs that passed FDR-correction at a p -value < 0.05 with a rate of 2-fold or greater were used for subsequent analysis, except for hierarchical clustering. Information about the fold-change, FDR-corrected p -value and function of DEGs is listed in Appendix C.

3.2 qPCR Validation of RNA-seq. Eight DEGs were chosen for qPCR validation of the RNA-seq results, of which four were down-regulated (*AT3G16770*, *AT3G16670*, *AT1G77330* and *AT1G74670*) and four were up-regulated (*AT1G21250*, *AT4G26260*, *AT4G14400* and *AT3G22231*) in response to AgNP treatment. Pfaffl-determined change in gene expression for DEGs in qPCR experiment were plotted against EDGE-determined change in gene expression in RNA-seq (Figure 2). Correlation between RNA-seq and qPCR expression levels were 0.9897. Statistical analysis of qPCR validation data using one-way ANOVA showed all eight DEGs had a p -value < 0.05 . These eight genes will be referred to as “biomarker genes” for the rest of this chapter.

3.3 Functional Categories of Differentially Expressed Genes. Hierarchical clustering demonstrated that chronic AgNP exposure induces distinct changes in gene expression in *Arabidopsis* (Figure 3). To shed light to the putative function of DEGs, gene ontology enrichment analysis was performed using GOrilla (Eden et.al., 2009). AgNP treatment caused

expression changes in genes responsive to stress, more specifically oxidative and pathogen-induced (biotic) stress, as well as genes involved in cell wall organization (Figure 4). Biotic stress-related ontologies, denoted as immune and defense response and systemic acquired resistance (SAR), contained similar genes which include two SAR-related transcripts, namely *AT5G10760* and *AT5G03350*, which increased in abundance (Appendix C). Response to oxidative stress included highly down-regulated peroxidase genes, namely *AT1G49570* and *AT5G19890*, and three other genes which are known to respond to oxidative stress (*AT3G16670*, *AT1G73120* and *AT2G41090*, see Appendix C). Plant cell wall-related ontologies contain two down-regulated root-specific genes *AT1G26240* and *AT1G26250* (Appendix C).

3.4 AgNP and AgNO₃ Affect *Arabidopsis* Root Length Differently. Data analysis of AgNP-treated *Arabidopsis* raised the possibility that the gene expression changes recorded above were due to the leakage of silver ions (Ag⁺) from the nanoparticle. To test this hypothesis, a secondary independent experiment was performed comparing control, Ag⁺ exposure (in the form of AgNO₃) and AgNP exposure. Phenotypic toxicity/response was determined by comparing the effects of AgNP and Ag⁺ on root length. The effect of treatment on root length was significant (*p*-value = 0.039) with the sample mean root length of AgNO₃ treatment being greater than the sample mean root length of AgNP treatment and control. There was no significant difference however, in sample means between the root length of AgNP-treated and control plants (Figure 5).

3.5 AgNP and AgNO₃ have Similar Gene Expression Patterns based on qPCR

Testing. To compare the effect of Ag⁺ and nanoparticle on gene expression, qPCR experiments were performed comparing gene expression on the biomarker genes on plants without treatment, with chronic AgNP exposure and with chronic AgNO₃ exposure.

Pfaffl-determined change in the transcript level of biomarker genes in response to AgNPs in qPCR experiment were plotted against EDGE-determined change in gene expression in RNA-seq (Figure 6). Correlation between RNA-seq and qPCR expression levels were 0.9514. Of the eight biomarker genes, only four passed one-way ANOVA statistical analysis: *AT3G16770*, *AT3G16670*, *AT1G77330*, and *AT1G74670* which had p-values of <0.0005, 0.002, 0.009 and 0.028, respectively.

Pfaffl-determined change in transcript level for biomarker genes in response to AgNO₃ in qPCR experiment were plotted against EDGE-determined change in gene expression in RNA-seq (Figure 7). Correlation between RNA-seq and qPCR expression levels were 0.9359. Of the eight biomarker genes, only four passed one-way ANOVA statistical analysis: *AT3G16770*, *AT3G16670*, *AT1G77330*, and *AT1G74670* which had p-values of 0.002, 0.004, 0.043 and 0.049, respectively.

4. Discussion

The lack of consistency in the literature on ENM-plant interactions suggests the need for a standardized method. This work in determining biomarker genes is a step in the direction for a simplified bioassay to enable the comparison of the effects of various ENMs in plants. The standardized growth and testing methods for the bioassay have produced consistent results and led to the identification of reliable biomarker genes. Importantly, this consistency has been verified by independently repeated experiments. In two independent gene expression studies, RT-qPCR validation of RNA-seq DEGs shows a correlation of 0.9897, and therefore, can confirm that the DEGs are differently expressed, and unlikely to be false-positives (Figure 2). In an additional independent growth-exposure experiment with AgNPs, qPCR data of the eight

biomarker genes against the original RNA-seq data shows a correlation of 0.9359, with four of the biomarker genes showing statistically significant gene expression changes when assayed with qPCR (Figure 6).

The biomarker genes in this bioassay were chosen based on their relative expression level in both untreated and treated samples as well as their relative gene expression changes between the two treatments. The biomarkers were moderately expressed genes and had at least 2-fold change in gene expression. These properties allowed for ease and repeatability in qPCR validation and testing. The functional role of these genes was not taken into consideration in the original selection for candidate biomarker genes; nonetheless, all eight of them were involved in response to stress, specifically defense response to fungal pathogens or oxidative stress.

The biomarkers have been validated and shown to consistently change in expression in response to AgNP exposure. Changes in the expression level of these genes can be detected despite our inability to measure phenotypic changes in the plants. This suggests that these biomarkers are highly sensitive to AgNP exposure and can be used to determine if plants are exposed to AgNP contamination. Since these biomarkers are consistently changing in response to AgNPs, the bioassay could possibly be simplified to include only qPCR testing for gene expression changes. The development of such a qPCR-based assay will deserve further experiments on a variety of AgNPs and other ENMs with various properties (shape, size, shell).

Results of previous studies have provided strong evidence that AgNPs can dissociate into Ag^+ , and physiological experiments have shown that both AgNPs and Ag^+ cause a phytotoxic response in plants (Geisler-Lee et al., 2013). It is possible therefore that the changes in the expression of the biomarker genes are caused by nanoparticle dissociation into ions. Root morphology, including root elongation rates, were reduced by exposure to both AgNPs and Ag^+ ,

but “brown tip” morphology was only seen in response to AgNP treatment (Geisler-Lee et al., 2013). Qian et al. (2013) showed that both AgNP and Ag⁺ are absorbed by *Arabidopsis*, but only AgNP caused significant damage to cellular structures (chloroplast) and reduced chlorophyll content. While both AgNPs and Ag⁺ produce ROS, AgNPs exhibit a more acute effect at lower concentrations than Ag⁺ (Nair and Chung, 2014). Therefore, the general consensus is that while dissociation into Ag⁺ may play a part in AgNP toxicity, phytotoxicity cannot be explained solely on the ion dissociation (Geisler-Lee et al., 2013; Cox et al., 2016). Our data on root length does not follow this general trend as Ag⁺ treatment (in the form of AgNO₃) increased root elongation while AgNP treatment did not show differences in root elongation when compared to control. The silver salt used as the source of Ag⁺ in this experiment contained nitrate, which is a macronutrient for plants, and is known to induce rapid growth. Future experiments should consider using a different silver salt to negate the effects of nitrate on plants. Unpublished data from Wait at Missouri State University observed that AgNP-treated plants had reduced carbon fixation rates at ambient and saturated light levels while AgNO₃-treated plants did not differ from untreated plants.

The lack of detection of physiological phytotoxicity due to AgNP exposure in our experiments could be due to experimental design and statistical analysis. Despite our methodology calling for 15 individual root length measurements per technical replicate, the blocked design reduced the sample size from what seems to be 135 samples per treatment to 9. This reduction in sample size causes an increase in the variance between samples within a treatment compared to the variance between treatments. Therefore, the calculated F-value for ANOVA was too low for a statistically significant *p*-value. This can also be seen by the blocking variable being statistically significant with a *p*-value of 0.004. To remedy this problem, the

experimental methods need to be changed in a way that they increase statistical power from blocked design. Statistical power could be increased by the removal of the blocked design, the addition of more blocks, or by growing each plant in an individual container.

Gene expression data collected in this experiment between AgNP- and AgNO₃-treated plants showed an overlap in DEGs, including *AT3G16770*, *AT3G16670*, *AT1G77330*, and *AT1G74670*. Independent experiments comparing RT-qPCR data for both AgNO₃ and AgNP treatment against RNA-seq data show correlations of 0.9514 and 0.9359, respectively. This suggests that the AgNP-induced changes may have been due to Ag⁺ leakage from the nanoparticles. However, we do not have direct experimental evidence for dissociation of Ag⁺ from the nanoparticles or for the presence of Ag⁺ in plants or in the growth medium. To unequivocally determine if the limited overlap in gene expression pattern is indeed caused by Ag⁺ leakage, additional experiments will be required. It is worth noting, however, that others have generated conclusive evidence for the leakage of Ag⁺ for AgNPs using inductively coupled plasma-mass spectrometry (Geiser-Lee et al., 2013) and that previous comparative transcriptomic studies have also demonstrated gene expression pattern overlap in AgNP and Ag⁺-exposed plants (Kaveh et al., 2013).

While there are 10 gene ontologies enriched, these gene ontologies are not mutually exclusive. Instead, several gene ontologies are related. For example, systemic acquired resistance (SAR) which are nested within defense response, which in turn falls under innate immune response, stress, and response to stimulus, sequentially. Response to oxidative stress is related to response to stress and response to stimulus, but independent from other categories.

AgNPs have been shown to accumulate along in the cell wall, plasmodesmata, and apoplast in *Arabidopsis* and rice in a size-dependent manner (Geiser-Lee et al., 2013; Bao et. al.,

2016). This accumulation can cause damage to the cell wall. Cell wall damage, specifically at the root, have been studied previously in response to AgNP treatment. Mirzajani et al. (2013) showed that in rice AgNPs penetrated the cell wall, causing disruption of cell morphology. GO enrichment analysis in our experiment shows an enrichment of DEGs in two categories concerning the cell wall, structural constituent of cell wall and plant-type cell wall organization, with enrichment values of 55.29 and 44.45, respectively. While the genes involved in cell wall organization in our study are down-regulated (*AT1G26240* and *AT1G26250*), these genes are only expressed in the root and directly involved in the structure of the cell wall (Berardini et al., 2015). While no direct cell wall or root cell damage was measured, we can infer from transcriptomic data that there was cell wall damage, specifically in the root, that could be due to the accumulation of the AgNPs at the cell wall. One of the first signals of cellular damage, including damage at the cell wall, is accumulation of reactive oxygen species (ROS), specifically hydrogen peroxide (H₂O₂).

Oxidative stress is consistently shown to be an effect of AgNP exposure and has been measured by examining an up-regulation in oxidative stress and peroxidase genes (Kaveh et al., 2013), increased protein precursors for oxidative stress tolerance (Mirzajani et al., 2014), and increased and accelerated ROS accumulation (Nair and Chung, 2014). The first sign of oxidative stress is the presence of ROS, such as singlet oxygen, superoxide, H₂O₂ and hydroxyl radical (Mourato et al., 2012). The most commonly produced ROS in response to AgNP exposure is H₂O₂ (Panda et al., 2011; Speranza et al., 2013; Nair and Chung, 2014; Thiruvengadam et al., 2015), which requires peroxidase enzymes to convert hydrogen peroxide into water and oxygen. While GO enrichment analysis shows an enrichment of DEGs in response to oxidative stress, these genes are typically down-regulated, including two peroxidase genes (*AT1G49570* and

AT5G19890). Kaveh et al. (2013) saw a trend of peroxidase up-regulation but found at least one peroxidase transcript (*AT5G19890*) down-regulated.

H₂O₂ is an intracellular signaling molecule that is involved in defense response to cell wall damage, oxidative stress and biotic stress. H₂O₂ and salicylic acid (SA) have been shown to be precursors for the activation of SAR (Lamb and Dixon, 1997), and therefore, the downregulation of peroxidase enzymes does not necessarily correlate with reductions of ROS within the plant cells. However, H₂O₂ might be regulated for the activation of SAR. We see enriched ontologies associated with SAR and defense response with enrichment values of 55.56 and 40.41, respectively, that contain two highly up-regulated SAR-related genes: *AT5G10760* and *AT5G03350*. These genes are involved in direct response to SA signaling, which is a common stress hormone induced during an attack by an obligate pathogen (Shah, 2003). These data are in contrast with previous results reported by Kaveh et al. (2013) and García-Sánchez et al. (2015) who detected the down-regulation of defense response-associated genes. Research has shown that response to nanoparticle treatments tend to cause a down-regulation in genes associated with the defense response (Kaveh et al., 2013; García-Sánchez et al., 2015). Our data are in contrast to these findings. It is possible therefore that *Arabidopsis* is not necessarily perceiving AgNPs as biotic stressors, but the AgNP exposure leads to a burst in H₂O₂ and elevated endogenous salicylic acid levels, which then causes an SAR-like stress response.

Research efforts have heavily focused on the potential phytotoxicity of silver nanomaterials, specifically on the phenotypic and physiologic impact in several plant species. However, there have only been two transcriptome-scale experiments to identify differentially expressed genes in response to silver-nanomaterial exposure (Kaveh et al., 2013; García-Sánchez et al., 2015). Both studies used microarray analysis, which is limited in the transcriptome

information it can provide. Microarrays rely on fluorescently-labeled cRNA, the hybridization of which to probes is measured with an analogue technology (Bunnik and Roch, 2013; Bumgarner, 2013). The inaccuracy inherent in analogue measurements and the limited number of transcripts the probes represent provide data that is more error-prone than the open-ended, digital system of RNA-seq (Bumgarner, 2013; Marioni et al., 2008; Oshlack et al., 2010; McGettigan, 2012; Zhang et al., 2014). This transcriptomic study is based on RNA-seq which gave us high confidence in our data and enabled us to identify novel transcripts. This is illustrated by the five unannotated and non-coding DEGs, not previously detected in microarray analysis, including *GLP6_2*, *AT2G15830*, *AT4G01870*, *CPuORF27* and *AT5G24200*.

The transcriptomic response due to chronic AgNP exposure suggests a biotic/pathogenic- and wounding-like response. Previous whole-transcriptome studies showed a different trend of reduction of root development and phosphate starvation genes (García-Sánchez et al., 2015) and strong response to oxidative stress with reduced response to biotic and hormonal stimuli (Kaveh et al., 2013; García-Sánchez et al., 2015). The cited studies have also used different techniques of growing and exposure. Kaveh et al. (2013) tested *Arabidopsis* which was chronically exposed to PVPP-shelled AgNP from germination through two weeks of growth, but growth involved long-day cycles (16-hour light). *Arabidopsis* grown in long-day cycles have a different gene expression profile than plants grown in short-day. García-Sánchez et al. (2015) grew plants for 4 weeks before doing a 48-hour exposure to nanoparticles while our experiments had the seedlings exposed to nanoparticles for 14 days. The shock-stress transcriptome likely triggers a different expression profile compared to chronic stress expression profiles. Physiological experiments have shown that AgNP effects on different phenotypes can be exposure-dependent, with toxicity being more acute with longer exposure time (reviewed Zuverza-Mena et al., 2017). Therefore,

differences in gene expression profiles could be due to differences in AgNP type, size, concentration, exposure method, exposure length and growth method, and the results of different studies cannot be directly compared.

With the presence of repeatable differential regulation of certain biomarker genes in response to AgNPs, a system for rapid detection of AgNP contamination can be developed. A detection system utilizing transgenic *Arabidopsis* plants in which the expression of fluorescence proteins are under the control DEG promoters could form the basis of rapid detection system for AgNP contamination in soil. Despite the consensus of AgNP phytotoxicity, we were not directly able to detect a toxic response in the phenology of *Arabidopsis*. However, *Arabidopsis* does mimic a stress response, as seen by the transcriptomic change. The impact of AgNP shape, size, shell deserve more scientific attention, as has been previously suggested by Cox et al. (2016) and Yen and Chen (2019). The next chapter will further investigate the effect of different characteristics on AgNP toxicity, specifically nanoparticle size.

References

- Babicki, S., Arndt, D., Marcu, A., Liang, Y., Grant, J.R., Maciejewski, A., Wishart, D.S., 2016. Heatmapper: web-enabled heat mapping for all. *Nucleic Acids Res.* 44, W147-W153.
- Bao, D., Oh, Z.G., Chen, Z., 2016. Characterization of silver nanoparticles internalized by *Arabidopsis* plants using single particle ICP-MS analysis. *Front. Plant Sci.* 7, 1-8.
- Berardini, T.Z., Reiser, L., Li, D., Mezheritsky, Y., Muller, R., Strait, E., Huala, E., 2015. The *Arabidopsis* information resource: Making and mining the “gold standard” annotated reference plant genome. *Genes.* 53, 474-484.
- Bumgarner, R., 2013. DNA microarrays: Types, applications, and their future. *Curr. Protoc. Mol. Biol.* 101, 22.1.1-22.1.11.
- Bunnik, E.M., Roch, K.G., 2013. An introduction to functional genomics and systems biology. *Advances Wound Care.* 2, 490-498.

- Cox, A., Venkatachalam, P., Sahi, S., Sharma, N., 2016. Silver and titanium dioxide nanoparticle in plants: A review of current research. *Plant Physiol. Biochem.* 107, 147-163.
- de la Rosa, G., López-Moreno, M.L., de Haro, D., Botez, C.E., Peralta-Videa, J.R., Gardea-Torresdey, J.L., 2013. Effects of ZnO nanoparticles in alfalfa, tomato, and cucumber at the germination stage: Root development and X-ray absorption spectroscopy studies. *Pure Appl. Chem.* 85, 2161-2174.
- Eden, E., Navon, R., Steinfeld, I., Lipson, D., Yakhini, Z., 2009. GOrilla: a tool for discovery and visualization of enriched GO terms in ranked gene lists. *BMC Bioinform.* 10:48.
- García-Sánchez, S., Bernales, I., Cristobal, S., 2015. Early response to nanoparticles in the *Arabidopsis* transcriptome compromises plant defence and root-hair development through salicylic acid signalling. *BMC Genom.* 16, 341.
- Geisler-Lee, J., Wang, Q., Yao, Y., Zhang, W., Geisler, M., Li, K., Huang, Y., Chen, Y., Kolmakov, A., Ma, X., 2013. Phytotoxicity, accumulation and transport of silver nanoparticles by *Arabidopsis thaliana*. *Nanotoxicol.* 7, 323-337.
- Hunt, S.E., McLaren, W., Gil, L., Thormann, A., Schuilenburg, H., Sheppard, D., Parton, A., Armean, I.M., Trevanion, S.J., Flicek, P., Cunningham, F., 2018. Ensembl variation resources. *Database.* 2018, 1-12.
- Kaveh, R., Li, Y.-S., Ranjbar, S., Tehrani, R., Brueck, C.L., Aken, B.V., 2013. Changes in *Arabidopsis thaliana* gene expression in response to silver nanoparticles and silver ions. *Environ. Sci. Technol.* 47, 10637-10644.
- Lamb, C., Dixon, R.A., 1997. The oxidative burst in plant disease resistance. *Annu. Rev. Plant Physiol. Plant Mol. Biol.* 48, 251-275.
- Liu, J., Williams, P.C., Geisler-Lee, J., Goodson, B.M., Fakharifar, M., Peiravi, M., Chen, D., Lightfoot, D.A., Gemeinhardt, M.E., 2018. Impact of wastewater effluent containing aged nanoparticles and other components on biological activities of the soil microbiome, *Arabidopsis* plants, and earthworms. *Environ. Res.* 164, 197-203.
- Marioni, J.C., Mason, C.E., Mane, S.M., Stephens, M., Gilad, Y. 2008. RNA-seq: An assessment of technical reproducibility and comparison with gene expression arrays. *Genome Research.* 18: 1509-1517.
- McGettigan, P.A., 2012. Transcriptomics in the RNA-seq era. *Curr. Opin. Chem. Biol.* 17, 1-8.
- Mirzajani, F., Askari, H., Hamzelou, S., Farzaneh, M., Ghassempour, A., 2013. Effect of silver nanoparticles on *Oryza sativa* L. and its rhizosphere bacteria. *Ecotoxicol. Environ. Saf.* 88, 48-54.

- Mirzajani, F., Askari, H., Hamzelou, S., Schober, Y., Römpp, A., Ghassempour, A., Spengler, B., 2014. Proteomics study of silver nanoparticles toxicity on *Oryza sativa* L. *Ecotoxicol. Environ. Saf.* 108, 335-339.
- Mohamed, M.S., Kumar, D.S., 2016. Effect of nanoparticles on plants with regard to physiological attributes. *Plant Nanotechnology*. Springer:pp. 119-153.
- Mourato, M., Reis, R., Martins, L.L., 2012. Characterization of plant antioxidative system in response to abiotic stresses: A focus on heavy metal toxicity. *Advances in Selected Plant Physiology Aspects*. IntechOpen:pp. 23-44.
- Nair, P.M.G., Chung, I.M., 2014. Assessment of silver nanoparticle-induced physiological and molecular changes in *Arabidopsis thaliana*. *Environ. Sci. Pollut.* 21, 8858-8869.
- Oshlack, A., Robinson, M.D., Young, M.D., 2010. From RNA-seq reads to differential expression results. *Genome Biol.* 11, 1-10.
- Panda, K.K., Achary, V.M.M., Krishnaveni, R. Padhi, B.K., Sarangi, S.N., Sahu, S.N., Panda, B.B., 2011. In vitro biosynthesis and genotoxicity bioassay of silver nanoparticles using plants. *Toxicol. In Vitro.* 25, 1097-1105.
- Panwar, J., Jain, N., Bhargaya, A., Akhtar, M., Yun, Y., 2012. Positive effect of zinc oxide nanoparticles on tomato plants: A step towards developing nano-fertilizers. *International Conference on Environmental Research and Technology (ICERT)*, Malaysia.
- Pfaffl, M.W., 2001. A new mathematical model for relative quantification in real-time RT-PCR. *Nucleic Acids Res.*, 9 e45.
- Qian, H., Peng, X., Han, X., Ren, J., Sun, L., Fu, Z., 2013. Comparison of the toxicity of silver nanoparticles and silver ions on the growth of terrestrial plant model *Arabidopsis thaliana*. *J. Environ. Sci.* 25, 1947-1955.
- Ramesh, M., Palanisamy, K., Babu, K., Sharma, N.K., 2014. Effects of bulk & nano-titanium dioxide and zinc oxide on physio-morphological changes in *Triticum aestivum* Linn. *J. Glob. Biosci.* 3, 415-422.
- Robinson, M.D. and Smyth, G.K., 2008. Small-sample estimation of negative binomial dispersion, with applications to SAGE data. *Biostat.* 9, 321-332.
- Shah, J., 2003. The salicylic acid loop in plant defense. *Curr. Opin, Plant Biol.* 6, 365-371.
- Speranza, A., Crinelli, R., Scoccianti, V., Taddei, A.R., Iacobucci, M., Bhattacharya, P., Ke, P.C., 2013. In vitro toxicity of silver nanoparticles to kiwifruit pollen exhibits peculiar traits beyond the cause of silver ion release. *Environ. Pollut.* 179, 258-267.

- Thiruvengadam, M., Gurunathan, S., Chung, I.-M., 2015. Physiological, metabolic, and transcriptional effects of biologically-synthesized silver nanoparticles in turnip (*Brassica rapa ssp. rapa* L.). *Protoplasma*. 252, 1031-1046.
- Vance, M.E., Kuiken, T., Vejerano, E.P., McGinnis, S.P., Hochella, M.F., Jr., Rejeski, D., Hull, M.S., 2015. Nanotechnology in the real world: Redeveloping the nanomaterial consumer products inventory. *Beilstein J. Nanotechnol.* 6, 1769-1780.
- Verma, S.K., Das, A.K., Patel, M.K., Shah, A., Kumar, V., Gantait, S., 2018. Engineered nanomaterials for plant growth and development: A perspective analysis. *Sci. Total Environ.* 630, 1413-1435.
- Wang, X., Yang, X., Chen, S., Li, Q., Wang, W., Hou, C., Gao, X., Wang, L., Wang, S., 2015. Zinc Oxide Nanoparticles Affect Biomass Accumulation and Photosynthesis in *Arabidopsis*. *Front. Plant Sci.* 6.
- Yan, A., Chen, Z., 2019. Impacts of silver nanoparticles on plants: a focus the phytotoxicity and underlying mechanism. *Int. J. Mol. Scie.* 20, 1-21.
- Ye, J., Coulouris, G., Zaretskaya, I., Cutcutache, I., Rozen, S., Madden, T.L., 2012. Primer-BLAST: A tool to design target-specific primers for polymerase chain reaction. *BMC Bioinform.* 13, 1-11.
- Zhang, Z.H., Jhaveri, D.J., Marshall, V.M., Bauer, D.C., Edson, J., Narayanan, R.K., Robinson, G.J., Lundberg, A.E., Bartlett, P.F., Wray, N.R., Zhao, Q., 2014. A comparative study of techniques for differential expression analysis on RNA-seq data. *PLoS ONE*. 9, e103207.
- Zuverza-Mena, N., Armendariz, R., Peralta-Videa, J.R., Gardea-Torresdey, J.L., 2016. Effects of silver nanoparticles on radish sprouts: root growth reduction and modifications in the nutritional value. *Front. Plant Sci.* 7, 90.
- Zuverza-Mena, N., Martínez-Fernández, D., Du, W., Hernandez-Viezcas, J.A., Bonilla-Bird, N., López-Moreno, M.L., Komárek, M., Peralta-Videa, J.R., Gardea-Torresdey, J.L., 2017. Exposure of engineered nanomaterials to plants: Insights into the physiological and biochemical responses-A review. *Plant Physiol. Biochem.* 110, 236-264.

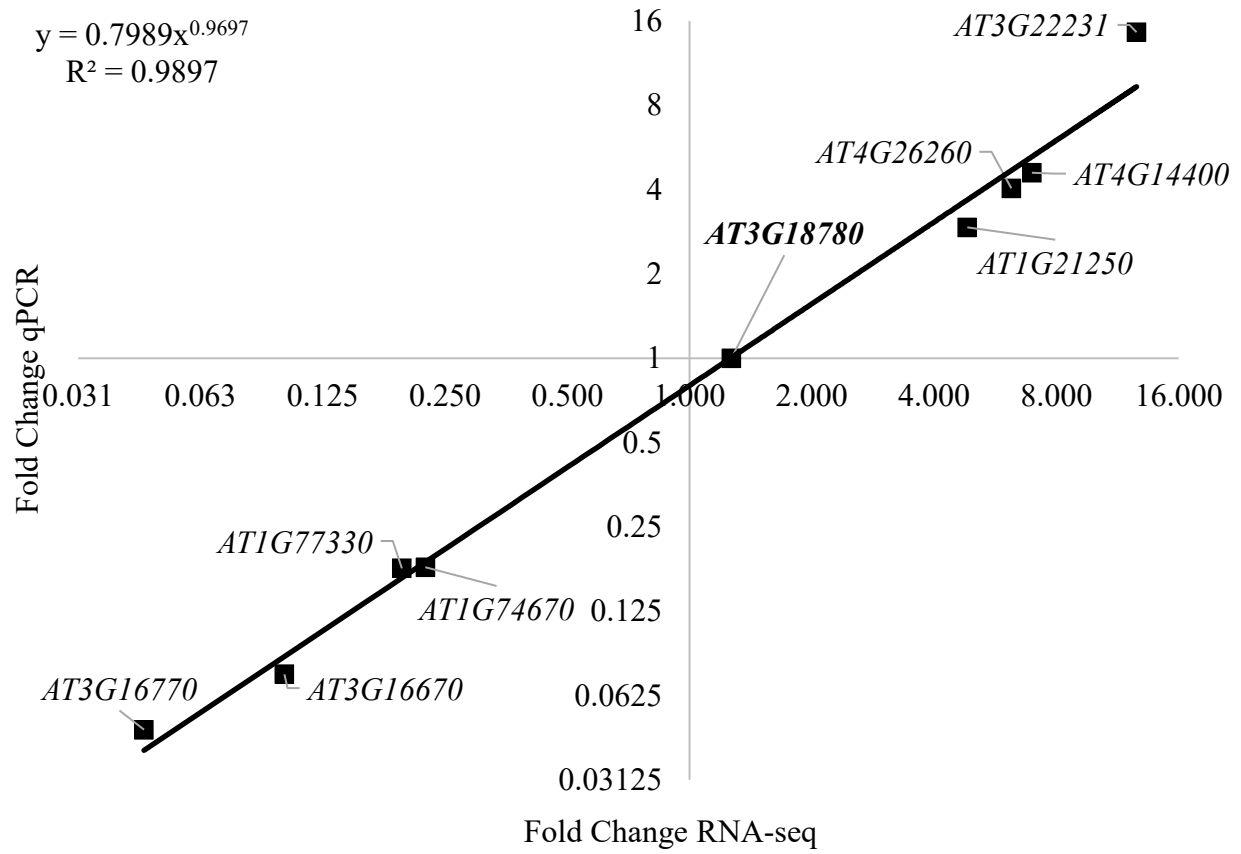


Figure 2. RT-qPCR validation of eight DEGs in response to chronic AgNP exposure. The trendline shows the power regression line with the equation and R^2 value of 0.9897. The x- and y-axis are in 2-base logarithmic scale. Fold-changes that are < 1 and > 1 correspond to down- and up-regulation, respectively. *AT3G18780* was used as a reference gene.

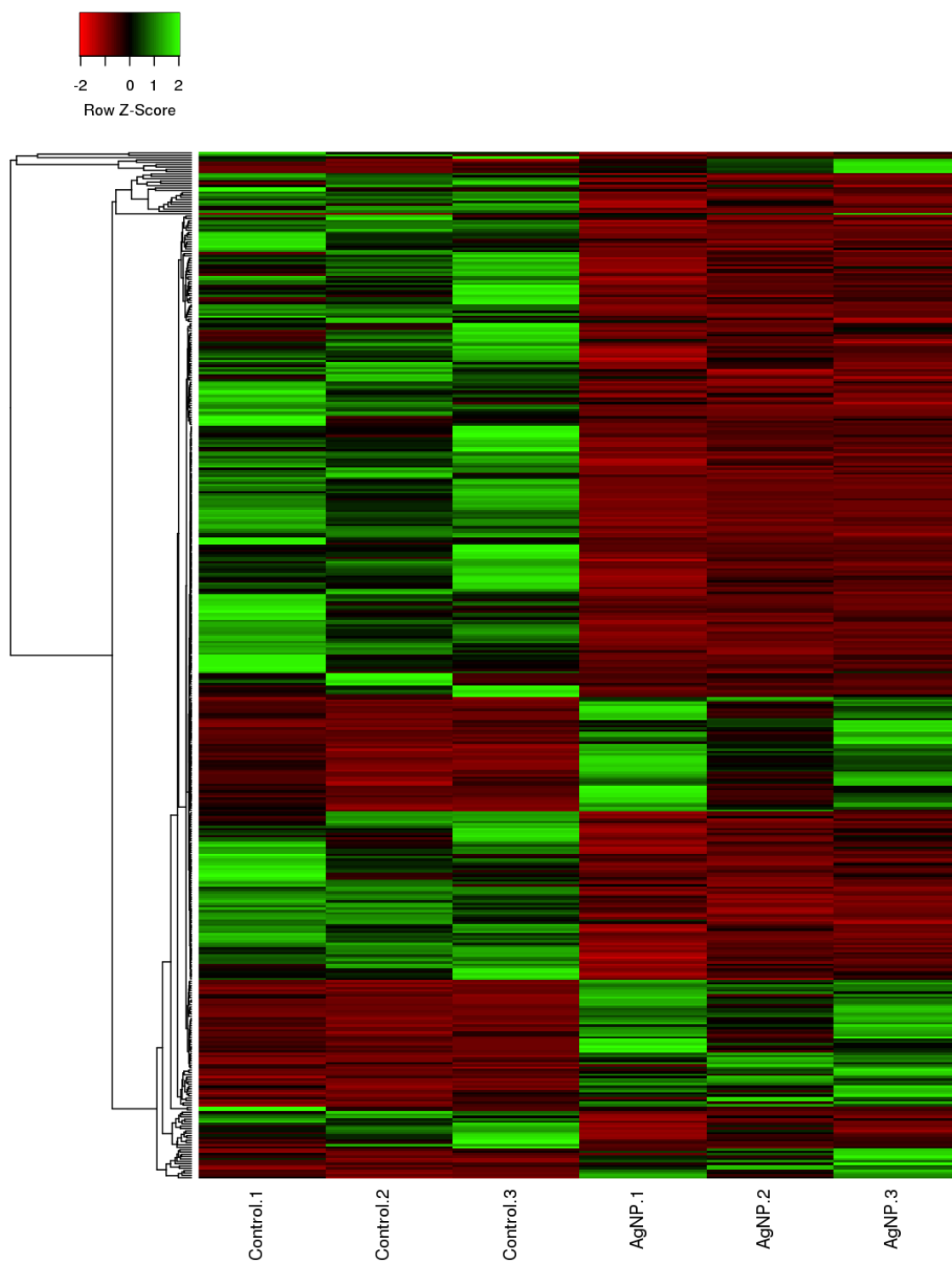


Figure 3. Hierarchical clustering of the expression data of DEGs in response to chronic AgNP exposure. Columns represent biological repeats for control and AgNP-treated plants while rows represent genes clustered via average linkage and calculations of Euclidean distance. Heatmap and clustering was performed with Heatmapper (Babicki et.al., 2016).

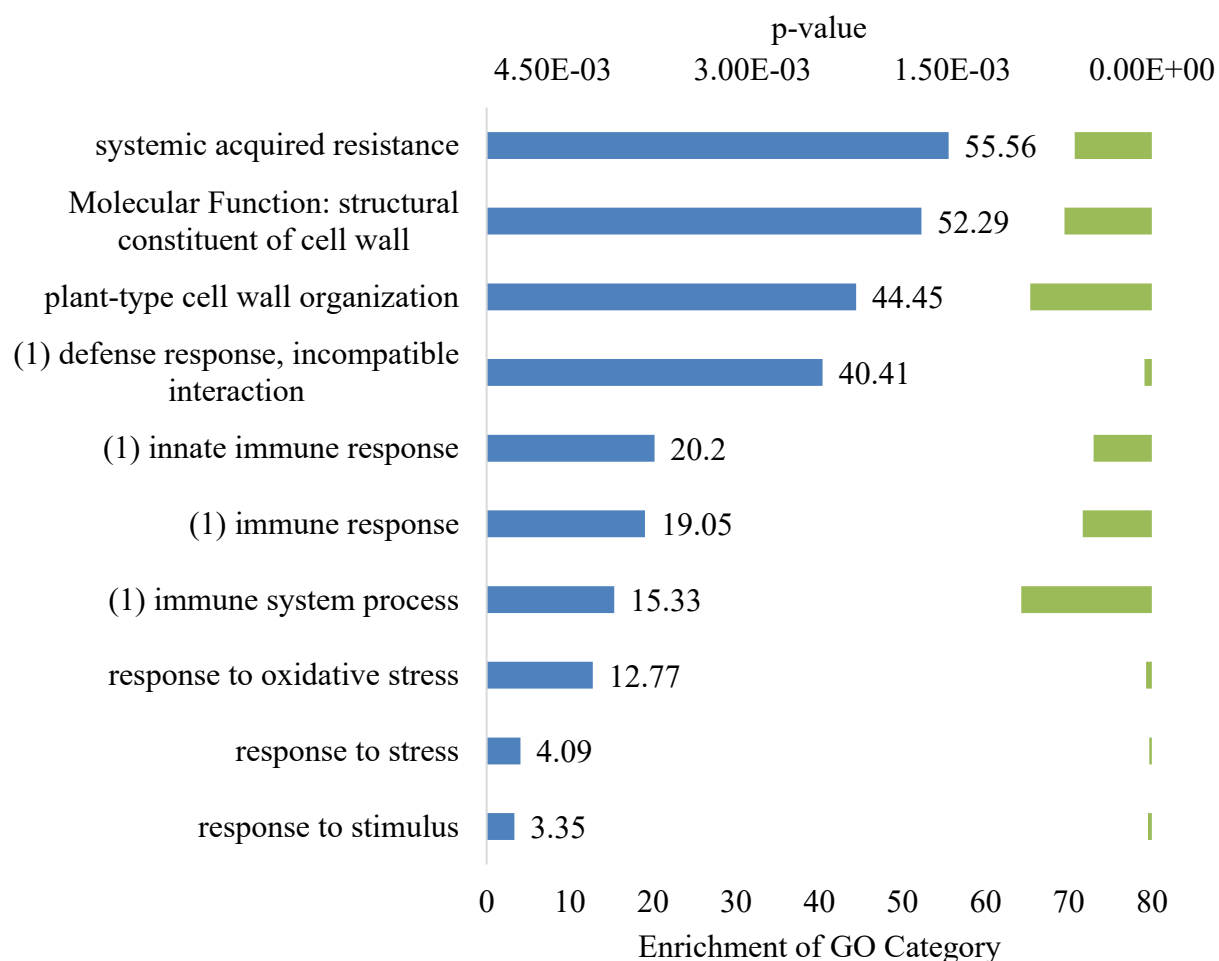


Figure 4. Enrichment of DEGs in various biological processes in AgNP-exposed *A. thaliana* seedlings. Gene ontology enrichment analysis was performed with GOrilla (Edan et. al., 2009) using the equation: $Enrichment = \frac{\binom{b}{n}}{\binom{B}{N}}$; where N is the total number of genes in the genome, B is the total number of genes in genome associated with a specific GO term, n is the number of differentially expressed genes, and b is the number of differentially expressed genes associated with the specified GO term. Ontologies with identical genes are marked with the same number.

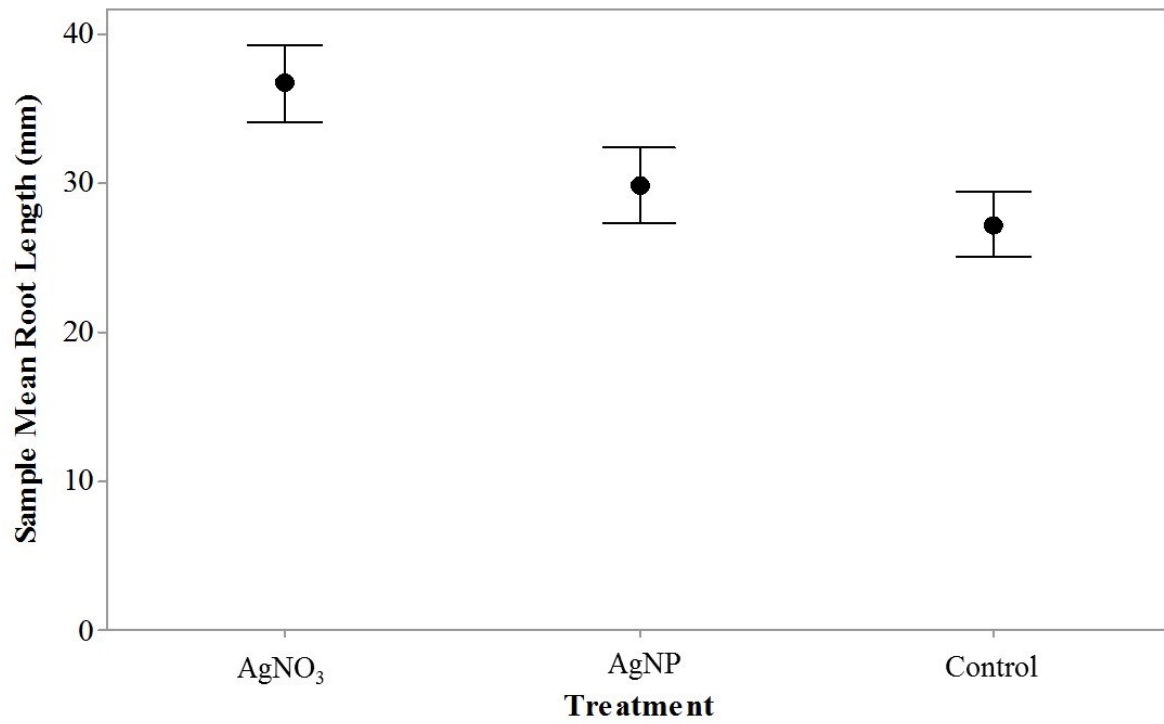


Figure 5. Sample mean root length in millimeters for different treatments. Error bars represent 95% confidence intervals.

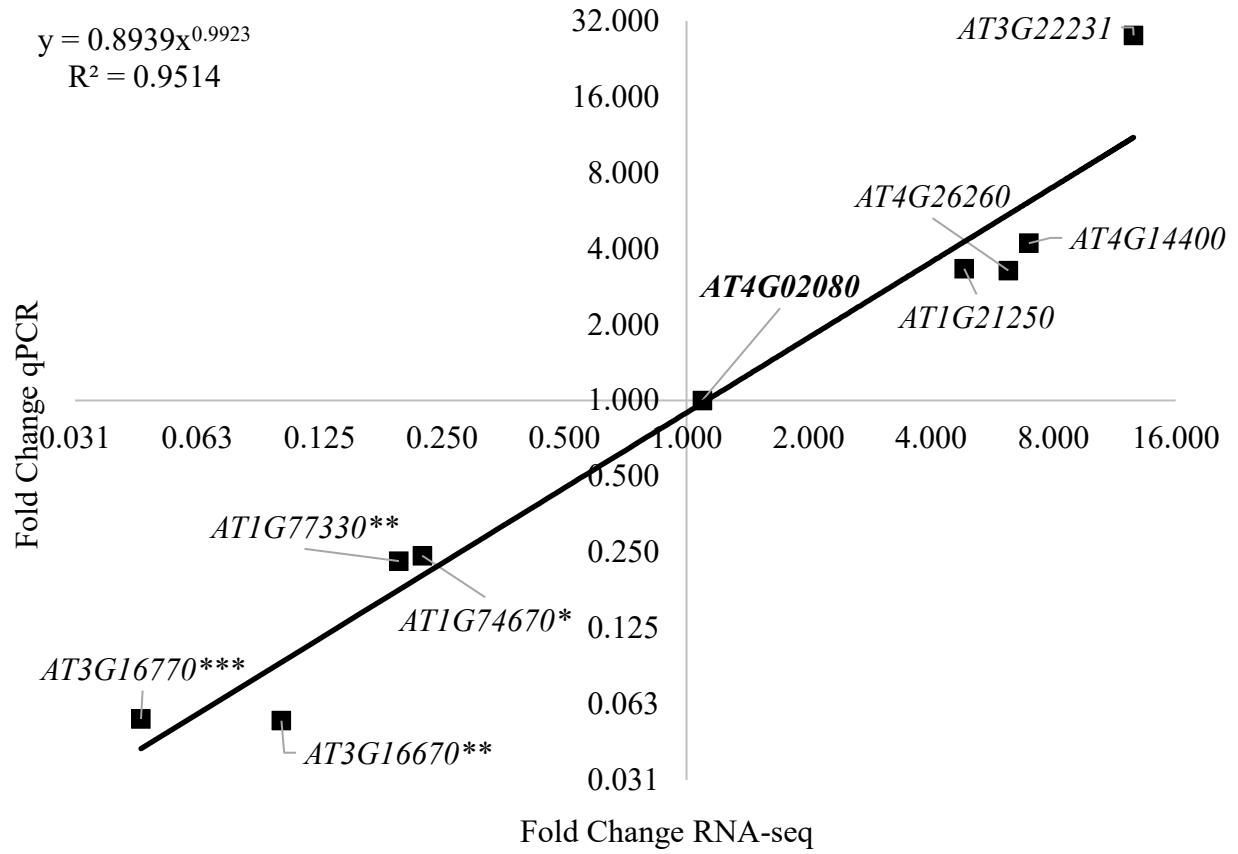


Figure 6. RT-qPCR validation of eight biomarker genes in response to AgNP treatment in an independent experiment. Trendline shows a power regression with the equation and R^2 value of 0.9514. The x- and y-axis are in 2-base logarithmic scale. Fold-changes that are < 1 and > 1 correspond to down- and up-regulation, respectively. Asterisks represent statistical significance (*, $p \leq 0.05$; **, $p \leq 0.005$) *AT4G02080* was used as a reference gene.

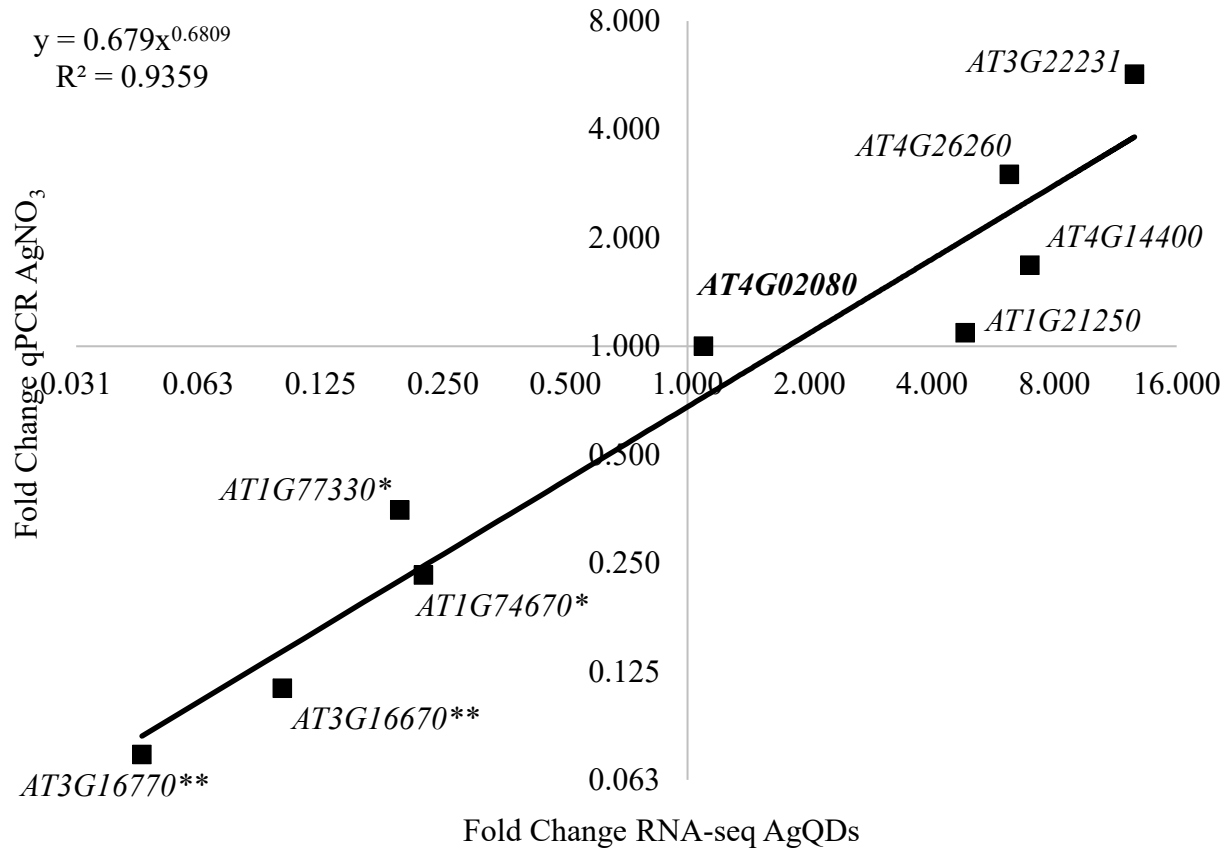


Figure 7. RT-qPCR validation of eight biomarker genes in response to AgNO₃ treatment. Trendline shows a power regression with the equation and R² value of 0.9359. The x- and y-axes are in 2-base logarithmic scale. Fold-changes that are < 1 and > 1 correspond to down- and up-regulation, respectively. Asterisks represent statistical significance (*, p ≤ 0.05; **, p ≤ 0.005). *AT4G02080* was used as a reference gene.

PARTICLE SIZE DOES NOT INFLUENCE GENE EXPRESSION IN SILVER AND GOLD NANOPARTICLE-EXPOSED *ARABIDOPSIS*

1. Introduction

Engineered nanomaterials (ENMs) are used in increasingly large quantities in consumer products. Of ENMs, silver-based nanomaterials are used most commonly in consumer products. Silver nanomaterials are of environmental concern, because they have been shown to readily leak from clothing and other products, and because they are present at detectable levels in rivers.

Silver nanoparticles (AgNPs) have been previously reported to be deleterious to microbes, yeasts, algae, plants and humans (reviewed by Aken, 2015). Plants are of primary concern, because their uptake of AgNPs potentially lead to bioaccumulation in higher organisms. It has been previously demonstrated that the dissociation of AgNPs into Ag^+ was weakly correlated with phytotoxicity (Kaveh et al., 2013; Geisler-Lee et al., 2013). However, it is generally agreed that the AgNP-triggered damage is caused by the particles themselves and that dissociated Ag^+ ions make very little or no contribution to toxicity (Yan and Chen, 2019). Therefore, recent studies have attempted to find correlation between AgNP toxicity and various nanomaterial characteristics, including particle shape, size, and the nature of the shell. Geisler-Lee et al. (2013) and Yan and Chen (2019) reported a negative correlation between AgNP particle size and the strength of impact on the physiology of the plant. These results lead to the hypothesis that larger surface area to mass ratio allows more atoms to directly interact with biological membranes (Wang et al., 2016). Experiments to better understand the influence of AgNP properties, including size, shape, and surface coating, on phytotoxicity have not produced unequivocal support for this hypothesis. A potential explanation for the unsettled questions is

that various experimenters have studied the physiological impact of AgNPs in different plant systems which likely differ in the way they take up, accumulate and internally transport nanoparticles. While most plant systems have higher phytotoxicity response to smaller-sized AgNP, larger AgNPs (150 nm diameter) had the tendency to more dramatically reduce seed germination and seedling growth than small AgNPs (20 nm diameter) in rice (Thuesombat et al., 2014). Yin et al. (2012) focused on the effect of surface coating (polyvinylpyrrolidone (PVP) and gum arabic (GA) on germination rates in eleven wetland plants and concluded that phytotoxicity was determined by both plant species and nanoparticle surface coating. Certain surface coating materials had an inhibitory effect on certain plant species but benefited others.

There has been limited scientific attention paid to the potential phytotoxicity of gold nanoparticles (AuNPs), likely because Au is considered an inert metal. Data reported so far revealed neither harmful, nor beneficial impact of AuNPs on plants, but have shown the ability of plants to take up and translocate AuNPs in a surface charge-dependent manner (Zhu et al., 2012; Koelmel et al., 2013). Negative effects of AuNP, including reduced growth and biomass and elevated oxidative stress (Verma et al., 2018), could only be induced when plants were exposed to high concentration. Such high concentrations could only result from biomagnification, (Judy et al., 2011), which is unlikely to occur in natural environment.

We sought to further understand the specific role of AgNP size on phytotoxicity by comparing an inert nanoparticle (AuNP) and AgNP at two different sizes while controlling for other factors known to influence phytotoxicity, including particle surface coating and concentration, plant system, and environmental conditions.

2. Methods

2.1 Nanoparticles. The nanoparticles used in this study were AgNPs and AuNPs, each applied as 20 nm- or 80 nm-diameter quasi-spherical neutral metal core particles surrounded by a citrate shell. They were obtained as colloidal preparations in 2 mM sodium citrate (PELCO® NanoXact™ particles, manufactured by Ted Pella, Inc., Redding, California). Upon arrival, the nanoparticles were stored at 4°C in dark. In visible light, the AgNP of 20 nm-diameter preparation had a yellow color, whereas AgNPs of 80 nm-diameter preparation had an opal color. This indicated that the material had size-dependent optical properties, and therefore the AgNP particles used in this study are considered to be quantum dots. Regardless of particle-size, AuNPs had a pink color in visible light.

2.2 Plant Material and Culture Conditions. This study was performed using *Arabidopsis thaliana* Col-0 ecotype seedlings. Seeds were sterilized for one hour in chlorine gas generated by mixing 3 mL of concentrated HCl with 100 mL of 6 % NaOCl (Clorox bleach). Additional sterilization was performed by washing the seeds in 70% ethanol for 2 min, followed by a 20 min incubation in a 10% bleach with 1% Triton solution. Seeds were washed with 4 rinses of sterile deionized water. The sterile seeds were then placed in an organized fashion on the surface of the agar-solidified plant culture media (see below) in Petri plates under axenic conditions. The plates were then wrapped with Parafilm, and the seeds were stratified at 4°C in the dark for 3 days. Following stratification, the Parafilm seal was removed, the plates were placed in a sandwich-sized plastic bags and transferred to a Conviron Adaptis A1000-AR Growth Chamber for 21 days. Plants were grown at 21°C, in a 10 hours light/14 hours dark diurnal cycle. During the entire 21-day growth period, the plates were randomly rearranged within the growth chamber daily to eliminate positional effect.

2.3 Plant Culture Media. Complete plant culture media was prepared using half-strength Murashige and Skoog nutrients with Gamborg's vitamins supplemented with 2.5% MOPS buffer and 0.8% agar. The final pH was adjusted to 7.0 using 100 mM KOH. It was necessary to maintain a neutral pH to prevent nanoparticle aggregation. Media were sterilized in an autoclave at 121°C for 20 minutes. Once cooled to 55°C, the media were supplemented with sterilized water (control) or aqueous solution AgNP or AuNP suspension for a final concentration of 8 µg/mL and sonicated for 2 minutes to prevent aggregation of nanoparticles. Following sonification, the media were supplemented with carbenicillin and Amphotericin B to 50 µg/mL and 1% final concentration to ensure axenic growth conditions.

2.4 Experimental Design and Collection of Plant Material. For each treatment, plants were grown in blocked environments with three technical replicates for each of the three biological repeats. All procedures to measure gene expression and phenotypic effects were performed on each replicate individually. For RNA-seq, replicates were pooled before library construction after RNA extraction and quantification.

Plant material was collected for root length phenotyping and total RNA extraction on 21-day old plants. In all experiments, plant material collection was performed 3 hours after the start of the light period to mitigate diurnal effect. Single plants were removed from culture media, and the root system was cut at the crown to remove it from the shoot system. The shoot system of the plants (consisting of cotyledons and rosettes) was flash-frozen in dry ice while the root was placed aside for length measurement. This process was repeated until 10 root and 20 shoot systems were collected from each replicate. The shoot material was stored at -80°C until total RNA extraction could be performed.

2.5 RNA Extraction, RNA-seq Library Construction and Sequencing. For total RNA extraction, the shoot material was first homogenized in liquid nitrogen, then suspended in Trizol reagent following the guidelines provided by the manufacturer. (Invitrogen, Carlsbad, California). RNA purification was performed using the RNeasy RNA-Extraction Kit by Qiagen (Hilden, Germany) following the manufacturer's guidelines. Total RNA was eluted in 50 μ L of DEPC-treated water, quantified using a Qubit 4.0 fluorimeter using the broad range RNA kit (ThermoFisher Scientific, Waltham, Massachusetts) and stored at -80°C .

mRNA purification and RNA-seq library construction were performed using the Universal Plus mRNA-seq kit by NuGEN Technologies (San Carlos, CA, USA) following the protocol without the optional AnyDeplete workflow. In brief, poly(A) mRNA was selected from 1 μ g of total RNA using poly(T) beads. The selected mRNA was fragmented, purified and reverse-transcribed into cDNA. The cDNA underwent library construction which consisted of end repair, adapter ligation and strand selection. Illumina adapters contain a nucleotide sequence barcode and primer-binding sites, which facilitates the assignment of reads to specific samples library and sequencing. The cDNA underwent strand selection so that only the forward strand was used for sequencing, making the cDNA library a "stranded" library. The stranded cDNA library was purified and amplified for a total of 15 libraries corresponding to the three biological repeats for control and the four nanoparticle treatments. Paired-end sequencing of 100-nt reads was performed on an Illumina NovaSeq 6000 Sequencing System at the Genome Sequencing Facility of the University of Kansas Medical Center.

2.6 RNA-seq analysis. RNA-seq analysis for differential gene expression was performed in the bioinformatics software CLC Genomics Workbench 11.0.1. Using an SSH file transfer protocol, raw read files were downloaded from the server of the sequencing center as zipped

FASTQ files, which were subsequently uploaded into CLC Genomics Workbench as unzipped paired Illumina reads. Reads were filtered based on length (between 15 and 1,000 bp), quality (limit 0.05) and ambiguities (limit 2) using default parameters and underwent automatic removal of read-through adapter sequences. Reads were mapped to the *Arabidopsis thaliana* TAIR10 reference genome sequence downloaded from ENSEMBL (Hunt et al., 2018), using default parameters in the forward direction. Expression data from mapped reads were normalized as the number of reads per kilobase per million mapped reads (RPKMs). Differentially expressed genes (DEGs) and differentially expressed variants were identified through pairwise comparison of control and each of the nanoparticle treatment libraries using the statistical tool Empirical Analysis of Differential Gene Expression (EDGE), which uses the Exact Test algorithm created by Robinson and Smyth (2008). False discovery rate (FDR)- and Bonferroni-correction of DEGs were performed to remove any false-positives. Genes that were differentially expressed 2-fold or higher and had a FDR-corrected *p*-value of less than 0.05 were used for subsequent data analysis.

2.7 qPCR Analysis. Real-time quantitative PCR (qPCR) validation of the RNA-seq gene expression results was performed for three transcripts using the same RNA samples that were used for the RNA-seq experiment. To normalize expression, *AT4G02080* was used as a reference gene. cDNA synthesis was performed using the SuperScript® II Reverse Transcriptase kit from Invitrogen, Inc., following the First-Strand cDNA Synthesis protocol with the following deviations: The starting amount of RNA was 1 µg; instead oligo-dTs, random primers were used at 100 ng/µL concentration; and finally, the RNA, primer and dNTP mix were incubated at 70°C instead of 65°C for 5 min. Following the addition of the reverse transcription buffer, DTT and RNaseOUT, the mixture was incubated at 25°C for 10 min, followed by the addition of the reverse transcriptase and incubations at 25°C for 10 min, at 42°C for 50 minutes and at 70°C for

15 min. cDNA sample concentrations were measured with a Qubit 4.0 fluorimeter using the ssDNA kit (ThermoFisher Scientific, Waltham, Massachusetts).

Primer pairs were designed using the Primer-BLAST platform provided by the National Center for Biotechnology Information (NCBI) database (Ye et.al, 2012) based on sequence data accessed at The *Arabidopsis* Information Resource (TAIR) website (Berardini et al., 2015). Primer oligonucleotides were synthesized by Integrated DNA Technologies, Inc (Coralville, Iowa) (Appendix D). qPCR experiments were performed on a MxPro 3005P instrument (Agilent Technologies, Santa Clara, California) using the GoTaq qPCR Master Mix (Promega Corp., Madison, Wisconsin). qPCR reaction mixtures were assembled and thermal cycling was performed following the manufacturer's guidelines, except that the reactions were performed in a volume of 20 μ L instead of recommended volume of 50 μ L. At the completion of the qPCR cycles, the following final dissociation thermal cycle segment was added: 95°C for 1 minute, 50°C for 30 seconds, and 95°C for 30 seconds. Cycle threshold (C_t) of 0.200 dRn fluorescence was used for primer efficiency calculations and differential expression analysis.

Primer efficiency for each primer pair was determined on a series of five five-time dilutions of cDNA sample in quadruplicates. The efficiency values for each replicate was accepted if the standard curve had an $r^2 > 0.985$ and efficiency was between 70% and 110%. qPCR analysis of differential expression for each gene was performed in three biological repeats in two technical replicates each, and with the inclusion of a no-template control. The average C_t value for each gene was used for differential expression analysis using the Pfaffl equation (Pfaffl, 2001). Statistical significance of differential expression was determined by measuring the difference in C_t values between target and reference genes for both control and treatment (Pfaffl,

2001). A one-way ANOVA was performed in Minitab 17 for each primer pair and considered significant at p -value < 0.05 .

2.8 Translucent Green Phenotyping. High-quality images of each replicate were taken on 20-day old plants. Images were taken on the 20th day to allow the plants remaining on the medium 24 hours to recover, before processing them for RNA-seq. The number of true leaves (rosettes) displaying translucent green (TG) phenotype were counted and compared to the total number of true leaves for each plate. The TG phenotype was defined as translucence on true leaves which maintained their green color (Figure 8). Data was analyzed as a ratio of TG leaves to total leaves.

The effect of nanoparticle treatment on TG phenotype was assessed using a multi-factor ANOVA. Nanoparticle treatment was treated as a fixed-effects factor, while biological repeat and replicate were treated as random-effects factors. Replicate was nested under treatment and biological repeat; otherwise, factors were crossed. All conclusions are based on a type-I error rate of 0.05. The analysis was performed using the general linear model (GLM) procedure of the software Minitab 17.

2.9 Root Length Phenotyping. High-quality images of 10 collected plant root systems (see section 2.4) were taken per replicate. The length of the longest root in millimeters was measured using the free-hand line tool of the software Image-J.

The effect of nanoparticle treatment on root length was assessed using a multi-factor ANOVA. Nanoparticle treatment was treated as a fixed-effects factor, while biological repeat and replicate were treated as random-effects factors. Replicate was nested under treatment and biological repeat; otherwise, factors were crossed. All conclusions are based on a type-I error rate of 0.05. The analysis was performed using the (GLM) procedure of Minitab 17.

3. Results

3.1 Exposure to Nanoparticle did not Influence Plant Phenotype. Statistical analysis did not reveal any significant effect of nanoparticle treatment on plant phenotype. TG plant frequency and root length measurement data showed that AgNP-treated plants differed from control at a p -value of 0.205 and 0.065, respectively (Figure 8).

3.2 Differential Expression of Genes in Response to Chronic Nanoparticle Exposure. RNA-seq averaged 79.5 million reads per library with an average of 91% of reads and 85% of fragments mapped to the TAIR10 reference genome sequence of *A. thaliana* (Appendix B-1, B-2). Libraries prepared from the first repeat of AgNP of 20 nm diameter treatment and the first repeat of AuNP of 80 nm diameter treatment had substantially lower percentage of reads (77.17% and 58.41%, respectively) and fragments mapped (68.90% and 57.84%, respectively) than average (Appendix E, F). Out of the 34,262 genes in the *Arabidopsis* genome, the number of genes differentially expressed (FDR-corrected p -value < 0.05, fold change rate 2-fold or greater) in response to exposure to 20 nm- and 80 nm-diameter AgNPs were 225 and 209, respectively. No DEGs were identified in response to AuNP exposure. DEGs that failed to pass FDR-correction at a p -value < 0.05 or that had lower than 2-fold change in transcript levels were excluded from subsequent analysis, except for hierarchical clustering, which included all DEGs. Fold-change, FDR-corrected p -value and putative DEG function data are listed in Appendix G for AgNP-treatment of 20 nm diameter and Appendix H for AgNP-treatment of 80 nm diameter.

3.3 Exposure to AgNPs of 20 nm and 80 nm in Diameter Induce Similar Transcriptional Changes in *Arabidopsis*. Hierarchical clustering demonstrated that chronic exposure to AgNPs at both 20 nm and 80 nm induced distinct changes in gene expression in *Arabidopsis* (Figure 9). The expression of 225 and 209 genes changed when the plants were

exposed to 20-nm and the 80-nm diameter AgNPs, respectively. Of these, 158 DEGs were shared between treatments at both particle sizes, (Figure 10). The correlation (r^2) of 0.9679 between the corresponding fold-change values of the 158 DEGs shared by the two treatments suggests that particle size had a relatively minor influence on the way AgNPs impact gene expression in the plant (Figure 11). Intriguingly, chronic exposure to AuNP at either 20 nm or 80 nm diameter did not induce changes in gene expression (Figure 9). Taken together, these data suggest that it is the metal content and not the size of the nanoparticle that is key in determining the impact.

3.4 qPCR Validation of RNA-seq. Three DEGs were chosen for the qPCR validation of RNA-seq results. Of these, one was down-regulated (*AT3G16670*) and two were up-regulated (*AT1G21250* and *AT1G14880*) in response to exposure to AgNP at both 20 nm and 80 nm diameter. For AgNP treatment of 20 nm diameter, Pfaffl-determined changes in gene expression for DEGs in qPCR experiment were plotted against EDGE-determined changes in gene expression in RNA-seq (Figure 12). Correlation between RNA-seq and qPCR expression levels were 0.9133. Of the three DEGs, only one passed one-way ANOVA statistical analysis: *AT1G14880* which had a *p*-value of 0.028. For AgNP treatment of 80 nm diameter, Pfaffl-determined changes in gene expression for DEGs in qPCR experiment were plotted against EDGE-determined changes in gene expression in RNA-seq (Figure 13). Correlation between RNA-seq and qPCR expression levels were 0.9969. All three DEGs passed one-way ANOVA statistical analysis: *AT3G16670*, *AT1G21250*, and *AT1G14880* which had a *p*-values of 0.001, 0.049, and 0.002, respectively.

3.5 Functional Categories of Differentially Expressed Genes. To shed light to the putative function of DEGs, gene ontology enrichment analysis was performed using GOrilla

(Eden et.al., 2009). Out of the 225 DEGs in response to exposure to AgNPs at 20 nm, only 89 DEGs were annotated and expressed at a level that could be included in the gene ontology enrichment assay. Thirty-three gene ontologies were enriched and 53 DEGs were found to be involved with these gene ontologies. Enriched gene ontologies primarily involved responses to stress, specifically wounding, oxidative, and pathogenic (biotic) stress (Figure 14). Biotic stress-related ontologies, denoted as immune/defense response and response to jasmonic acid contained upregulated genes involving controlling fungal infections, including *AT1G73805*, *AT2G34810*, *AT2G38870*, *AT2G39030*, *AT2G43530*, *AT3G11340*, *AT3G51450*, *AT3G51660*, *AT4G08870*, *AT5G03350*, *AT5G05600*, *AT5G10760*, *AT5G23820*, *AT5G38900*, *AT5G45410*, and *AT5G6180* (Appendix G). The ontology for regulation of systemic acquired resistance was highly enriched at 80.93 and contained two upregulated genes *AT1G73805* and *AT4G01895* (Appendix G). Response to wounding ontology contained upregulated genes which are also involved in biotic or oxidative stress, including *AT1G72520*, *AT2G20340*, *AT2G34810*, *AT2G38870*, and *AT3G51450* (Appendix G). Oxidative stress ontologies, denoted as the molecular function of oxidoreductase activity and dioxygenase activity, contained mostly upregulated genes involved in the oxidation-reduction process, including *AT1G06620*, *AT1G06640*, *AT1G14120*, *AT1G26390*, *AT1G72520*, *AT2G34810*, *AT2G38240*, *AT5G05340*, and *AT5G05600* (Appendix G). There were overlaps of genes between multiple enriched ontologies, showing that these ontologies were related (Figure 15).

Out of the 209 DEGs in response to AgNP at 80 nm exposure, only 86 DEGs were annotated and expressed at a level that could be included in the gene ontology enrichment assay. Thirty-six gene ontologies were enriched and 54 DEGs were found to be included in them. Enriched gene ontologies primarily involved responses to stress, specifically wounding and

pathogenic (biotic) stress, as well as genes involved in cell wall organization (Figure 16). Biotic stress-related ontologies, denoted as immune/defense response and response to jasmonic acid contained upregulated genes involving controlling fungal infections, including *AT1G66100*, *AT2G34810*, *AT2G34930*, *AT2G38240*, *AT2G38870*, *AT2G39030*, *AT2G43530*, *AT3G51450*, *AT5G03350*, *AT5G05600*, *AT5G10760*, *AT5G23820*, *AT5G38900*, and *AT5G61890* (Appendix H). Response to wounding ontology contained upregulated genes which also are involved in biotic stress, including *AT2G34810*, *AT2G38870*, and *AT3G51450* (Appendix H). The plant cell wall-related ontology contained six up-regulated defense-response or cell wall organization genes (*AT1G17860*, *AT2G34930*, *AT2G38870*, *AT3G15720*, *AT5G03350*, and *AT5G05340*) and three down-regulated abiotic-stress related genes (*AT4G16260*, *AT5G47550*, and *AT5G64100*) (Appendix H). There were overlap of genes among multiple enriched ontologies, showing that these ontology functions were related (Figure 17).

3.6 AuNPs Induce Splicing Variation that is Dependent on Nanoparticle Size.

Despite lack of DEGs, differential frequency in two splice variants were detected due to AuNP exposure at 80 nm, *AT1G57720_2* and *CPN60B1_1*, with these splice variants being drastically down-regulated. These two splice variants passed statistically significance (FDR-corrected p-value < 0.05; fold change rate 2-fold or greater).

4. Discussion

When comparing differences in size of nanoparticles in response to root elongation, there are several factors that need to be taken in consideration. Geiser-Lee et al. (2013) showed that root elongation in response to AgNP treatment is not only dependent on size but on concentration of the nanoparticle and method of exposure as well. Siegel et al. (2018) recently

reported that the physiological impact of AuNPs is both particle size- and concentration-dependent. They found that, for AuNPs to impact root elongation at a diameter of 18 nm (the largest particle size studied), it had to be applied at a concentration as high as 100 mg/L. This concentration is 10 times higher than the concentration applied in our experiments. It is possible therefore, that we could also have detected an impact on gene expression if we used AuNPs at size below 20 nm and higher concentrations. Clearly, when making conclusions about the phytotoxicity of various engineered nanoparticles, one must consider all factors that may influence their physiological impact. It will require extensive testing at various sizes, concentrations, with different coating materials, and using a wide range of plant species to perceive any overall effects of a given engineered nanomaterial.

The TG phenotype has been previously described in transgenic *Arabidopsis*, with overexpression in key aquaporin genes, including *AT2G36830* (Zhu et. al., 2014), which leads to water dysregulation. In these experiments, *AT2G36830* and other aquaporin genes were not found differentially regulated in any of the nanoparticle-treated plants. While no significant differences could be detected between nanoparticle treatments and control, in the TG phenotype, the possibility of nanoparticles causing water dysregulation deserves further attention.

Our data suggest that metal composition of the nanoparticle is a more important factor in impacting the transcriptome than particle size. As the hierarchical clustering of the expression data of DEGs demonstrates (Figure 9), independently repeated AgNP-exposure of plants induced similar gene expression patterns, which were barely influenced by particle size. The control and AuNP-exposure of plants on the other hand induced a strikingly different expression pattern. The AgNP-treated plants had DEGs of 225 and 209 for 20 nm and 80 nm diameter, respectively, of which 158 genes were shared (Figure 10). When these shared DEGs were mapped, the r^2 value

of the trendline was 0.9679, which represents a strong correlation (Figure 11). García-Sánchez et al. (2015) compared nanoparticles of different size and composition for their impact on the transcriptome of *Arabidopsis*. While their results show a general trend of down-regulation of the transcriptome and correlation to abiotic stress through gene ontology, our data suggest the opposite. We tend to see a general trend of upregulation of the transcriptome with many of the genes involved in biotic stress response. These discrepancies could be due to differences in exposure methods as well as transcriptome analysis. García-Sánchez et al. (2015) performed a 48-hour shock-treatment experiment and measured gene expression changes with microarray, whereas our data represent the result chronic exposure with measurements made using next generation sequencing. While DEGs were similar between sizes of AgNP, RNA-seq provides the option to compare differences in alternative splicing between samples. The possibility that there are alternative splicing differences in response to different sizes of AgNP particles deserves further investigations.

Most research on the effect of AgNP size on phytotoxicity focused on the physiological effects on plants, including accumulation of AgNPs (Geisler-Lee et al., 2013; Wang et al., 2013), root tip browning (Geisler-Lee et al., 2013), and plant growth (Yin et al., 2012). Each of these studies concluded that AgNP phytotoxicity is negatively correlated with AgNP size. Our data does not show this trend as root length measurements, TG phenotype and gene expression data show no difference between treatments with AgNPs at 20 nm and 80 nm. The same conclusions are true to AuNPs.

Cell wall pores are typically 3-5 nm, while the nanoparticles used for this study are 20 and 80 nm in diameter. Geiser-Lee et al. (2013) has shown that AgNPs with diameters between 10-40 nm can accumulate in the cell wall and plasmodesma. Another study showed that AgNP

that are 10 nm in diameter accumulated in the apoplast region of root tissues (Bao et. al., 2016). The apoplastic presence of the particles can cause damage to the cell wall. Other metal oxide- and metal-based nanomaterials have also been shown to be taken up into the root and accumulate in different regions surrounding the cell (reviewed in Verma et. al., 2018). Cell wall damage, specifically at the root, have been studied previously in response to AgNP treatment. Studies in rice showed that AgNPs penetrated the cell wall, causing disruption of cell morphology (Mirzajani et al, 2013). Our data shows enriched ontologies of cell wall and external encapsulating structure are for AgNP at 80 nm exposure. Since most of the genes found in the cell wall-enriched ontology are involved in cell wall organization, it is safe to assume the AgNPs at 80 nm significantly impacts damage to plant cell walls. Surprisingly, a previous experiment focusing on the effects of AgNPs at 20 nm diameter at concentrations of 4 $\mu\text{g/ml}$ had DEGs in enriched ontologies involving cell wall organization (Chapter 1). The effects of AgNPs are known to be concentration-dependent (Geiser-Lee et al., 2013; Thuesombat et al., 2014), therefore, the lack of cell wall-related GO enrichment could have been due to the application of lower concentrations of AgNPs in our previous experiments.

Oxidative stress is a well-established phytotoxic response to ENM exposure in plants. Previous studies have reported an increase in the level of AgNP-induced oxidative stress by detecting an up-regulation in genes encoding peroxidases (Kaveh et. al., 2013) and precursors of oxidative stress tolerance proteins (Mirzajani et. al, 2014), as well as increased and accelerated ROS accumulation (Nair and Chung, 2014). Our gene ontology enrichment provides further support for the induction of oxidative stress through the enriched molecular function ontologies of dioxygenase activity for AgNPs at both 20 nm and 80 nm (enrichment value of 14.28 and 12.32, respectively) and oxidoreductase activity for AgNPs at 20 nm (enrichment value of 3.29).

Most of these genes are involved in the oxidation-reduction process, with a single upregulated peroxidase gene (*AT5G05340*) for AgNPs at 20 nm. The first sign of oxidative stress is the presence of reactive oxygen species (ROS), such as singlet oxygen, superoxide, hydrogen peroxide (H₂O₂) and hydroxyl radical (Mourato et al., 2012). The most commonly produced ROS in response to AgNP exposure was reported to be H₂O₂ (Panda et al., 2011; Speranza et al., 2013; Nair and Chung, 2014; Thiruvengadam et al., 2015), which required peroxidase enzymes to convert H₂O₂ into water and oxygen. H₂O₂ is well established as an intracellular signal produced rapidly as a first response to pathogenic stress and damage to the cell wall. In combination with Ca²⁺ influx, a burst of H₂O₂ acts as a key signal to set the plant immune response into motion.

There are several plant stress hormones involved in biotic and abiotic stress responses. It has been proposed that during a pathogen attack, the transport and concentration of biotic stress hormones, such as salicylic acid (SA), increase whereas the concentration of abiotic stress hormones, such as jasmonic acid (JA) and ethylene are decreasing in the plant (reviewed by Caarls et al., 2015 and by Kazan, 2015). This concept, however, has been challenged as too simplistic, and it is more likely that gene expression regulation in response to pathogen attack is borne out of the interplay between the SA and JA signaling networks (reviewed in Dar et al., 2015).

We saw an enrichment of ontologies for biotic stress and defense response. For AgNP at 20 nm exposure, ontologies included pathogenic stress response through activation of the systemic acquired resistance (SAR) and the JA signaling pathway. The gene ontology regulation of SAR has an enrichment value of 80.93, and contains two upregulated SA-signaling genes, *AT1G73805* and *AT4G01895* (Figure 14). In plants, SA concentration is known to increase as

part of the defense response to obligate fungal pathogenic infections (Durrant and Dong, 2004). H₂O₂ and SA have been shown to be precursors for the activation of SAR (Lamb and Dixon, 1997). Increase in JA levels and the activation of the JA signaling pathway can be deduced through the enrichment of three ontologies: molecular function of JA hydrolases (enrichment value of 134.89), regulation of JA-mediated signaling pathway (enrichment value of 44.96), and response to JA (enrichment value of 22.48). The two genes in the enriched ontology of JA hydrolases are jasmonate-induced oxygenase, which are upregulated, implying that there is an increase in jasmonic acid within the plant. Recently, however, it has been found that JA cross-talks other stress hormones, including SA, to protect against a wide variety of biotic stress (Glazebrook, 2005; Howe, 2004; reviewed in Dar et. al., 2015). This can be seen in our data, as genes involved in JA-related ontologies overlap with genes of fungal defense-related ontologies, or as the gene annotations include responses to JA (*AT2G39030*, *AT3G51450*, and *AT4G08870*, see Appendix G).

While the ontology of regulation of SAR was not enriched from AgNP at 80 nm exposure, other pathogenic defense responses ontologies were enriched (Figure 16), which included defense response to fungus, incompatible interaction (enrichment value of 59.83), defense response to fungus (enrichment value 22.9), and response to biotic stimulus (enrichment value of 9.14). As described with AgNPs at 20 nm, increase in JA and the activation of the JA signaling pathway can be deduced through the enrichment of three ontologies: molecular function of JA hydrolases (enrichment value of 139.60), regulation of JA mediated signaling pathway (enrichment value of 46.53), and response to JA (enrichment value of 23.27). Again, overlap between pathogenic stressor ontologies and JA-related ontologies can be perceived as expression changes in *AT2G39030* and *AT3G51450* (Appendix H).

For AgNPs at both 20 nm and 80 nm, the enriched ontology of response to wounding is interesting as it is the only direct abiotic-like stress response seen. However, two genes involved in the enriched ontology overlap with the ontologies for defense response and response to fungus. These genes respond to wounding induced by fungal attack or herbivory. These genes include *AT2G38870* and *AT3G51450* (Appendix G, H). Two of the genes observed in the enriched response to wounding ontology are also enriched in JA related ontologies. These genes include *AT2G34810* and *AT3G51450*, of which *AT3G51450* can be seen in biotic defense response ontologies as well (Appendix G, H). What can be reason for the response similar to defense signaling in AgNP-exposed plants? One potential explanation may be the oxidative stress and elevated levels of H₂O₂, which are consistently observed in studies on AgNP-exposed plants (reviewed by Yan and Chen, 2019). Because hydrogen peroxide produced at the cell wall is a key signal to set off the defense response, plant cells may respond to AgNP-triggered hydrogen peroxide with defense-like response, complete with signaling reminiscent of SAR.

Our experiments failed to detect gene expression changes in response to AuNP exposure. Previously, others have demonstrated a transcriptomic impact of Au ions in salts that are typically used to synthesize AuNP (Taylor et al., 2014). To our knowledge, our study is the first to directly examine transcriptomic response to AuNP in plants. It has been hypothesized that different shells reduce the rate of dissociation of nanoparticles into the metal ions, thereby reducing the nanoparticle toxicity (Koelmel et al., 2013). This hypothesis needs to be explored further considering that the AuNP used in this study had a citrate shell, and the rate at which the citrate shell causes dissociation into Au ions is unknown. With previous research of Au ions showing strong negative impact of the transcriptome, it should be observed if the citrate shell surrounding the AuNPs used in this experiment played a role in the lack of transcriptomic

changes. As stated before, next generation sequencing technology allows for comparing differences in alternative splicing variants. While AuNP show no statistically differential gene expression, there were two splice variants (*ATIG57720_2* and *CPN60B1_1*) that was drastically reduced in response to AuNP at 80 nm diameter exposure. These two transcripts have yet to be annotated, so the biological significance of this finding is not known.

In terms of resources, the immune response is known to incur a cost in plants. It is therefore difficult to reconcile our findings on the activated immune response and our inability to detect significant phenotypic differences between AgNP-treated and control plants. It is therefore important to experiment with different experimental design which reduces or eliminates the blocking effects of the replicates. Other aspects of plant physiology, primarily photosynthesis, also warrant further investigations. Collection of additional data on the carbon fixation rates, chlorophyll content and dried biomass in response to nanoparticle-treatment using a similar experimental design described is already under way.

References

- Aken, B.V., 2015. Gene expression changes in plants and microorganisms exposed to nanomaterials. *Curr. Opin. Biotechnol.* 33, 206-209.
- Babicki, S., Arndt, D., Marcu, A., Liang, Y., Grant, J.R., Maciejewski, A., Wishart, D.S., 2016. Heatmapper: web-enabled heat mapping for all. *Nucleic Acids Res.* 44, W147-W153.
- Bao, D., Oh, Z.G., Chen, Z., 2016. Characterization of silver nanoparticles internalized by *Arabidopsis* plants using single particle ICP-MS analysis. *Front. Plant Sci.* 7, 1-8.
- Berardini, T.Z., Reiser, L., Li, D., Mezheritsky, Y., Muller, R., Strait, E., Huala, E., 2015. The *Arabidopsis* information resource: Making and mining the “gold standard” annotated reference plant genome. *Genes.* 53, 474-484.
- Caarls, L., Pieterse, C.M.J., Van Wees, S.C.M., 2015. How salicylic acid takes transcriptional control over jasmonic acid signaling. *Front. Plant Sci.* 6, 1-9.

- Dar, T.A., Uddin, M., Khan, M.M.A., Hakeem, K.R., Jaleel, H., 2015. Jasmonates counter plant stress: A review. *Environ. Exp. Botany*. 115, 49-57.
- Durrant, W.E., Dong, X., 2004. Systemic acquired resistance. *Annu. Rev. Phytopathol.* 42, 185-209.
- Eden, E., Navon, R., Steinfeld, I., Lipson, D., Yakhini, Z., 2009. GOrilla: a tool for discovery and visualization of enriched GO terms in ranked gene lists. *BMC Bioinform.* 10:48.
- García-Sánchez, S., Bernales, I., Cristobal, S., 2015. Early response to nanoparticles in the *Arabidopsis* transcriptome compromises plant defence and root-hair development through salicylic acid signalling. *BMC Genom.* 16, 341.
- Geisler-Lee, J., Wang, Q., Yao, Y., Zhang, W., Geisler, M., Li, K., Huang, Y., Chen, Y., Kolmakov, A., Ma, X., 2013. Phytotoxicity, accumulation and transport of silver nanoparticles by *Arabidopsis thaliana*. *Nanotoxicol.* 7, 323-337.
- Glazebrook, J., 2005. Contrasting mechanisms of defence against biotrophic and necrotrophic pathogens. *Annu. Rev. Phytopathol.* 43, 205-227.
- Howe, G.A., 2004. Jasmonates as signals in the wound response. *J. Plant Growth Regul.* 23, 223-237.
- Hunt, S.E., McLaren, W., Gil, L., Thormann, A., Schuilenburg, H., Sheppard, D., Parton, A., Armean, I.M., Trevanion, S.J., Flicek, P., Cunningham, F., 2018. Ensembl variation resources. *Database*. 2018, 1-12.
- Judy, J.D., Unrine, J.M., Bertsh, P.M., 2011. Evidence for biomagnification of gold nanoparticles within a terrestrial food chain. *Environ. Sci. Technol.* 45, 776-781.
- Kaveh, R., Li, Y.-S., Ranjbar, S., Tehrani, R., Brueck, C.L., Aken, B.V., 2013. Changes in *Arabidopsis thaliana* gene expression in response to silver nanoparticles and silver ions. *Environ. Sci. Technol.* 47, 10637-10644.
- Kazan, K., 2015. Diverse roles of jasmonates and ethylene in abiotic stress tolerance. *Trend Plant Sci.* 20, 219-229.
- Koelmel, J., Leland, T., Wang, H., Amarasiriwardena, D., Xing, B., 2013. Investigation of gold nanoparticles uptake and their tissue level distribution in rice plants by laser ablation-inductively coupled-mass spectrometry. *Environ. Pollut.* 174, 222-228.
- Lamb, C., Dixon, R.A., 1997. The oxidative burst in plant disease resistance. *Annu. Rev. Plant Physiol. Plant Mol. Biol.* 48, 251-275.

- Mirzajani, F., Askari, H., Hamzelou, S., Farzaneh, M., Ghassempour, A., 2013. Effect of silver nanoparticles on *Oryza sativa* L. and its rhizosphere bacteria. *Ecotoxicol. Environ. Saf.* 88, 48-54.
- Mirzajani, F., Askari, H., Hamzelou, S., Schober, Y., Römpp, A., Ghassempour, A., Spengler, B., 2014. Proteomics study of silver nanoparticles toxicity on *Oryza sativa* L. *Ecotoxicol. Environ. Saf.* 108, 335-339.
- Mourato, M., Reis, R., Martins, L.L., 2012. Characterization of plant antioxidative system in response to abiotic stresses: A focus on heavy metal toxicity. *Advances in Selected Plant Physiology Aspects*. IntechOpen:pp. 23-44.
- Nair, P.M.G., Chung, I.M., 2014. Assessment of silver nanoparticle-induced physiological and molecular changes in *Arabidopsis thaliana*. *Environ. Sci. Pollut.* 21, 8858-8869.
- Panda, K.K., Achary, V.M.M., Krishnaveni, R. Padhi, B.K., Sarangi, S.N., Sahu, S.N., Panda, B.B., 2011. In vitro biosynthesis and genotoxicity bioassay of silver nanoparticles using plants. *Toxicol. In Vitro.* 25, 1097-1105.
- Pfaffl, M.W., 2001. A new mathematical model for relative quantification in real-time RT-PCR. *Nucleic Acids Res.*, 9 e45.
- Robinson, M.D. and Smyth, G.K., 2008. Small-sample estimation of negative binomial dispersion, with applications to SAGE data. *Biostat.* 9, 321-332.
- Siegel, J., Záruba, K., Švorčík, V., Kroumanová, K., Burketová, L., Martinec, J., 2018. Round-shape gold nanoparticles: effect of particle size and concentration on *Arabidopsis thaliana* root growth. *Nanoscale Res. Lett.* 13, 1-7.
- Speranza, A., Crinelli, R., Scoccianti, V., Taddei, A.R., Iacobucci, M., Bhattacharya, P., Ke, P.C., 2013. In vitro toxicity of silver nanoparticles to kiwifruit pollen exhibits peculiar traits beyond the cause of silver ion release. *Environ. Pollut.* 179, 258-267.
- Supek, F., Bošnjak, M., Škunca, N., Šmuc, T., 2011. REVIGO summarizes and visualizes long lists of gene ontology terms. *PLoS ONE.* 6, e21800.
- Taylor, A.F., Rylott, E.L., Anderson, C.W., Bruce, N.C., 2014. Investigating the toxicity, uptake, nanoparticle formation and genetic response of plants to gold. *PLoS ONE.* 9, e93793.
- Thiruvengadam, M., Gurunathan, S., Chung, I.-M., 2015. Physiological, metabolic, and transcriptional effects of biologically-synthesized silver nanoparticles in turnip (*Brassica rapa* ssp. *rapa* L.). *Protoplasma.* 252, 1031-1046.
- Thuesombat, P., Hannongbua, S., Akasit, S., Chadchawan, S., 2014. Effect of silver nanoparticles on rice (*Oryza sativa* L. cv. *KDML 105*) seed germination and seedling growth. *Ecotoxicol. Environ. Saf.* 104, 302-309.

- Verma, S.K., Das, A.K., Patel, M.K., Shah, A., Kumar, V., Gantait, S., 2018. Engineered nanomaterials for plant growth and development: A perspective analysis. *Sci. Total Environ.* 630, 1413-1435.
- Wang, J., Koo, Y., Alexander, A., Yang, Y., Westerhof, S., Zhang, Q., Schnoor, J.L., Colvin, V.L., Braam, J., Alvarez, P.J.J., 2013. Phytostimulation of poplars and *Arabidopsis* exposed to silver nanoparticles and Ag⁺ at sublethal concentrations. *Environ. Sci. Technol.* 47, 5442-5449.
- Wang, P., Lombi, E., Zhao, F.-J., Kopittke, P.M., 2016. Nanotechnology: A new opportunity in plant sciences. *Trends Plant Sci.* 21, 699-712.
- Yan, A., Chen, Z., 2019. Impacts of silver nanoparticles on plants: a focus the phytotoxicity and underlying mechanism. *Int. J. Mol. Scie.* 20, 1-21.
- Ye, J., Coulouris, G., Zaretskaya, I., Cutcutache, I., Rozen, S., Madden, T.L., 2012. Primer-BLAST: A tool to design target-specific primers for polymerase chain reaction. *BMC Bioinform.* 13, 1-11.
- Yin, L., Colman, B.P., McGill, B.M., Wright, J.P., Bernhardt, E.S., 2012. Effects of silver nanoparticle exposure on germination and early growth of eleven wetland plants. *PLoS ONE.* 7, e47674.
- Zhu, Z.-J., Wang, H., Yan, B., Zheng, H., Jiang, Y., Miranda, O.R., Rotello, V.M., Xing, B., Vachet, R.W., 2012. Effect of surface charge on the uptake and distribution of gold nanoparticles in four plant species. *Environ. Sci. Technol.* 46, 12391-12398.
- Zhu, D., Wu, Z., Coa, G., Li, J., Wei, J., Tsuge, T., Gu, H., Aoyama, T., Qu, L.-J., 2014. TRANSLUCENT GREEN, an ERF family transcription factor, controls water balance in *Arabidopsis* by activating the expression of aquaporin genes. *Mol. Plant.* 7, 601-615.

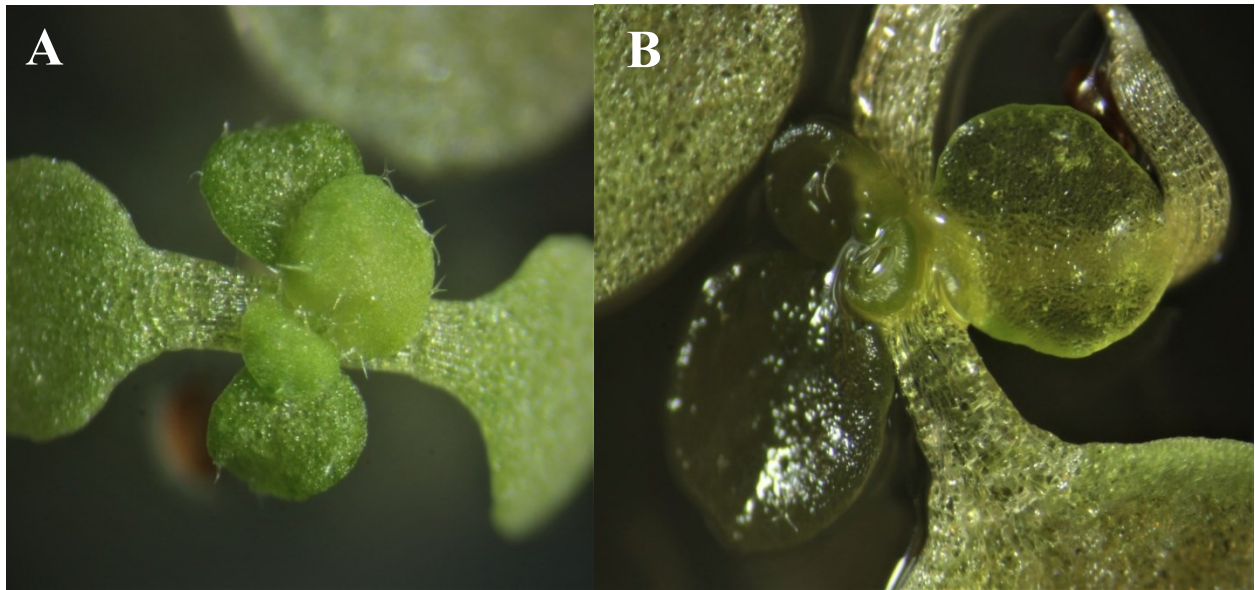


Figure 8. The translucent green phenotype. *Arabidopsis* seedlings growing on AgNP-containing medium with (A) normal non-translucent and (B) translucent leaves.

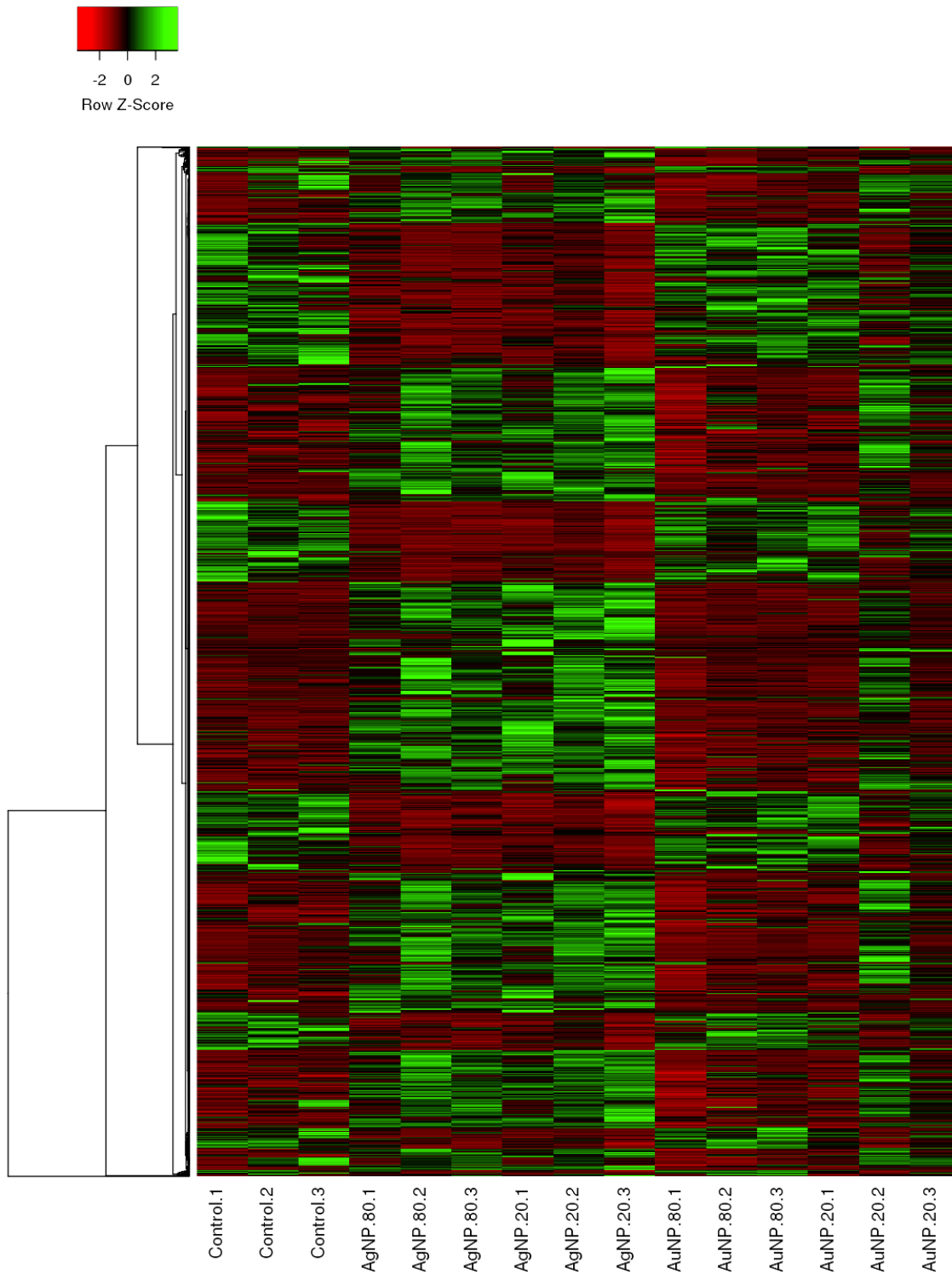


Figure 9. Hierarchical clustering of rate of expression change of DEGs in response to chronic nanoparticle exposure. Columns represent biological repeats for control and nanoparticle-treated plants while rows represent genes clustered via average linkage and Euclidean distance values. Heatmap and clustering was performed with Heatmapper (Babicki et al., 2016).

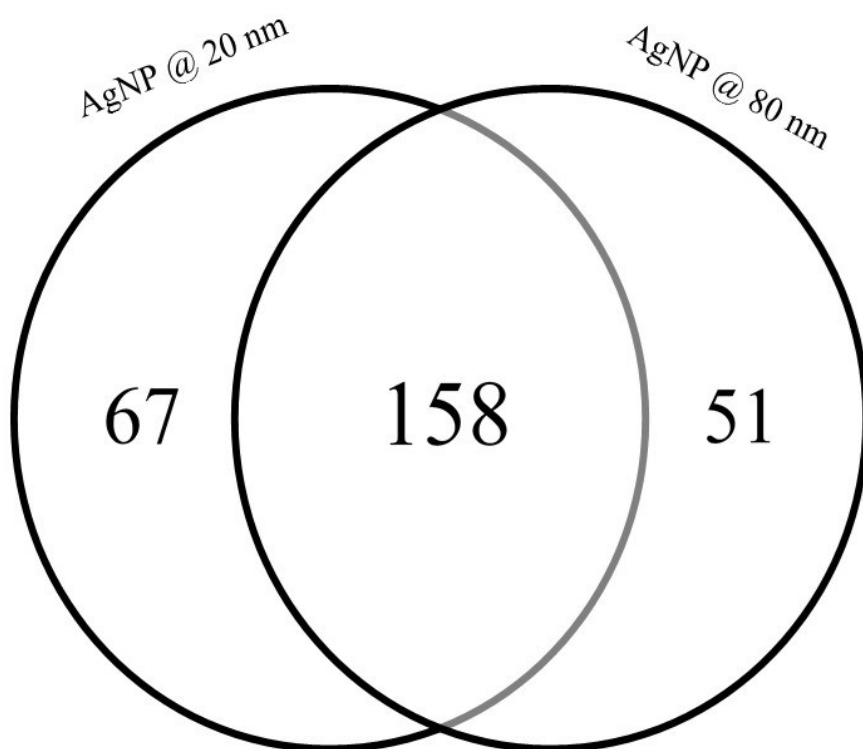


Figure 10. Number of differentially expressed genes responsive to AgNPs at only 20 nm, at only 80 nm particle size and at both sizes.

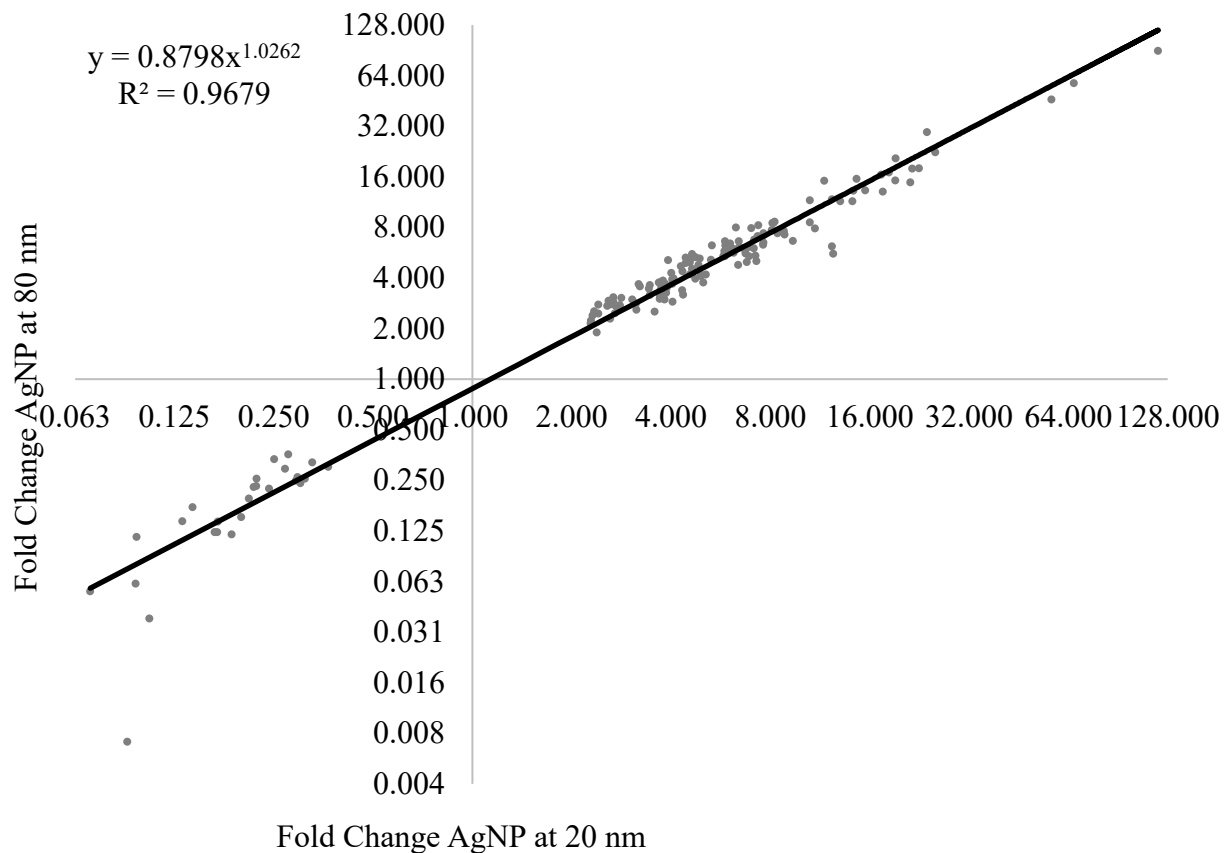


Figure 11. Fold-change of the 158 genes differentially expressed in response to AgNP at both 20 nm and 80 nm sizes. Trendline shows an exponential regression with the equation and R^2 value of 0.9679. The x and y axes are in a 2-base logarithmic scale. Fold-changes that are < 1 and > 1 correspond to down-and up-regulation, respectively.

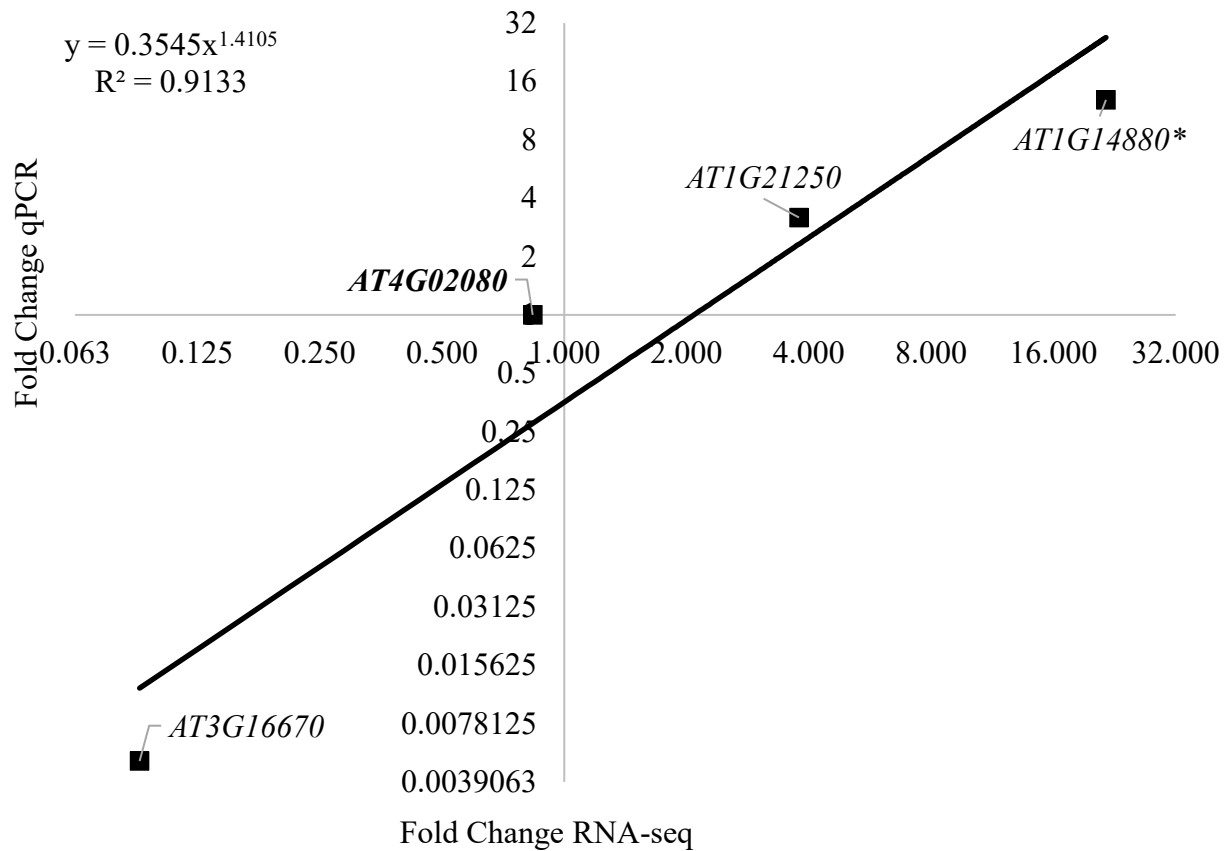


Figure 12. qPCR validation of three genes in response to AgNP at 20 nm treatment. The trendline shows the power regression line with the equation and R^2 value of 0.9133. The x- and y-axes are in 2-base logarithmic scale. Fold-changes that are < 1 and > 1 correspond to down-and up-regulation, respectively. Asterisks represent statistical significance. *AT4G02080* was used as a reference gene.

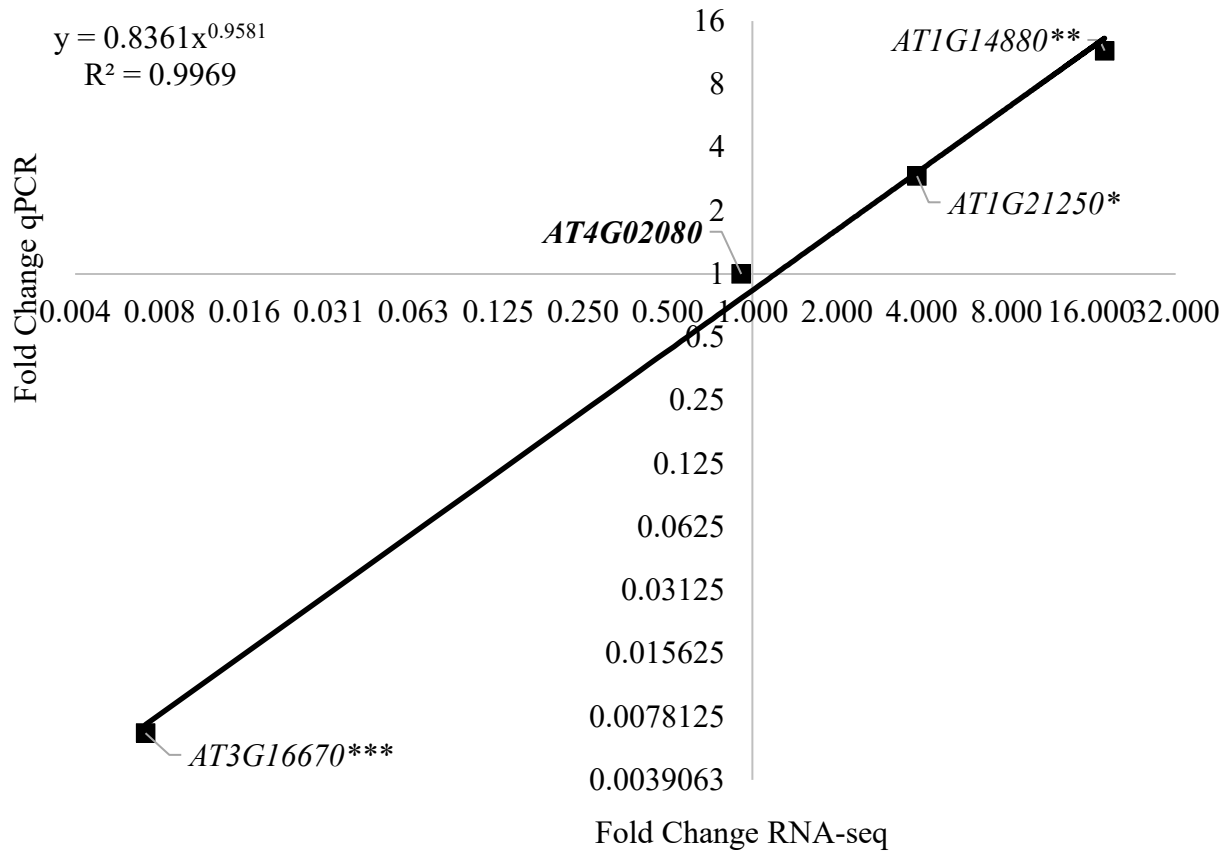


Figure 13. qPCR validation of three genes in response to AgNP at 80 nm treatment. The trendline shows the power regression line with the equation and R^2 value of 0.9969. The x- and y-axes are in 2-base logarithmic scale. Fold-changes that are < 1 and > 1 correspond to down- and up-regulation, respectively. Asterisks represent statistical significance. *AT4G02080* was used as a reference gene.

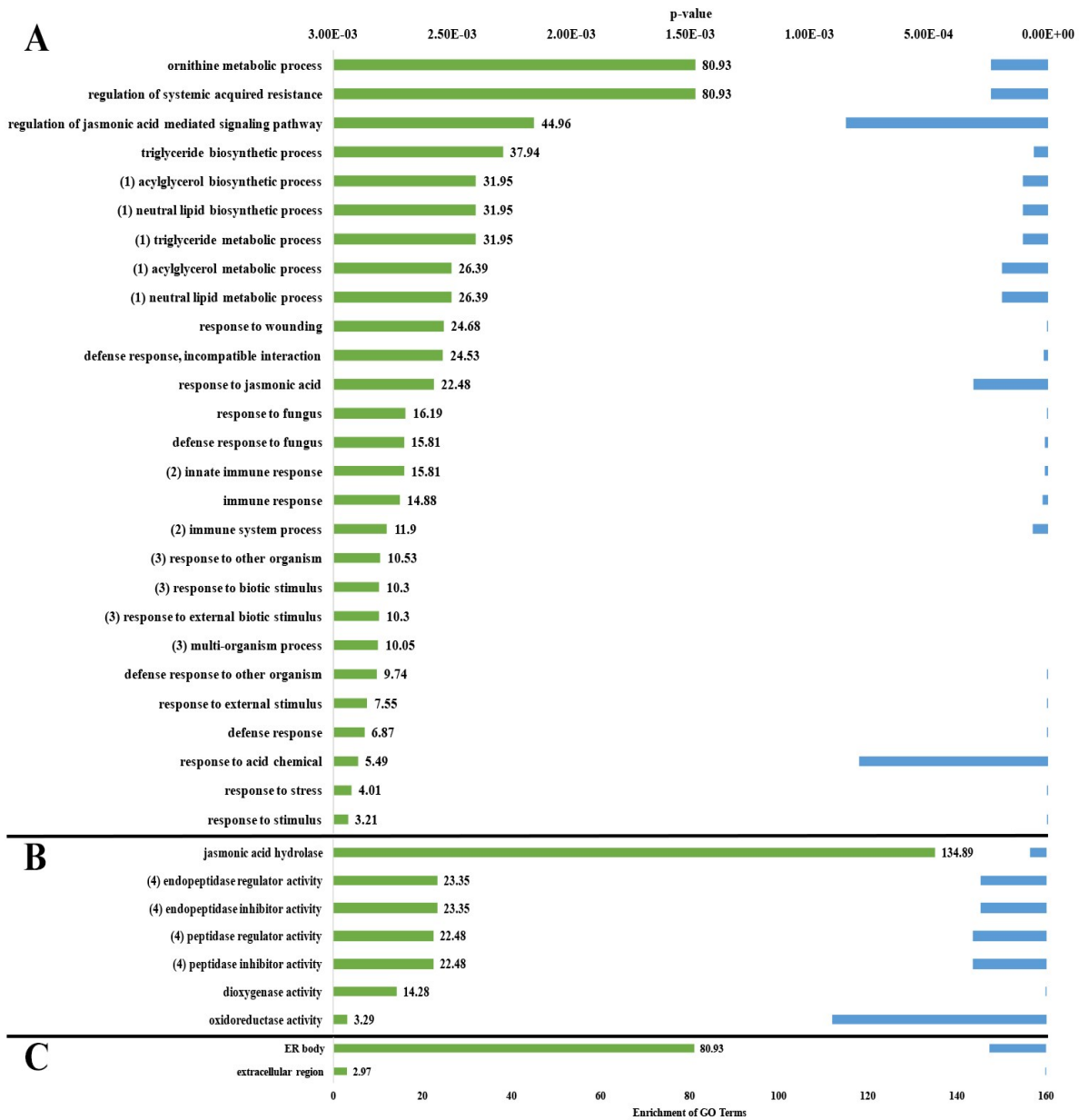


Figure 14. Enrichment of differentially expressed genes in (A) biological processes, (B) molecular functions and (C) cellular components in response to exposure to AgNPs at 20 nm. Gene ontology enrichment analysis was performed with GOrilla (Edan et. al., 2009) using the equation described in Fig. 4.

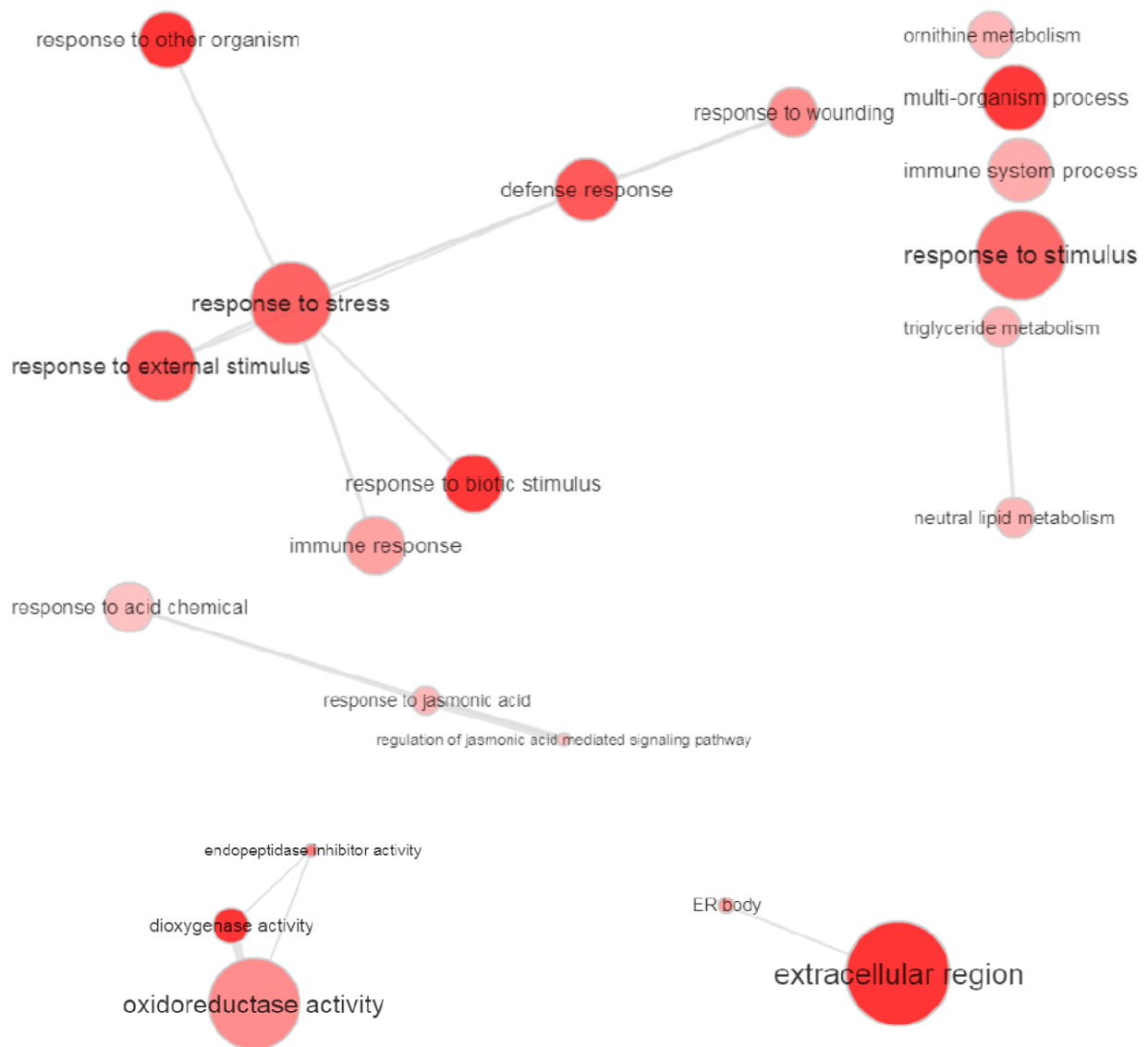


Figure 15. Relatedness among GO terms from Gene Ontology Enrichment Analysis of DEGs in response to AgNP at 20 nm after removal of redundant GO terms. Bubble color is related to p-value and bubble size is related to the enrichment of each GO term. Similar GO terms are linked together with edges whose width indicates degree of similarity. Analysis was performed using REVIGO (Supek et al., 2011).

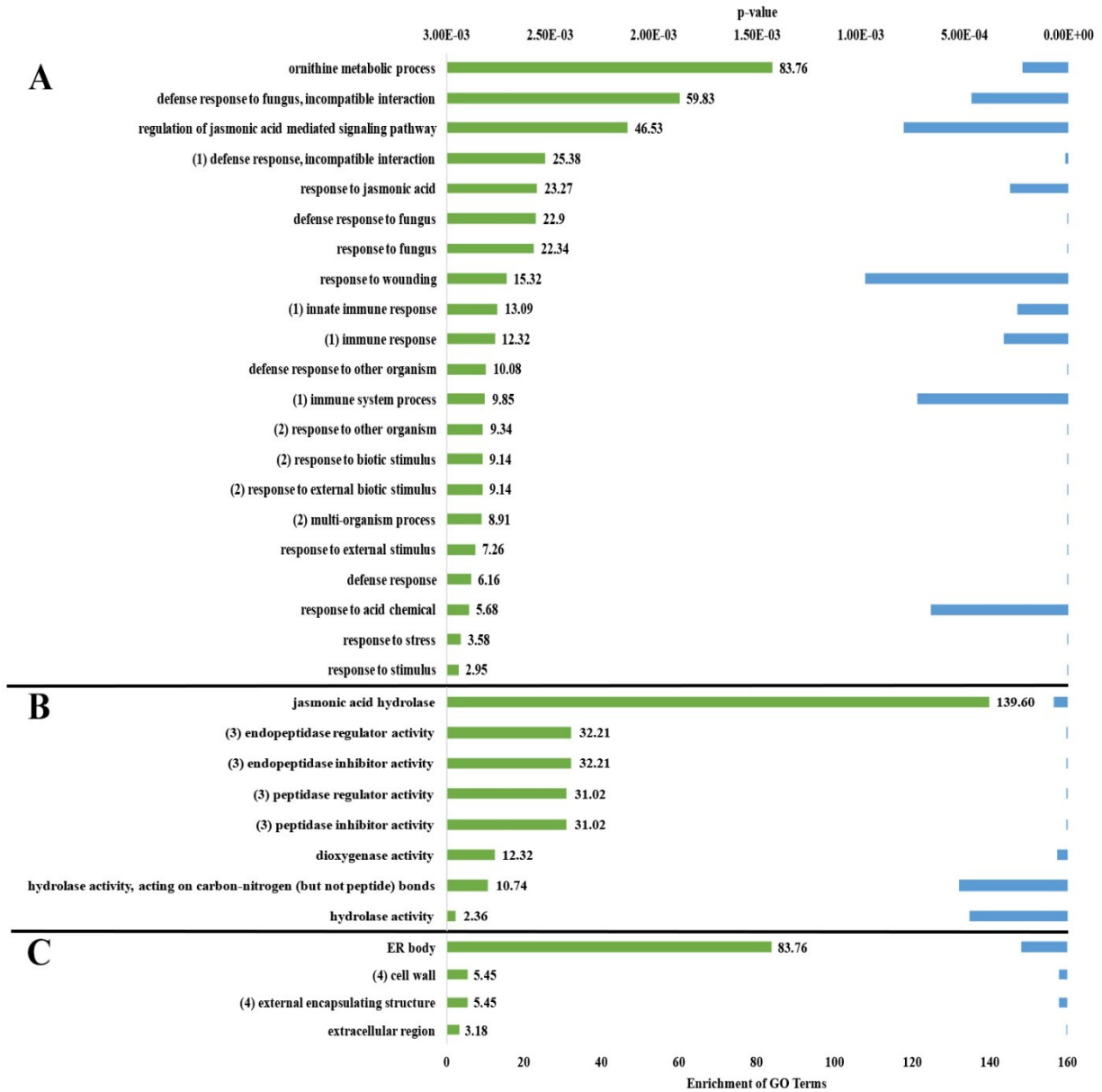
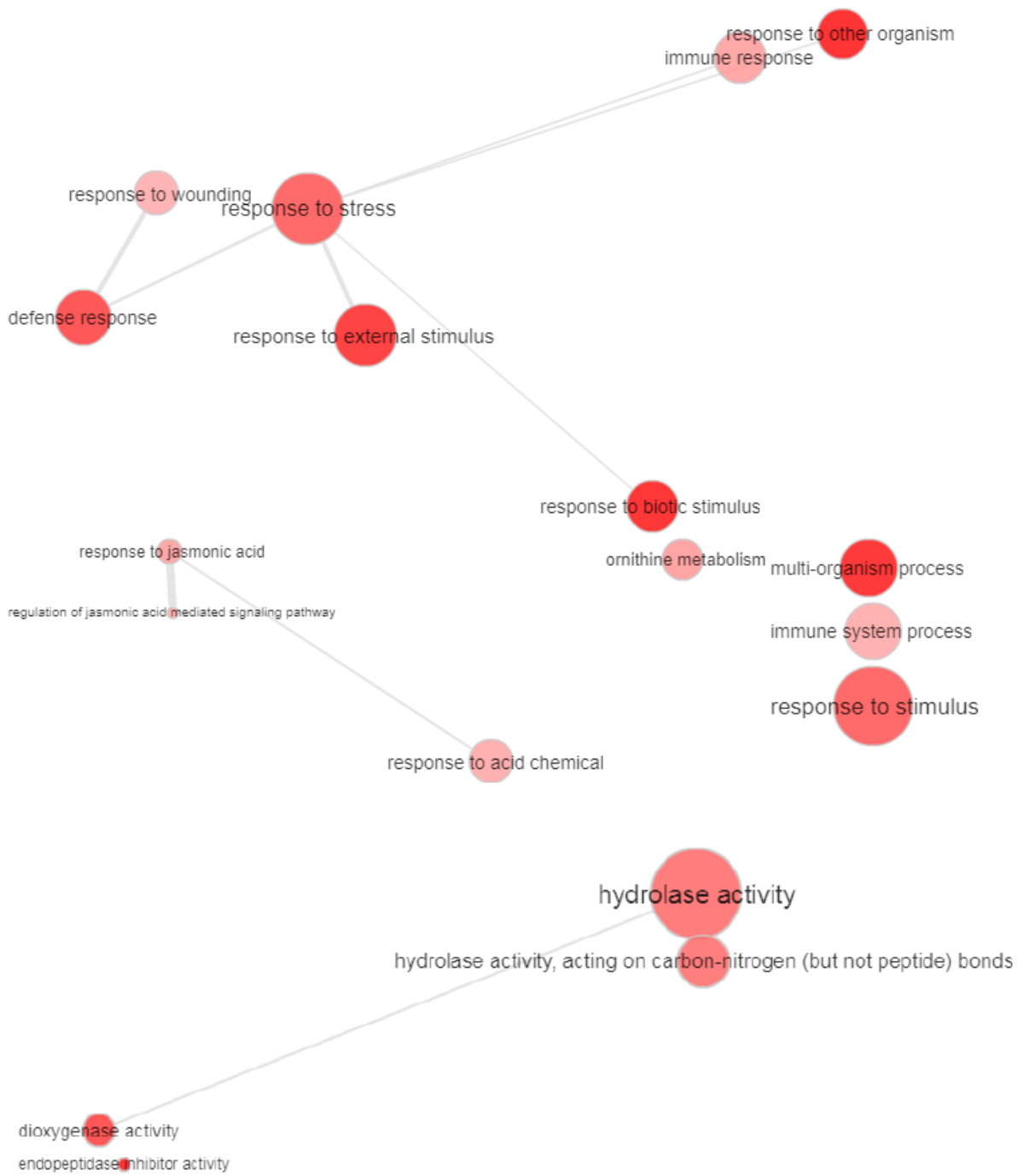


Figure 16. Enrichment of differentially expressed genes in (A) biological processes, (B) molecular functions and (C) cellular components in response exposure to AgNP at 80 nm. Gene ontology enrichment analysis was performed with GOrilla (Edan et. al., 2009) using the equation described in Fig. 4.



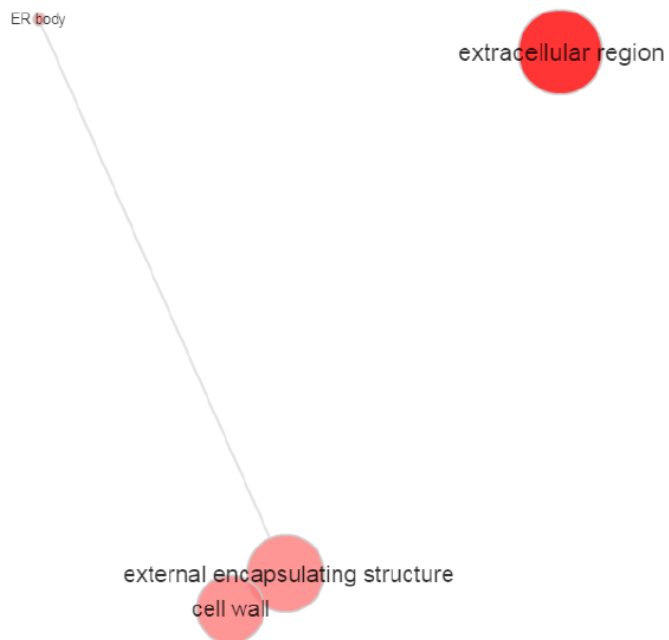


Figure 17. Relatedness among GO terms from Gene Ontology Enrichment Analysis of DEGs in response to AgNP at 80 nm after removal of redundant GO terms as described in Fig. 15. Analysis was performed using REVIGO (Supek et al., 2011).

SUMMARY

The purpose of this thesis research was to examine gene expression changes underlying the physiological impact of AgNP exposure in an *Arabidopsis* model system and to develop a gene expression-based standardized plant bioassay for comparative studies on various ENMs. The first chapter reports on experiments on the transcriptomic and phenotypic impact of Ag⁺ in the form of AgNO₃ to mimic the AgNP disassociation into Ag⁺. Gene expression results reveal that there is a similarity between the impact of Ag⁺ and AgNP on the transcriptome. This suggests that AgNP toxicity may be due to Ag⁺ dissociation from the nanoparticles, which had been previously demonstrated by others (Geisler-Lee et al., 2013), though not by us. However, in our experiments, root length is not impacted negatively by AgNPs. In fact, the root system grew significantly longer in the presence of high concentration of Ag⁺, suggesting that the Ag⁺ may not be responsible for the phytotoxicity typically seen by AgNP exposure (Kaveh et al., 2013; Geisler-Lee et al., 2013). The second chapter reports on experiments on the role of particle size in AgNP-induced phytotoxicity and transcriptomic impact. Previous studies on a wide-variety of plant species found that AgNP phytotoxicity is in general negatively correlated with AgNP size, such that the smaller AgNP is more toxic than larger AgNPs (Geisler-Lee et al., 2013; Yan and Chen, 2019). However, our phenotypic data on root length and TG leaves did not show any statistically significant difference between the smaller-sized AgNP (20 nm diameter) and larger-sized AgNP (80 nm diameter). García-Sánchez et al. (2015) examined the transcriptomic impact of different sizes of AgNP, carbon nanotubes (CNTs) and titanium dioxide nanoparticles (TiO) and concluded that all ENMs had a similar impact on the *Arabidopsis* transcriptome despite size, shape and metal composition differences. While our data shows that size does not influence

transcriptomic changes, we see that the metal composition does play a significant role. AuNPs and AgNPs had completely different gene expression profiles, while the two different sizes for each metal triggered similar gene expression patterns.

The inconsistent and contrasting results of studies performed on AgNP phytotoxicity in plants indicate that plant responses are determined by AgNP properties, the plant species used, and the methods employed. The development of a standardized, gene expression-based bioassay in *Arabidopsis* is an attempt to establish a sensitive system in which the impact of AgNPs on plants can be detected. Our results of repeatable and consistent AgNP-triggered expression changes in a handful of biomarker genes demonstrate that the establishment of such a system is achievable.

ADDITIONAL REFERENCES

- Aken, B.V., 2015. Gene expression changes in plants and microorganisms exposed to nanomaterials. *Curr. Opin. Biotechnol.* 33, 206-2019.
- Bagherzadeh Homaei, M., Eshampour, A.A., 2016. Silver nanoparticles and silver ions: Oxidative stress responses and toxicity in potato (*Solanum tuberosum* L.) grown in vitro. *Hortic. Environ. Biotechnol.* 57, 544-553.
- Buzea, C., Pacheco, I.I., Robbie, K., 2007. Nanomaterials and nanoparticles: Sources and toxicity. *Biointerphases*. 2, MR17-MR71.
- Colman, B.P., Arnaout, C.L., Anciaux, S., Gunsch, C.K., Hochella, M.F. Jr., Kim, B., Lowry, G.V., McGill, B.M., Reinsch, B.C., Richardson, C.J., Unrine, J.M., Wright, J.P., Yin, L., Bernhardt, E.S., 2013. Low concentrations of silver nanoparticles in biosolids cause adverse ecosystem responses under realistic field scenario. *PLoS ONE*. 8, e57189.
- García-Sánchez, S., Bernales, I., Cristobal, S., 2015. Early response to nanoparticles in the *Arabidopsis* transcriptome compromises plant defence and root-hair development through salicylic acid signalling. *BMC Genom.* 16, 341.
- Geisler-Lee, J., Wang, Q., Yao, Y., Zhang, W., Geisler, M., Li, K., Huang, Y., Chen, Y., Kolmakov, A., Ma, X., 2013. Phytotoxicity, accumulation and transport of silver nanoparticles by *Arabidopsis thaliana*. *Nanotoxicol.* 7, 323-337.
- Geisler-Lee, J., Brooks, M., Gerfen, J.R., Wang, Q., Fotis, C., Sparer, A., Ma, X., Berg, R.H., Geisler, M., 2014. Reproductive toxicity and life history study of silver nanoparticle effect, uptake and transport in *Arabidopsis thaliana*. *Nanomater.* 4, 301-318.
- Jiang, H.-S., Qui, X.-N., Li, G.-B., Li, W., Yin, L.-Y., 2014. Silver nanoparticles induced accumulation of reactive oxygen species and alteration of antioxidant systems in the aquatic plant *Spirodela polyrhiza*. *Environ. Toxicol. Chem.* 33, 1398-1405.
- Kaveh, R., Li, Y.-S., Ranjbar, S., Tehrani, R., Brueck, C.L., Aken, B.V., 2013. Changes in *Arabidopsis thaliana* gene expression in response to silver nanoparticles and silver ions. *Environ. Sci. Technol.* 47, 10637-10644.
- Liu, X., Lee, P.Y., Ho, C.M., Lui, V.C., Chen, Y., Che, C.M., Tam, P.K., Wong, K.K., 2010. Silver nanoparticles mediate differential responses in keratinocytes and fibroblasts during skin wound healing. *Chem. Med. Chem.* 5, 468-475.

- Liu, J., Williams, P.C., Geisler-Lee, J., Goodson, B.M., Fakharifar, M., Peiravi, M., Chen, D., Lightfoot, D.A., Gemeinhardt, M.E., 2018. Impact of wastewater effluent containing aged nanoparticles and other components on biological activities of the soil microbiome, *Arabidopsis* plants, and earthworms. *Environ. Res.* 164, 197-203.
- Massarsky, A., Trudeau, V.L., Moon, T.W., 2014. Predicting the environmental impact of nanosilver. *Environ. Toxicol. Pharmacol.* 38, 861-873.
- Nair, P.M.G., Chung, I.M., 2014a. Physiological and molecular level effects of silver nanoparticles exposure in rice (*Oryza sativa* L.) seedlings. *Chemosphere.* 112, 105-113.
- Nair, P.M.G., Chung, I.M., 2014b. Assessment of silver nanoparticle-induced physiological and molecular changes in *Arabidopsis thaliana*. *Environ. Sci. Pollut.* 21, 8858-8869.
- Panda, K.K., Achary, V.M.M., Krishnaveni, R. Padhi, B.K., Sarangi, S.N., Sahu, S.N., Panda, B.B., 2011. In vitro biosynthesis and genotoxicity bioassay of silver nanoparticles using plants. *Toxicol. In Vitro.* 25, 1097-1105.
- Sun, T.Y., Mitrano, D.M., Bornhöft, N.A., Scheringer, M., Hungerbühler, K., Nowack, B., 2017. Envisioning nano release dynamics in a changing world: Using dynamic probabilistic modeling to assess future environmental emissions of engineered nanomaterials. *Environ. Sci. Technol.* 51, 2854-2863.
- Sharma, V.K., Siskova, K.M., Zboril, R., Gardea-Torresday, J.L., Organic-coated silver nanoparticles in biological and environmental conditions: Fate, stability and toxicity. *Adv. Colloid Interface Sci.* 204, 15-34.
- Thuesombat, P., Hannongbua, S., Akasit, S., Chadchawan, S., 2014. Effect of silver nanoparticles on rice (*Oryza sativa* L. cv. *KDML 105*) seed germination and seedling growth. *Ecotoxicol. Environ. Saf.* 104, 302-309.
- Vance, M.E., Kuiken, T., Vejerano, E.P., McGinnis, S.P., Hochella, M.F., Jr., Rejeski, D., Hull, M.S., 2015. Nanotechnology in the real world: Redeveloping the nanomaterial consumer products inventory. *Beilstein J. Nanotechnol.* 6, 1769-1780.
- Vishwakarma, K., Upadhyay, N., Singh, J., Liu, S., Singh, V.P., Prasad, S.M., Chauhan, D.K., Tripathi, D.K., Sharma, S., 2017. Differential phytotoxic impact of plant mediated silver nanoparticles (AgNPs) and silver nitrate (AgNO₃) on *Brassica* sp. *Front. Plant Sci.* 8, 1-12.
- Yan, A., Chen, Z., 2019. Impacts of silver nanoparticles on plants: a focus the phytotoxicity and underlying mechanism. *Int. J. Mol. Scie.* 20, 1-21.
- Yin, L., Colman, B.P., McGill, B.M., Wright, J.P., Bernhardt, E.S., 2012. Effects of silver nanoparticle exposure on germination and early growth of eleven wetland plants. *PLoS ONE.* 7, e47674.

APPENDICES

Appendix A

qPCR primer information for RNA-seq validation.

	Forward Primer Sequence	T _m (°C)	Reverse Primer Sequence	T _m (°C)	Primer Efficiency
<i>AT3G18780</i>	ACTTTCATCAGCCGTTTTGA	52.6	ACGATTGGTTGAATATCATCAG	50.6	1.773
<i>AT4G02080</i>	GCTGTGTTATTATTAAGCCGTAAG	52.0	AAAGCTAGGTACGGTTTAAGAC	52.3	1.942
<i>AT3G16770</i>	CACCAACCAAGTTAACGTGAAAGA	55.7	TTTCCCCATGGACGCTTACG	57.6	1.893
<i>AT3G16670</i>	TGGGGTTCTCTTTTGCACCA	57.1	GGACGACCGCATTAGCGAAA	57.9	1.951
<i>AT4G26260</i>	AGGTTTCTGCATTCGAGAAGAGT	56.2	TCGGCATCGAAAATCCTCCG	57.6	1.881
<i>AT4G14400</i>	CTGCCACTTGGTTTGCGATG	57.3	CTGTGAGAGAAATCTTTCCGTTGA	54.9	1.882
<i>AT1G74670</i>	AGTCATGGCCAAACTCATAACT	54.3	TCAGACTTCCTGGTCCATAACTT	55.4	1.871
<i>AT3G22231</i>	GACAAACTCCAAGGGCGTCA	57.7	CGCAGCAGAAGATACACTCCA	56.9	1.884
<i>AT1G77330</i>	CGGCGAGTGGATCGATGTTC	58.2	ACTCTTGTACCTTCCGTTGCTA	55.7	1.831
<i>AT1G21250</i>	TATGCGGTGGGAACAGCACT	59.2	ATTGACGTCTTGGCAACCAGC	58.4	1.894

Appendix B

Summary of RNA-seq data between samples. For each biological repeat, the total number of reads and the percentage of reads mapped are listed for each sample. Reads were mapped to the *Arabidopsis thaliana* TAIR10 reference genome.

	Control		AgNP	
	Number of RNA Reads	Percent Mapped	Number of RNA Reads	Percent Mapped
Repeat 1	33,538,008	94.60%	33,687,566	93.10%
Repeat 2	27,417,701	89.40%	29,042,251	91.50%
Repeat 3	26,191,008	87.80%	36,447,804	91.10%

Appendix C

Differentially expressed genes in response to AgNP treatment along with the relative FDR-corrected p-value, fold change and function.

TAIR ID	FDR-corrected p-value	Fold Change	Product Function
<i>AT1G49570</i>	2.48E-12	-195.63	Peroxidase
<i>AT5G19890</i>	4.03E-12	-136.30	Peroxidase
<i>AT5G57760</i>	1.73E-03	-37.57	Hypothetical protein
<i>AT3G15510</i>	7.27E-12	-26.44	Positive regulation of DNA transcription
<i>AT5G50335</i>	2.68E-03	-24.50	Hypothetical protein
<i>AT3G16770</i>	5.63E-18	-23.35	Ethylene response factor (ERF). Responsive under abiotic stress.
<i>AT1G26240</i>	3.16E-02	-18.84	Proline-rich extension-like family protein.
<i>AT1G43160</i>	4.31E-03	-16.62	Ethylene response factor (ERF). Responsive to abiotic stress.
<i>AT2G05510</i>	2.48E-19	-13.91	Glycine-rich family protein
<i>AT5G02760</i>	1.13E-04	-13.42	Phosphatase functioning in sustaining leaf longevity and preventing early senescence.
<i>AT2G47880</i>	1.39E-02	-12.88	Cell redox homeostasis; cellular response to nitrogen starvation; related to glutaredoxins.
<i>AT3G23150</i>	3.44E-02	-12.67	Response to ethylene signaling.
<i>AT5G59320</i>	1.43E-02	-11.13	Lipid transfer protein; predicted pathogenesis-related protein.
<i>AT1G52890</i>	3.44E-02	-10.86	NAC transcription factor responsive to drought and high salt stress.
<i>AT2G44080</i>	4.86E-06	-10.30	AGROS-like protein; cell expansion-dependent organ growth.
<i>AT3G16670</i>	2.90E-10	-10.17	Response to oxidative stress.
<i>AT4G02270</i>	1.93E-03	-9.74	Root hair specific protein involved with cell wall biogenesis.
<i>AT4G25820</i>	1.52E-02	-9.12	Xyloglucan endotransglycosylase that hydrolyze O-glycosyl compounds; cell wall biogenesis and organization.
<i>AT1G05680</i>	3.53E-10	-7.30	Encodes a UDP-glucosyltransferase that acts on IBA (indole-3-butyric acid) and affects auxin homeostasis. Responsive to hydrogen peroxide.
<i>AT3G54040</i>	5.18E-06	-6.78	Hypothetical protein.
<i>AT5G63660</i>	2.61E-05	-6.69	Plant defensin family protein (PDF) response to fungal pathogen infection.
<i>AT1G26250</i>	2.92E-06	-6.65	Proline-rich extension-like family protein; cell wall organization.

Appendix C (continued). DEGs in response to AgNP treatment.

TAIR ID	FDR-corrected p-value	Fold Change	Product Function
<i>AT5G01210</i>	6.95E-07	-5.90	HXXXD-type acyl-transferase family protein.
<i>GLP6_2</i>	3.10E-03	-5.57	Unknown function.
<i>AT1G73830</i>	2.28E-02	-5.54	Encodes brassinosteroid signaling component "BEE3" and positively modulates shade avoidance.
<i>AT1G73120</i>	1.23E-03	-5.49	F-box superfamily protein; response to oxidative stress.
<i>AT2G43590</i>	7.00E-04	-5.40	Chitinase family protein.
<i>AT1G77330</i>	1.24E-05	-5.31	Defense response. Involved in ethylene signaling pathway and oxidation-reduction process.
<i>AT2G22860</i>	6.27E-03	-5.21	Plant peptide growth factor. Involved in cell differentiation and proliferation.
<i>AT4G15550</i>	1.50E-03	-5.04	Encodes a UDP-glucosyltransferase that acts on IBA (indole-3-butyric acid).
<i>AT2G27550</i>	5.48E-03	-4.99	Negative regulation on flower development.
<i>AT4G30670</i>	4.59E-03	-4.96	Putative membrane lipoprotein.
<i>AT4G12470</i>	6.28E-04	-4.94	Defense response. Priming of salicylic acid induction and systematic immunity triggered by pathogenic infection.
<i>AT4G16260</i>	1.66E-04	-4.80	Defense response to fungal pathogen.
<i>AT1G74670</i>	2.52E-02	-4.59	Gibberellin-regulated family protein.
<i>AT2G15830</i>	1.64E-02	-4.56	Hypothetical protein.
<i>AT2G47270</i>	1.31E-03	-4.48	Encodes UPBEAT1, which regulates peroxidases to modulate balance of ROS and maintain normal cell differentiation and proliferation.
<i>AT2G39980</i>	3.11E-03	-4.40	HXXXD-type acyl-transferase family protein.
<i>AT3G01970</i>	1.54E-03	-4.37	WRKY transcription factor.
<i>AT5G13330</i>	1.15E-03	-4.04	Ethylene response factor (ERF). Responsive under abiotic stress.
<i>AT5G49700</i>	2.11E-02	-4.03	Putative AT-hook DNA-binding family protein.
<i>AT5G25350</i>	7.44E-05	-3.92	EIN3-binding F-box protein 2 (EBF2). Involved in ethylene-response pathway.
<i>AT5G39190</i>	2.28E-02	-3.66	Germin-like protein.
<i>AT4G16146</i>	6.28E-04	-3.52	cAMP-regulated phosphoprotein 19-related protein.

Appendix C (continued). DEGs in response to AgNP treatment.

TAIR ID	FDR-corrected p-value	Fold Change	Product Function
<i>AT5G22300</i>	2.01E-03	-3.51	Encodes a nitrilase isomer and involved in cyanide detoxification pathway.
<i>AT5G15780</i>	8.35E-03	-3.35	Extensin family protein.
<i>AT5G17860</i>	3.16E-02	-3.17	Calcium exchanger protein involved in sodium and potassium ion transport.
<i>AT2G40940</i>	2.28E-02	-3.02	Ethylene response sensor (ERS). Involved in negative regulation of ethylene signaling pathway.
<i>AT4G01870</i>	2.84E-02	-2.58	Hypothetical protein.
<i>AT5G14780</i>	2.52E-02	-2.43	Encodes a NAD-dependent formate dehydrogenase. Involved in oxidation-reduction and wounding response.
<i>AT5G10380</i>	2.59E-02	2.56	Defense response to fungal pathogen and involved in programmed cell death.
<i>AT3G20370</i>	2.28E-02	2.59	TRAF-like family protein.
<i>AT5G51550</i>	2.72E-02	3.16	EXORDIUM-like protein.
<i>AT2G44670</i>	1.16E-04	3.17	Senescence-associated family protein.
<i>AT2G41090</i>	8.53E-03	3.20	Encodes a calcium binding calmodulin variant that interacts with phosphomannomutase to increase ascorbic acid biosynthesis.
<i>AT3G50770</i>	7.16E-03	3.28	Calmodulin-like protein. Involved in calcium ion binding.
<i>AT1G14250</i>	1.05E-02	3.40	GDA1/CD39 nucleoside phosphatase family protein.
<i>AT5G44568</i>	3.16E-02	3.51	Transmembrane protein.
<i>AT1G10340</i>	3.31E-03	3.53	Ankyrin repeat family protein.
<i>AT2G25510</i>	4.34E-03	3.81	Transmembrane protein.
<i>AT5G62130</i>	4.25E-03	4.14	PER1-like family protein.
<i>AT4G12545</i>	2.52E-02	4.29	Bifunctional inhibitor/lipid-transfer protein/seed storage 2S albumin superfamily protein.
<i>AT1G21250</i>	1.15E-03	4.36	Encodes a cell wall-associated kinase that functions as an extracellular signaling receptor. Defense response to fungal pathogen.
<i>AT3G47480</i>	6.28E-04	4.89	Calcium-binding EF-hand family protein.
<i>CPuORF27</i>	1.48E-07	5.44	Upstream open reading frames (uorfs) in the 5' UTR of a mature mRNA, and can potentially mediate translational regulation of the major, ORF (morf)

Appendix C (continued). DEGs in response to AgNP treatment.

TAIR ID	FDR-corrected p-value	Fold Change	Product Function
<i>AT4G22590</i>	1.48E-07	5.46	Haloacid dehalogenase-like hydrolase (HAD) superfamily protein. Involved in trehalose biosynthetic process.
<i>AT4G26260</i>	1.57E-04	6.27	Encodes a myo-inositol oxygenase. Involved in oxidation-reduction process.
<i>AT4G14400</i>	3.91E-04	6.28	Accelerated Cell Death 6. Involved in resistance to certain fungal pathogens and programmed cell death.
<i>AT5G03350</i>	1.49E-04	6.94	Systematic acquired resistance gene. Response to salicylic acid stimulus.
<i>AT1G14880</i>	2.25E-02	8.06	Plant cadmium resistance 1.
<i>AT5G10760</i>	9.82E-09	8.37	Systematic acquired resistance gene. Involved in protein catabolism.
<i>AT5G18840</i>	2.05E-10	9.68	Major facilitator superfamily protein that is integral component of the plasmid membrane.
<i>AT5G24200</i>	3.14E-05	10.67	Hypothetical protein.
<i>AT3G22231</i>	5.93E-03	10.94	Pathogen and circadian controlled 1. Regulated by circadian clock. Defense response to fungal pathogen.
<i>AT4G12550</i>	2.05E-10	12.08	Auxin-induced root cultures 1. Involved in lateral root morphogenesis and response to auxin.
<i>AT2G04450</i>	1.05E-08	12.73	NAD pyrophosphatase activity. Involved in regulation of salicylic acid signaling and response to another organism.

Appendix D

qPCR primers used for RNA-seq data validation.

	Forward Primer Sequence	T _m (°C)	Reverse Primer Sequence	T _m (°C)	Primer Efficiency
<i>AT4G02080</i>	GCTGTGTTATTATTAAGCCGTAAG	52.0	AAAGCTAGGTACGGTTTAAGAC	52.3	1.942
<i>AT3G16670</i>	TGGGGTTCTCTTTTGCACCA	57.1	GGACGACCGCATTAGCGAAA	57.9	1.951
<i>AT1G14880</i>	TTGCTTCTCTGACTGCCGAA	56.6	CAGCCGCACAACACGATTT	56.7	1.979
<i>AT1G21250</i>	TATGCGGTGGGAACAGCACT	59.2	ATTGACGTCTTGGCAACCAGC	58.4	1.894

Appendix E

Summary of RNA-seq data from AgNP-treated samples. For each biological repeat, the total number of reads, the percentage of reads mapped, and the percentage of reads mapped in pairs. Reads were mapped to the *Arabidopsis thaliana* TAIR10 reference genome.

	Control			AgNP @ 20nm			AgNP @ 80nm		
	# of RNA Reads	% Mapped	% Mapped Paired	# of RNA Reads	% Mapped	% Mapped Paired	# of RNA Reads	% Mapped	% Mapped Paired
Repeat 1	103,540,742	92.18%	84.75%	89,571,540	77.17%	68.90%	74,683,356	90.99%	83.06%
Repeat 2	80,237,038	94.32%	87.03%	85,093,250	91.17%	87.25%	69,356,484	97.76%	91.53%
Repeat 3	73,149,362	96.83%	90.25%	74,213,952	93.87%	86.50%	72,086,010	97.29%	91.62%

Appendix F

Summary of RNA-seq data from AuNP-treated samples. For each biological repeat, the total number of reads, the percentage of reads mapped, and the percentage of reads mapped in pairs. Reads were mapped to the *Arabidopsis thaliana* TAIR10 reference genome.

	Control			AuNP @ 20nm			AuNP @ 80nm		
	# of RNA Reads	% Mapped	% Mapped Paired	# of RNA Reads	% Mapped	% Mapped Paired	# of RNA Reads	% Mapped	% Mapped Paired
Repeat 1	103,540,742	92.18%	84.75%	77,294,098	94.75%	86.85%	100,691,102	58.41%	57.84%
Repeat 2	80,237,038	94.32%	87.03%	71,474,280	96.80%	90.26%	71,059,066	96.38%	87.40%
Repeat 3	73,149,362	96.83%	90.25%	70,076,702	96.96%	90.49%	76,760,608	88.41%	80.70%

Appendix G

Genes differentially expressed in response to exposure to AgNP at 20 nm. Asterisks in column GO denote genes which belong to enriched gene ontology categories.

TAIR ID	FDR-corrected p-value	Fold Change	GO	Production Function
<i>AT1G04800</i>	4.99E-05	-4.94		Hypothetical glycine-rich protein.
<i>AT1G06620</i>	7.90E-10	8.55	*	Involved in oxidation-reduction process.
<i>AT1G06640</i>	4.92E-02	2.74	*	Involved in oxidation-reduction process.
<i>AT1G08830</i>	2.36E-06	6.29		Copper-zinc superoxide dismutase 1. Detoxifies superoxide radicals and regulated by stress.
<i>AT1G12520</i>	5.42E-07	5.29		Copper-zinc superoxide dismutase copper chaperone. Transports and delivers copper to superoxide dismutase.
<i>AT1G13300</i>	1.57E-03	-12.31		GARP family of transcription factors. Involved in nitrate/phosphotase signaling in root.
<i>AT1G14120</i>	3.03E-04	9.04	*	Indoleacetic acid (auxin) oxidase expressed in root cap cells. Involved in auxin homeostasis.
<i>AT1G14250</i>	6.91E-07	10.97		GDA1/CD39 nucleoside phosphatase family protein that is an integral component of cell membrane.
<i>AT1G14880</i>	1.96E-02	21.98		Plant cadmium resistance 1.
<i>AT1G17380</i>	5.10E-02	4.85		Jasmonate-Zim-Domain Protein 5. Involved in defense response and jasmonic acid-mediated pathway.
<i>AT1G17420</i>	2.16E-04	4.84		Lipoxygenase-3. Involved in anther and pollen development, and lipid oxidation.
<i>AT1G19300</i>	7.64E-04	3.98		Galacturonosyl Transferase-Like 1. Synthesizes Dylan and other carbohydrates.
<i>AT1G19670</i>	3.05E-02	3.68		Coronatine-Induced Protein 1. Initiates chlorophyll breakdown.
<i>AT1G20510</i>	2.89E-02	2.57		CoA Lipase 1. Involved in metabolism of jasmonic acid and phenylpropanoids, and response to wounding.
<i>AT1G21250</i>	3.35E-02	4.08		Cell Wall-Associated Kinase 1. Cell surface receptor that is involved in intercellular signaling and defense response.
<i>AT1G21310</i>	1.75E-05	13.48		Extensin 3. Involved in cell wall synthesis.

Appendix G (continued). DEGs in response to AgNP at 20 nm treatment.

TAIR ID	FDR-corrected p-value	Fold Change	GO	Product Function
<i>AT1G21313</i>	1.19E-04	19.38		Transmembrane Protein.
<i>AT1G21550</i>	1.54E-04	3.68		Calcium Binding EF-hand Family Protein. Involved in calcium ion binding.
<i>AT1G22690</i>	4.04E-03	-3.43	*	Gibberellin-Related Family Protein. Involved in cell signaling mediated by gibberellin.
<i>AT1G24147</i>	3.45E-02	5.00	*	Transmembrane Protein.
<i>AT1G26390</i>	2.98E-05	11.95	*	FAD-Binding Berberine Family Protein. Involved in FAD binding in cellular respiration.
<i>AT1G27130</i>	5.26E-02	-2.74		Glutathione-S Transferase TAU 13. Involved in glutathione metabolism.
<i>AT1G28480</i>	8.09E-15	22.19		GRX480. Regulates protein redox state.
<i>AT1G29920</i>	5.28E-04	-13.88		Chlorophyll A/B-Binding Protein 2. Involved in light absorption in photosystem II.
<i>AT1G31580</i>	1.90E-02	4.98		ESC1. Part of the cell wall.
<i>AT1G32940</i>	3.10E-04	7.07		Subtilase Family Protein. Involved in protein breakdown and control of growth.
<i>AT1G33811</i>	4.70E-03	-4.12	*	GDSL-motif esterase/acyltransferase/lipase. Involved in lipid catabolism.
<i>AT1G33960</i>	1.42E-07	7.51		Immune Associated Nucleotide Binding 8. Defense against bacterial infections.
<i>AT1G35230</i>	5.17E-04	3.86		Arabinogalactan Protein 5. Embedded in cellular membranes in shoot systems.
<i>AT1G36622</i>	8.01E-04	4.29	*	Transmembrane Protein.
<i>AT1G44350</i>	3.63E-04	4.62		IAA-Resistant Leucine-Like 6. Involved in metabolic processes within the chloroplast.
<i>AT1G51680</i>	7.09E-04	3.32		4-Coumarate: CoA Ligase 1. Involved in phenylpropanoid metabolism.
<i>AT1G51760</i>	2.76E-04	3.70		IAA-Alanine Resistant 3. Involved in protein breakdown and wound response.
<i>AT1G51820</i>	3.62E-02	2.93		Stress Induced Factor 4. Kinase enzyme (phosphorylates proteins).
<i>AT1G52000</i>	1.27E-02	6.21		Mannose-Binding Lectin Superfamily Protein. Binds carbohydrates.
<i>AT1G52040</i>	7.79E-04	14.38		Myrosinase-Binding Protein 1. Aids defense response in flowers.
<i>AT1G52100</i>	1.15E-11	7.36		Mannose-Binding Lectin Superfamily Protein. Involved in carbohydrate binding.

Appendix G (continued). DEGs in response to AgNP at 20 nm treatment.

TAIR ID	FDR-corrected p-value	Fold Change	GO	Product Function
<i>AT1G52400</i>	3.52E-02	6.52		Beta-Glucosidase 18. Involved in many functions including metabolism, cellular signaling, and defense.
<i>AT1G52410</i>	2.55E-04	6.89		TSK-Associating Protein 1. Defends against fungal infection.
<i>AT1G53625</i>	7.79E-04	4.59		Hypothetical protein.
<i>AT1G53885</i>	2.05E-03	4.47		Linoleate 9S-Lipoxygenase-4 Protein-Mitochondrial.
<i>AT1G53903</i>	7.79E-04	4.80		Linoleate 9S-Lipoxygenase-4 Protein. Mitochondrial protein expressed in guard cells.
<i>AT1G60260</i>	3.84E-03	3.00		Beta-glucosidase 5. Plasma membrane protein involved in carbohydrate metabolism.
<i>AT1G61120</i>	8.04E-04	33.57		Geranylalanol Synthase. Repairs cellular damage.
<i>AT1G62380</i>	3.32E-02	-2.45		ACC Oxidase 2. Responds to extracellular stimuli.
<i>AT1G64200</i>	6.24E-03	3.01		Vacuolar H ⁺ -ATPase Subunit E Isoform 3. Transports protons during ATP metabolism.
<i>AT1G64710</i>	2.43E-02	-2.83	*	GroES-Like Zinc-Binding Alcohol Dehydrogenase Family Protein. Catabolizes formaldehyde.
<i>AT1G65481</i>	9.74E-09	12.62		Transmembrane Protein.
<i>AT1G65486</i>	8.71E-05	3.80	*	Transmembrane Protein.
<i>AT1G65490</i>	2.42E-04	4.60		Transmembrane Protein
<i>AT1G65500</i>	2.48E-05	4.36		Transmembrane Protein
<i>AT1G65730</i>	9.81E-03	4.53		Yellow Stripe-Like 7. Transports biomolecules across membranes.
<i>AT1G65845</i>	1.42E-07	3.06		Transmembrane Protein
<i>AT1G66100</i>	4.78E-03	11.95	*	Predicted pathogenesis-related protein belonging to the plant thionin (PR-13) family.
<i>AT1G68620</i>	3.63E-04	4.11		Predicted alpha/beta-hydrolases superfamily protein.
<i>AT1G69720</i>	2.24E-02	3.29		Heme Oxygenase 3. Encodes a member of the heme oxygenase family.
<i>AT1G69870</i>	6.17E-05	3.01		Nitrate Transporter 1.7. Involved in source-sink remobilization of nitrate.

Appendix G (continued). DEGs in response to AgNP at 20 nm treatment.

TAIR ID	FDR-corrected p-value	Fold Change	GO	Product Function
<i>AT1G70700</i>	1.28E-07	4.37		Jasmonate-zim-domain protein 5. Presumed to be involved in jasmonate signaling and defense response.
<i>AT1G70850</i>	1.84E-02	-5.37		MLP-like protein 24. Involved in defense response.
<i>AT1G71880</i>	5.45E-02	2.16		Sucrose-Proton Symporter 1. Involved in carbohydrate and proton transportation. Responsive to nematodes.
<i>AT1G72520</i>	3.14E-02	3.49	*	Lipoxygenase 4. Involved in anther/pollen development and defense response to wounding.
<i>AT1G73325</i>	1.60E-03	25.48	*	Kunitz family trypsin and protease inhibitor protein.
<i>AT1G73600</i>	8.73E-04	-6.33	*	Phosphoethanolamine Methyltransferase 3. Responsive to phosphate and phosphite in roots which then catalyzes methylation.
<i>AT1G73805</i>	2.63E-02	3.97	*	SAR Deficient 1. A key regulator of Isochorismate Synthesis 1 (ICS1) and salicylic acid synthesis.
<i>AT1G76930</i>	1.06E-03	5.73		Extensin 1/4. Involved in cell wall organization and strength.
<i>AT2G01520</i>	4.52E-02	-10.32		(Zusammen-CA)-Enhanced 1. MLP-Like Protein 328. Plays a role in promoting vegetative growth and delaying flowering.
<i>AT2G02850</i>	7.35E-04	8.24		Plantacyanin one of blue copper proteins. Involved in anther development and pollination.
<i>AT2G03980</i>	3.78E-02	2.31	*	GDSL-motif esterase/acyltransferase/lipase. Involved in lipid and non-lipid catabolism.
<i>AT2G06050</i>	3.10E-03	2.86		Oxophytodienoate-Reductase 3. Involved in the biosynthetic process of jasmonic acid and stamen development.
<i>AT2G14560</i>	2.26E-03	10.21		Late Upregulated in Response to Hyaloperonospora Parasitica (LUPRA1). Response to fungal pathogen and salicylic acid.
<i>AT2G16660</i>	2.00E-02	4.02	*	Major facilitator superfamily protein.
<i>AT2G20340</i>	4.52E-02	2.68	*	Aromatic Aldehyde Synthase. Involved in L-phenylalanine catabolism and amino acid metabolism.

Appendix G (continued). DEGs in response to AgNP at 20 nm treatment.

TAIR ID	FDR-corrected p-value	Fold Change	GO	Product Function
<i>AT2G21140</i>	2.29E-02	-2.83		Proline-Rich Protein 2. Involved in cell wall organization.
<i>AT2G22770</i>	2.34E-02	4.17		Regulation of ER body development. Involved in fungal pathogen defense response.
<i>AT2G23010</i>	2.76E-03	7.44		Serine Carboxypeptidase-Like 9. Involved in protein metabolism.
<i>AT2G23560</i>	1.50E-02	6.97		Methyl Esterase 7. Involved in salicylic acid metabolism by hydrolyzing methyl-salicylate. Involved in systemic acquired resistance and fungal defense response.
<i>AT2G24850</i>	1.28E-05	20.26		Tyrosine Aminotransferase 3. Responsive to jasmonic acid.
<i>AT2G25440</i>	4.02E-02	4.87		Receptor Like Protein 20.
<i>AT2G25510</i>	2.85E-05	7.05		Transmembrane protein.
<i>AT2G26010</i>	3.58E-02	-3.67		Plant Defensin 1.3. Predicted to encode a pathogenesis-related protein involved in a defense response to fungus.
<i>AT2G28190</i>	8.76E-05	7.58		Copper/Zinc Superoxide Dismutase 2. Involved in response to oxidative stress by detoxifying superoxide radicals.
<i>AT2G29090</i>	2.16E-04	5.46		CYP707A gene family. Involved in abscisic acid catabolic process.
<i>AT2G29350</i>	2.68E-02	11.51		Senescence-Associated Gene 13. Involved in insect defense response and oxidation-reduction process.
<i>AT2G30490</i>	2.27E-03	2.96		Cinnamate 4-Hydroxylase. Involved in developmental and oxidation-reduction process.
<i>AT2G32690</i>	2.73E-04	-3.35		Glycine-Rich Protein 23. Response to salicylic acid and abscisic acid.
<i>AT2G34600</i>	1.74E-04	5.50		Jasmonate-Zim-Domain Protein 7. Response to jasmonic acid, wounding and pathogen.
<i>AT2G34810</i>	2.98E-05	4.87	*	FAD-binding berberine family protein. Response to jasmonic acid and wounding. Involved in oxidation-reduction process.
<i>AT2G37040</i>	3.21E-04	4.14		Phenylalanine Ammonia-Lyase 1. Involved in L-phenylalanine and salicylic acid catabolism, defense response, response to wounding and oxidative stress.

Appendix G (continued). DEGs in response to AgNP at 20 nm treatment.

TAIR ID	FDR-corrected p-value	Fold Change	GO	Product Function
<i>AT2G38240</i>	2.71E-03	10.95	*	Jasmonate-Induced Oxygenase 4. Part of the oxidation-reduction process.
<i>AT2G38760</i>	2.00E-02	4.59		Annexin 3. Calcium binding proteins that are involved in response to abiotic stress.
<i>AT2G38870</i>	1.74E-08	5.36	*	Predicated to encode a pathogenesis-related protein involved in a defense response to fungus.
<i>AT2G39030</i>	1.13E-06	19.40	*	N-Acetyltransferase Activity 1. Involved in defense response and response to jasmonic acid and abscisic acid.
<i>AT2G39310</i>	6.24E-03	2.87		Jacalin-Related Lectin 22.
<i>AT2G39330</i>	2.64E-02	15.81		Jacalin-Related Lectin 23.
<i>AT2G39420</i>	1.33E-04	6.19		Alpha/Beta-Hydrolasas Family Protein.
<i>AT2G40750</i>	3.65E-03	6.27		WRKY DNA-Binding Protein 54. Involved in response to bacterial and fungal pathogens and response to stress-hormones.
<i>AT2G40940</i>	7.07E-03	-2.98		Ethylene Response Sensor 1. Involved in response to ethylene and defense response to fungus.
<i>AT2G42360</i>	1.46E-04	4.03		RING/U-Box Superfamily Protein.
<i>AT2G42610</i>	6.84E-04	-6.64		Light Sensitive Hypocotyls 10. Involved in response to light stimulus.
<i>AT2G43510</i>	1.50E-05	5.25		Trypsin Inhibitor Protein 1. Involved in defense response against fungus and herbivores.
<i>AT2G43530</i>	1.44E-04	4.01	*	Encodes a defense-like family protein that is involved in the fungal defense response.
<i>AT2G43590</i>	2.69E-02	-8.27	*	Involved in macromolecular catabolism at the cell wall, including chitin.
<i>AT2G44290</i>	2.81E-04	2.57	*	Involved in lipid transport.
<i>AT2G47800</i>	2.80E-02	2.55		ATP-Binding Cassette C4. An ATPase transporter involved in drug transport and response to abiotic stimuli.
<i>AT3G05727</i>	2.17E-04	-4.68	*	Encodes a defense-like family protein that is involved in the fungal defense response.
<i>AT3G07390</i>	8.10E-06	4.12		Auxin-Induced in Root Cultures 12. Involved in root morphogenesis and response to auxin.
<i>AT3G09270</i>	6.68E-03	2.65		Gluthathione S-Transferase TAU 8. Involved in glutathione metabolism.

Appendix G (continued). DEGs in response to AgNP at 20 nm treatment.

TAIR ID	FDR-corrected p-value	Fold Change	GO	Product Function
<i>AT3G09520</i>	3.41E-02	5.14		Exocyst Subunit EXO70 Family Protein H4. Involved in exocytosis.
<i>AT3G09940</i>	2.27E-03	17.28		Monodehydroascorbate Reductase 3. Involved in regulation of symbiosis between <i>Arabidopsis</i> and root colonizing fungus.
<i>AT3G11340</i>	4.76E-02	2.87	*	UDP-Dependent Glycosyltransferase 76B1. Involved in the conjugation of isoleucic acid that modulates plant defense and senescence.
<i>AT3G11660</i>	5.28E-02	2.11		NHL1. Involved in defense response to virus.
<i>AT3G12145</i>	2.99E-02	4.05		Floral Transition at the Meristem 4. Involved in reproduction regulation and flowering.
<i>AT3G13790</i>	1.45E-08	4.00		Cell Wall Invertase 1. Involved in response to wounding and fungus.
<i>AT3G14210</i>	5.39E-02	-2.98		Epithiospecifier Modifier 1. Involved as a defense response against insects and pathogens, and glucosinolate catabolism.
<i>AT3G16400</i>	3.88E-05	5.00		Nitrile Specific Protein 1. Involved in nitrile biosynthetic process and response to herbivore.
<i>AT3G16450</i>	7.84E-06	4.35	*	Jacalin-related lectin 33. Involved in response to cold and zinc ion.
<i>AT3G16470</i>	4.24E-02	2.80		Jacalin-Like 1. Involved in plant development via jasmonic acid signaling.
<i>AT3G16670</i>	2.68E-02	-10.19	*	Response to oxidative stress.
<i>AT3G18830</i>	4.89E-04	2.92		Polyol/Monosaccharide Transporter 5. Involved in transport of linear polyols, cyclic polyols and monosaccharides.
<i>AT3G21230</i>	6.60E-05	7.69		4-coumarate: CoA ligase 5. Involved in phenylpropanoid metabolism.
<i>AT3G21351</i>	3.54E-05	5.24	*	Encodes a transmembrane protein.
<i>AT3G22231</i>	2.29E-02	26.19		Pathogen and circadian controlled 1. Regulated by circadian clock. Defense response to fungal pathogen.
<i>AT3G22235</i>	1.54E-02	19.23		Cysteine-Rich Transmembrane Module 8.
<i>AT3G23250</i>	2.77E-05	8.46		MYB Domain Protein 15. Involved in response to abiotic stressors and stress-related hormones.

Appendix G (continued). DEGs in response to AgNP at 20 nm treatment.

TAIR ID	FDR-corrected p-value	Fold Change	GO	Product Function
<i>AT3G25760</i>	1.41E-02	2.31		Allene Oxide Cyclase 1. Involved in the catalysis of an important step in the jasmonic acid biosynthetic pathway.
<i>AT3G25770</i>	9.81E-03	2.33		Allene Oxide Cyclase 2. Involved in the catalysis of an important step in the jasmonic acid biosynthetic pathway.
<i>AT3G25780</i>	2.24E-02	5.42		Allene Oxide Cyclase 3. Involved in the catalysis of an important step in the jasmonic acid biosynthetic pathway.
<i>AT3G26830</i>	1.85E-04	14.91		Phytoalexin Deficient 3. Involved in the camalexin biosynthetic process and defense response to fungus, including systemic acquired resistance.
<i>AT3G26840</i>	1.01E-02	5.16	*	Phytol Ester Synthase 2. Involved in the phytol metabolic process that serves to maintain photosynthetic membrane integrity in chloroplasts.
<i>AT3G28220</i>	2.63E-03	5.13		TRAF-like family protein.
<i>AT3G28540</i>	2.17E-04	5.27		P-Loop Containing Nucleoside Triphosphate Hydrolases Superfamily Protein.
<i>AT3G44720</i>	1.92E-03	2.46		Arogenate Dehydratase 4. Involved in the L-phenylalanine biosynthetic process.
<i>AT3G44860</i>	6.81E-07	19.18		Farnesoic Acid Carboxyl-O-Methyltransferase. Involved in DNA methylation.
<i>AT3G44990</i>	4.56E-04	-9.16		Xyloglucan Endotransglucosylase/Hydrolyse 31. Involved in cell wall biogenesis and organization.
<i>AT3G45060</i>	1.19E-05	19.58		High Affinity Nitrate Transporter 2.6. Involved in nitrate assimilation and transport.
<i>AT3G45140</i>	4.66E-05	9.56		Lipoxygenase 2. Involved in jasmonic induced-defense response to wounding.
<i>AT3G47480</i>	3.67E-06	5.32		Calcium binding EF-hand family protein.
<i>AT3G47780</i>	1.81E-03	5.10		ABC2 Homolog 6. Involved in transmembrane lipid transport.
<i>AT3G47960</i>	1.20E-02	2.88		Glucosinolate Transporter 1. Involved in glucosinolate transport to seeds.

Appendix G (continued). DEGs in response to AgNP at 20 nm treatment.

TAIR ID	FDR-corrected p-value	Fold Change	GO	Product Function
<i>AT3G49120</i>	4.29E-05	7.03		Peroxidase CB/34. Involved in generating hydrogen peroxide in/around the cell wall as a defense response against pathogens.
<i>AT3G49580</i>	6.48E-06	8.62		Response to Low Sulfur 1. Involved in sulfur starvation.
<i>AT3G51450</i>	6.82E-07	8.62	*	Involved in the response to several stressors including stress hormones, fungal pathogens and wounding.
<i>AT3G51660</i>	2.10E-02	2.81	*	A MIF-superfamily protein.
<i>AT3G54420</i>	3.65E-03	3.90		Chitinase family protein. Involved in the cell wall macromolecular catabolic process and defense against fungus.
<i>AT3G55970</i>	1.42E-07	13.98		Jasmonate-Induced Oxygenase 3. Part of the oxidation-reduction process.
<i>AT3G56240</i>	3.62E-04	-4.46		Copper Chaperone. Involved in copper ion homeostasis and transport.
<i>AT3G56400</i>	3.41E-02	4.14		WRKY DNA-Binding Protein 70. Functions as an activator of salicylic acid-dependent defense gene and repressor of jasmonic acid-regulator genes.
<i>AT3G57260</i>	1.84E-02	10.12		Pathogenesis-Related Protein 2. Involved in systemic acquired resistance.
<i>AT3G60415</i>	4.59E-02	3.17		Phosphoglycerate Mutase Family Protein.
<i>AT3G60530</i>	2.89E-02	-2.51		GATA Transcription Factor 4. Involved in transcription regulation.
<i>AT3G61280</i>	8.91E-05	7.60	*	O-glucosyltransferase rumi-like protein that is an integral component of the plasmid membrane.
<i>AT4G00050</i>	2.55E-02	2.89		Unfertilized Embryo Sac 10. Involved in double fertilization forming a zygote and endosperm.
<i>AT4G01070</i>	1.74E-02	4.01		UDP-Glucose-Dependent Glucosyltransferase 72 B1. Involved in the metabolism of xenobiotica.
<i>AT4G01700</i>	3.78E-02	2.67	*	Chitinase family protein. Involved in the cell wall macromolecular catabolic process and defense against fungus.
<i>AT4G01895</i>	3.55E-02	4.54	*	Encodes a protein that is a regulator of the systemic acquired resistance response.
<i>AT4G04490</i>	4.28E-03	6.71		Cysteine-Rich Receptor-Like Protein Kinase 36.

Appendix G (continued). DEGs in response to AgNP at 20 nm treatment.

TAIR ID	FDR-corrected p-value	Fold Change	GO	Product Function
<i>AT4G04490</i>	5.76E-04	6.81		Cysteine-Rich Receptor-Like Protein Kinase 36.
<i>AT4G08870</i>	2.26E-03	6.19	*	Arginine Amidohydrolase 2. Encodes an arginase that is involved in fungal defense and ornithine metabolism. Gene expression is enhanced in response to jasmonate.
<i>AT4G12495</i>	4.92E-02	7.49		Transmembrane protein.
<i>AT4G13510</i>	2.40E-02	2.23		Ammonium Transport 1. Involved in the uptake and transport of ammonium.
<i>AT4G15440</i>	3.26E-02	5.13		Hydroperoxide Lyase 1. Involved in the oxidation-reduction process and fatty acid metabolism.
<i>AT4G15630</i>	2.00E-02	2.49		Hypothetical Protein.
<i>AT4G16146</i>	1.30E-02	-4.20		cAMP-regulated phosphoprotein 19-related protein.
<i>AT4G16980</i>	2.99E-02	2.77		Arabinogalactan-protein family.
<i>AT4G21830</i>	9.74E-09	97.54		Methionine Sulfoxide Reductase B7. Involved in the oxidation-reduction process.
<i>AT4G21850</i>	5.44E-03	7.92		Methionine Sulfoxide Reductase B9. Involved in the oxidation-reduction process.
<i>AT4G21910</i>	5.21E-02	2.52		MATE Efflux Family Protein. Involved in drug transmembrane transport.
<i>AT4G22490</i>	6.36E-04	-4.19	*	Bifunctional inhibitor/lipid-transfer protein/seed storage 2S albumin superfamily protein
<i>AT4G22505</i>	4.90E-02	-5.31		Bifunctional inhibitor/lipid-transfer protein/seed storage 2S albumin superfamily protein
<i>AT4G22513</i>	2.72E-02	-3.15		Protease inhibitor/seed storage/LTP family protein.
<i>AT4G22517</i>	1.33E-02	-3.15		Protease inhibitor/seed storage/LTP family protein.
<i>AT4G22755</i>	1.64E-03	2.81		Methylsterol Monooxygenase 1-3.
<i>AT4G23170</i>	1.28E-02	2.80		Cysteine-Rich Receptor-Like Protein Kinase 9. Involved in response to salicylic acid, systemic acquired resistance, and programmed cell death.

Appendix G (continued). DEGs in response to AgNP at 20 nm treatment.

TAIR ID	FDR-corrected p-value	Fold Change	GO	Product Function
<i>AT4G23210</i>	4.07E-06	6.07		Cysteine-Rich Receptor-Like Protein Kinase 13. Involved in hypersensitive cell death as a defense mechanism against pathogens by increasing salicylic acid.
<i>AT4G27860</i>	1.84E-02	3.38	*	Membrane of ER Body 1. Involved in manganese and iron transport and homeostasis.
<i>AT4G31870</i>	6.00E-04	3.35		Glutathione Peroxidase 7. Involved in the degradation of hydrogen peroxide into water using glutathione as an electron donor.
<i>AT4G34230</i>	7.16E-03	3.98		Cinnamyl Alcohol Dehydrogenase 5. Involved in the oxidation-reduction process.
<i>AT4G36220</i>	2.91E-04	3.49		Ferulic Acid 5-Hydroxylase 1. Involved in lignan biosynthetic and oxidation-reduction process.
<i>AT4G36990</i>	1.87E-02	2.28		Heat Shock Factor Protein. Encodes factors that regulate heat shock proteins that response to heat.
<i>AT4G37150</i>	1.31E-02	3.82		Methyl Esterase 9. Involved in salicylic acid metabolism by hydrolyzing methyl-salicylate. Involved in systemic acquired resistance and fungal defense response.
<i>AT5G01540</i>	5.45E-02	3.02		Lectin Receptor Kinase A4-1. Regulates pattern-triggered immunity and negatively regulates abscisic acid response.
<i>AT5G02940</i>	8.04E-04	2.60		Ion channel protein involved in potassium transport.
<i>AT5G03350</i>	3.33E-05	8.76	*	Involved in systemic acquired resistance and response to salicylic acid.
<i>AT5G05340</i>	1.97E-02	6.00	*	Peroxidase 52. Involved in hydrogen peroxide catabolism and lignin biosynthesis.
<i>AT5G05600</i>	2.76E-03	2.96	*	Jasmonate-Induced Oxygenase 2. Part of the oxidation-reduction process.
<i>AT5G06870</i>	1.50E-04	5.03		Polygalacturonase Inhibiting Protein 2. Involved in plant defense response against fungal pathogens.

Appendix G (continued). DEGs in response to AgNP at 20 nm treatment.

TAIR ID	FDR-corrected p-value	Fold Change	GO	Product Function
<i>AT5G10760</i>	3.03E-04	8.03	*	Apoplatic/EDS1-Dependent 1. Involved in proteolysis and systemic acquired resistance.
<i>AT5G12420</i>	3.63E-04	4.09	*	WSD1-like family protein. Involved in triglyceride biosynthetic process and in maintaining plasmid membrane integrity.
<i>AT5G13220</i>	4.78E-04	6.12		Jasmonate-Zim-Domain Protein 10. Involved in defense response, response to jasmonic acid and wounding, and regulation of systemic acquired resistance.
<i>AT5G14780</i>	1.47E-02	-2.56		Formate Dehydrogenase. Involved in oxidation-reduction process and response to wounding.
<i>AT5G19110</i>	2.76E-03	20.50	*	Eukaryotic aspartyl protease family protein.
<i>AT5G19875</i>	1.21E-03	4.11	*	Transmembrane protein.
<i>AT5G22570</i>	1.34E-03	28.28		WRKY DNA-Binding Protein 38. Involved in defense response to bacterium and response to salicylic acid signaling.
<i>AT5G23820</i>	1.72E-02	4.32	*	MD2-Related Lipid Recognition 3. Involved in defense response and regulated by stress hormones, including ethylene and jasmonate.
<i>AT5G24150</i>	4.08E-03	3.35		Squalene Monooxygenase 5. Involved in the oxidation-reduction process.
<i>AT5G24200</i>	5.93E-07	8.43		Alpha/Beta-Hydrolasas Family Protein.
<i>AT5G24380</i>	2.25E-04	-5.41		Yellow Stripe-Like 2. Transports biomolecules across membranes.
<i>AT5G24420</i>	2.13E-02	4.84		6-Phosphogluconolactonase 5. Involved in the oxidative pentose-phosphate pathway.
<i>AT5G24570</i>	1.19E-02	-3.11		Hypothetical Protein.
<i>AT5G25460</i>	1.40E-02	-4.28	*	Transmembrane protein.
<i>AT5G25840</i>	2.17E-03	-3.68		DUF1677 Family Protein.
<i>AT5G26260</i>	1.27E-02	6.63	*	TRAF-like family protein.
<i>AT5G26270</i>	6.88E-06	4.67		Transmembrane Protein.
<i>AT5G38900</i>	4.10E-03	4.88	*	Protein Disulfide Isomerase. Involved in fungal defense response.
<i>AT5G39610</i>	2.89E-02	-9.45		NAC Domain Containing Protein. Involved in age-related cell death, senescence in leaves, and response to salt stress.

Appendix G (continued). DEGs in response to AgNP at 20 nm treatment.

TAIR ID	FDR-corrected p-value	Fold Change	GO	Product Function
<i>AT5G40780</i>	4.76E-02	2.75		Lysine Histidine Transporter 1. Involved in amino acid uptake and transportation.
<i>AT5G44050</i>	1.94E-02	7.42		MATE Efflux Family Protein. Involved in drug transmembrane transport.
<i>AT5G44567</i>	1.74E-02	10.94		Hypothetical Protein.
<i>AT5G44568</i>	2.17E-06	7.83		Transmembrane Protein.
<i>AT5G45410</i>	3.83E-02	2.13	*	Non Host Resistance 2A. Plastid localized protein involved in defense response to bacterium.
<i>AT5G46350</i>	1.61E-04	6.43		WRKY DNA-Binding Protein 8. Involved in defense response to bacterium, fungus and virus.
<i>AT5G47550</i>	4.47E-02	-3.74	*	Cysteine Proteinase Inhibitor 5. Involved in heat stress tolerance.
<i>AT5G48930</i>	5.21E-02	2.35		Hydroxycinnamoyl-CoA Shikimate/Quinate Hydroxycinnamoyl Transferase. Involved in the phenylpropanoid pathway and cell wall organization.
<i>AT5G50950</i>	1.21E-05	7.90		Fumarase 2. Involved in accumulation of fumarate which helps with nitrogen assimilation and cold acclimation.
<i>AT5G52120</i>	2.43E-02	2.84		Phloem Protein 2-A14. Involved in protein ubiquitination.
<i>AT5G54160</i>	2.68E-02	2.53		Caffeate O-Methyltransferase 1. Involved in flavanol biosynthesis.
<i>AT5G54610</i>	5.00E-02	9.82		Ankyrin. Involved in innate immune response and response to salicylic acid.
<i>AT5G55050</i>	1.81E-04	15.32	*	GDSL-motif esterase/acyltransferase/lipase. Involved in lipid and non-lipid catabolism.
<i>AT5G57480</i>	6.00E-04	7.04		Protein involved in ATP binding.
<i>AT5G57785</i>	1.43E-03	3.30		Hypothetical protein.
<i>AT5G60900</i>	3.63E-04	10.42		Receptor Like Protein Kinase 1. Involved in protein phosphorylation.
<i>AT5G61890</i>	1.92E-03	13.00	*	Ethylene Response Factor 114. Involved in response to ethylene and defense response to fungus.
<i>AT5G62130</i>	3.24E-06	7.14		PER1-like family protein.

Appendix G (continued). DEGs in response to AgNP at 20 nm treatment.

TAIR ID	FDR-corrected p-value	Fold Change	GO	Product Function
<i>AT5G65020</i>	2.68E-02	4.20		Annexin 2. Calcium binding proteins that are involved in response to abiotic stress and in polysaccharide transport.
<i>AT5G65870</i>	9.81E-03	2.44		Phytosulfokine 5 Precursor. Encodes a plant peptide growth factor involved in cell differentiation.

Appendix H

Genes differentially expressed in response to exposure to AgNP at 80 nm. Asterisks in column GO denote genes which belong to enriched gene ontology categories.

TAIR ID	FDR-corrected p-value	Fold Change	GO	Product Function
<i>AT1G04800</i>	1.03E-06	-7.63		Hypothetical glycine-rich protein.
<i>AT1G06620</i>	2.46E-10	8.90	*	Involved in oxidation-reduction process.
<i>AT1G06640</i>	3.17E-02	2.86	*	Involved in oxidation-reduction process.
<i>AT1G08830</i>	5.53E-07	7.05		Copper-zinc superoxide dismutase 1. Detoxifies superoxide radicals and regulated by stress.
<i>AT1G12080</i>	5.38E-02	-4.53		Vacuolar calcium-binding protein-like protein
<i>AT1G12520</i>	3.55E-07	5.59		Copper-zinc superoxide dismutase copper chaperone. Transports and delivers copper to superoxide dismutase.
<i>AT1G13300</i>	8.20E-04	-15.36		GARP family of transcription factors. Involved in nitrate/phosphotase signaling in root.
<i>AT1G14120</i>	4.16E-03	7.32	*	Indoleacetic acid (auxin) oxidase expressed in root cap cells. Involved in auxin homeostasis.
<i>AT1G14250</i>	2.17E-05	8.90	*	GDA1/CD39 nucleoside phosphatase family protein that is an integral component of cell membrane.
<i>AT1G14880</i>	3.97E-02	18.41		Plant cadmium resistance 1.
<i>AT1G17380</i>	2.02E-02	5.36		Jasmonate-Zim-Domain Protein 5. Involved in defense response and jasmonic acid-mediated pathway.
<i>AT1G17420</i>	1.21E-04	5.14		Lipoxygenase-3. Involved in anther and pollen development, and lipid oxidation.
<i>AT1G17860</i>	4.18E-02	2.35	*	Kunitz Trypsin Inhibitor 5. Involved in defense response against insects.
<i>AT1G19300</i>	5.00E-03	3.53		Galacturonosyl Transferase-Like 1. Synthesizes Dylan and other carbohydrates.
<i>AT1G19670</i>	3.02E-02	3.72		Coronatine-Induced Protein 1. Initiates chlorophyll breakdown.
<i>AT1G20510</i>	4.47E-03	2.92		CoA Lipase 1. Involved in metabolism of jasmonic acid and phenylpropanoids, and response to wounding.

Appendix H (continued). DEGs in response to AgNP at 80 nm treatment.

TAIR ID	FDR-corrected p-value	Fold Change	GO	Product Function
<i>AT1G20900</i>	1.95E-02	-6.37		AT-Hook Motif Nuclear-Localized Protein 27. Involved in flower development and immune response.
<i>AT1G21250</i>	3.95E-02	4.08		Cell Wall-Associated Kinase 1. Cell surface receptor that is involved in intercellular signaling and defense response.
<i>AT1G21310</i>	5.67E-03	6.62		Extensin 3. Involved in cell wall synthesis.
<i>AT1G21550</i>	1.16E-03	3.34		Calcium Binding EF-hand Family Protein. Involved in calcium ion bonding.
<i>AT1G22690</i>	1.15E-02	-3.17	*	Gibberellin-Related Family Protein. Involved in cell signaling mediated by gibberellin.
<i>AT1G26390</i>	8.89E-05	11.33	*	FAD-Binding Berberine Family Protein. Involved in FAD binding in cellular respiration.
<i>AT1G27020</i>	1.43E-02	-2.42		Hypothetical Protein.
<i>AT1G28480</i>	6.91E-11	17.48		GRX480. Regulates protein redox state.
<i>AT1G32640</i>	2.33E-02	2.26		Jasmonate Insensitive 1. Transcription factor involved in regulation of growth, jasmonic acid-dependent functions, and defense responses to insects and ROS.
<i>AT1G32940</i>	4.09E-03	5.80		Subtilase Family Protein. Involved in protein breakdown and control of growth.
<i>AT1G33811</i>	9.76E-03	-3.96	*	GDSL-motif esterase/acyltransferase/lipase. Involved in lipid catabolism.
<i>AT1G33960</i>	1.09E-05	6.25		Immune Associated Nucleotide Binding 8. Fights against bacterial infections.
<i>AT1G44350</i>	5.36E-04	4.62		IAA-Resistant Leucine-Like 6. Involved in metabolic processes within the chloroplast.
<i>AT1G51680</i>	1.93E-03	3.18		4-Coumarate: CoA Ligase 1. Involved in phenylpropanoid metabolism.
<i>AT1G51760</i>	1.99E-04	3.82		IAA-Alanine Resistant 3. Involved in protein breakdown and wound response.
<i>AT1G52000</i>	2.44E-02	5.75		Mannose-Binding Lectin Superfamily Protein. Binds carbohydrates.
<i>AT1G52040</i>	4.34E-03	11.73		Myrosinase-Binding Protein 1. Aids defense response in flowers.
<i>AT1G52100</i>	9.25E-08	5.64		Mannose-Binding Lectin Superfamily Protein. Involved in carbohydrate binding.

Appendix H (continued). DEGs in response to AgNP at 80 nm treatment.

TAIR ID	FDR-corrected p-value	Fold Change	GO	Product Function
<i>AT1G52400</i>	4.36E-02	6.30		Beta-Glucosidase 18. Involved in many functions including metabolism, cellular signaling, and defense.
<i>AT1G52410</i>	1.40E-03	6.20		TSK-Associating Protein 1. Defends against fungal infection.
<i>AT1G53170</i>	5.38E-02	-5.35		Ethylene Response Element Binding Factor 4. Involved in the ethylene signaling pathway.
<i>AT1G53885</i>	5.63E-04	4.84		Linoleate 9S-lipoxygenase-4 Protein-Mitochondrial.
<i>AT1G53903</i>	1.44E-04	5.38		Linoleate 9S-Lipoxygenase-4 Protein. Mitochondrial protein expressed in guard cells.
<i>AT1G60260</i>	7.63E-03	2.92		Beta-glucosidase 5. Plasma membrane protein involved in carbohydrate metabolism.
<i>AT1G61120</i>	5.77E-03	28.85		Geranylgeranyl Synthase. Repairs cellular damage.
<i>AT1G64200</i>	3.10E-03	3.19		Vacuolar H ⁺ -ATPase Subunit E Isoform 3. Transports protons during ATP metabolism.
<i>AT1G65481</i>	1.23E-02	5.63		Transmembrane Protein.
<i>AT1G65486</i>	5.38E-02	2.66	*	Transmembrane Protein.
<i>AT1G65490</i>	8.69E-03	3.60		Transmembrane Protein
<i>AT1G65500</i>	7.78E-03	3.09		Transmembrane Protein
<i>AT1G66100</i>	1.13E-03	15.56	*	Predicted pathogenesis-related protein belonging to the plant thionin (PR-13) family.
<i>AT1G66180</i>	8.73E-03	-5.85	*	Putative Aspartyl Protease. Involved in protein catabolism and lysis and responds to light.
<i>AT1G68290</i>	3.02E-02	8.22		Endonuclease 2. Involved in nucleic acid catabolism.
<i>AT1G68620</i>	6.98E-03	3.44	*	Predicted alpha/beta-hydrolases superfamily protein.
<i>AT1G69870</i>	1.61E-04	2.91		Nitrate Transporter 1.7. Involved in source-sink remobilization of nitrate.
<i>AT1G70700</i>	3.89E-07	4.25		Jasmonate-zim-domain protein 5. Presumed to be involved in jasmonate signaling and defense response.

Appendix H (continued). DEGs in response to AgNP at 80 nm treatment.

TAIR ID	FDR-corrected p-value	Fold Change	GO	Product Function
<i>AT1G70850</i>	1.09E-02	-6.37		MLP-like protein 24. Involved in defense response.
<i>AT1G73325</i>	4.09E-03	22.33	*	Kunitz family trypsin and protease inhibitor protein.
<i>AT1G73600</i>	4.34E-03	-5.26		Phosphoethanolamine Methyltransferase 3. Responsive to phosphate and phosphite in roots which then catalyzes methylation.
<i>AT1G74950</i>	5.38E-02	2.35		Jasmonate-Zim-Domain Protein 2. Involved in defense responses and response to jasmonic acid.
<i>AT2G04450</i>	1.11E-02	5.15		Nucleoside Diphosphate Linked to Some Moiety 6. Involved in regulation of salicylic acid mediated signaling pathway.
<i>AT2G05510</i>	8.66E-03	-16.70		Glycine-rich family protein
<i>AT2G06050</i>	2.98E-04	3.26		Oxophytodienoate-Reductase 3. Involved in the biosynthetic process of jasmonic acid and stamen development.
<i>AT2G14560</i>	2.51E-02	7.24		Late Upregulated in Response to Hyaloperonospora Parasitica (LUPRA1). Response to fungal pathogen and salicylic acid.
<i>AT2G16660</i>	1.76E-02	4.11	*	Major facilitator superfamily protein.
<i>AT2G21140</i>	1.76E-02	-2.90		Proline-Rich Protein 2. Involved in cell wall organization.
<i>AT2G22770</i>	1.15E-02	4.41		Regulation of ER body development. Involved in fungal pathogen defense response.
<i>AT2G23010</i>	5.00E-03	7.12		Serine Carboxypeptidase-Like 9. Involved in protein metabolism.
<i>AT2G23560</i>	3.69E-02	6.53		Methyl Esterase 7. Involved in salicylic acid metabolism by hydrolyzing methyl-salicylate. Involved in systemic acquired resistance and fungal defense response.
<i>AT2G24850</i>	8.10E-04	14.05		Tyrosine Aminotransferase 3. Responsive to jasmonic acid.
<i>AT2G25510</i>	1.05E-03	5.18		Transmembrane protein.
<i>AT2G25625</i>	3.25E-03	-4.72		Chloroplast Vesiculation.
<i>AT2G28190</i>	3.74E-05	8.47		Copper/Zinc Superoxide Dismutase 2. Involved in response to oxidative stress by detoxifying superoxide radicals.

Appendix H (continued). DEGs in response to AgNP at 80 nm treatment.

TAIR ID	FDR-corrected p-value	Fold Change	GO	Product Function
<i>AT2G29090</i>	3.97E-03	4.43		CYP707A gene family. Involved in abscisic acid catabolic process.
<i>AT2G29740</i>	3.07E-02	-4.26		UDP-Glucosyl Transferase 71C2.
<i>AT2G30490</i>	4.47E-03	2.87		Cinnamate 4-Hydroxylase. Involved in developmental and oxidation-reduction process.
<i>AT2G32690</i>	9.01E-03	-2.61		Glycine-Rich Protein 23. Response to salicylic acid and abscisic acid.
<i>AT2G34600</i>	1.21E-05	6.39		Jasmonate-Zim-Domain Protein 7. Response to jasmonic acid, wounding and pathogen.
<i>AT2G34810</i>	1.81E-04	4.43	*	FAD-binding berberine family protein. Response to jasmonic acid and wounding. Involved in oxidation-reduction process.
<i>AT2G34930</i>	9.92E-03	9.09	*	Disease Resistance Family Protein (LRR). Involved in defense response to fungus.
<i>AT2G37040</i>	1.01E-03	3.91		Phenylalanine Ammonia-Lyase 1. Involved in L-phenylalanine and salicylic acid catabolism, defense response, response to wounding and oxidative stress.
<i>AT2G38240</i>	1.96E-03	11.96	*	Jasmonate-Induced Oxygenase 4. Part of the oxidation-reduction process.
<i>AT2G38750</i>	3.85E-02	6.71		Annexin 4. Calcium binding proteins that are involved in response to abiotic stress.
<i>AT2G38760</i>	4.09E-03	5.39		Annexin 3. Calcium binding proteins that are involved in response to abiotic stress.
<i>AT2G38870</i>	1.16E-06	4.46	*	Predicted to encode a pathogenesis-related protein involved in a defense response to fungus.
<i>AT2G39030</i>	2.17E-05	15.42	*	N-Acetyltransferase Activity 1. Involved in defense response and response to jasmonic acid and abscisic acid.
<i>AT2G39420</i>	7.35E-05	6.51	*	Alpha/Beta-Hydrolasas Family Protein.
<i>AT2G40330</i>	2.19E-02	-3.88		Regulatory Components of ABA Receptor 9. Abscisic acid sensors involved in the regulation of the abscisic acid-activated signaling pathway.
<i>AT2G40750</i>	9.17E-03	5.97		WRKY DNA-Binding Protein 54. Involved in response to bacterial and fungal pathogens and response to stress-hormones.

Appendix H (continued). DEGs in response to AgNP at 80 nm treatment.

TAIR ID	FDR-corrected p-value	Fold Change	GO	Product Function
<i>AT2G40940</i>	1.01E-03	-3.63		Ethylene Response Sensor 1. Involved in response to ethylene and defense response to fungus.
<i>AT2G42360</i>	3.37E-02	3.11		RING/U-Box Superfamily Protein.
<i>AT2G42610</i>	1.01E-03	-6.22		Light Sensitive Hypocotyls 10. Involved in response to light stimulus.
<i>AT2G43510</i>	2.78E-05	5.13		Trypsin Inhibitor Protein 1. Involved in defense response against fungus and herbivores.
<i>AT2G43530</i>	1.61E-04	4.04	*	Encodes a defense-like family protein that is involved in the fungal defense response.
<i>AT2G43590</i>	4.47E-03	-20.28	*	Involved in macromolecular catabolism at the cell wall, including chitin.
<i>AT2G44080</i>	2.79E-02	-14.53		ARGOS-Like. Involved in cell expansion-dependent organ growth and responds to brassinosteroid.
<i>AT2G44290</i>	4.08E-02	2.03	*	Involved in lipid transport.
<i>AT2G44790</i>	3.95E-02	-3.60		Uclacyanin 2. Proteins that are anchored components of cell/plasma membranes.
<i>AT3G05727</i>	1.21E-05	-6.16	*	Encodes a defense-like family protein that is involved in the fungal defense response.
<i>AT3G05730</i>	1.61E-02	-4.58	*	Defensin-Like Family Protein. Involved in defense response to fungus.
<i>AT3G05937</i>	1.62E-02	-3.66		Hypothetical Protein.
<i>AT3G07390</i>	1.11E-03	3.19		Auxin-Induced in Root Cultures 12. Involved in root morphogenesis and response to auxin.
<i>AT3G09940</i>	4.34E-03	16.25		Monodehydroascorbate Reductase 3. Involved in regulation of symbiosis between <i>Arabidopsis</i> and root colonizing fungus.
<i>AT3G13790</i>	1.02E-05	3.21		Cell Wall Invertase 1. Involved in response to wounding and fungus.
<i>AT3G14610</i>	8.69E-03	-3.77		Putative Cytochrome P450. Involved in the oxidation-reduction process.
<i>AT3G15720</i>	3.95E-02	4.11	*	Pectin Lyase-Like Superfamily Protein. Involved in cell wall organization.
<i>AT3G16150</i>	5.25E-02	-6.71	*	Asparaginase B1. Involved in the catabolism of asparagine.

Appendix H (continued). DEGs in response to AgNP at 80 nm treatment.

TAIR ID	FDR-corrected p-value	Fold Change	GO	Product Function
<i>AT3G16400</i>	9.49E-05	4.81		Nitrile Specific Protein 1. Involved in nitrile biosynthetic process and response to herbivore.
<i>AT3G16450</i>	2.17E-05	4.19	*	Jacalin-related lectin 33. Involved in response to cold and zinc ion.
<i>AT3G16470</i>	2.49E-02	2.94		Jacalin-Like 1. Involved in plant development via jasmonic acid signaling.
<i>AT3G16670</i>	1.61E-04	-84.99	*	Response to oxidative stress.
<i>AT3G16770</i>	1.50E-04	-45.83		Ethylene response factor (ERF).
<i>AT3G18830</i>	4.47E-03	2.61		Polyol/Monosaccharide Transporter 5. Involved in transport of linear polyols, cyclic polyols and monosaccharides.
<i>AT3G21230</i>	1.99E-04	7.40		4-coumarate: CoA ligase 5. Involved in phenylpropanoid metabolism.
<i>AT3G22235</i>	4.55E-02	14.17		Cysteine-Rich Transmembrane Module 8.
<i>AT3G23250</i>	3.23E-04	7.37		MYB Domain Protein 15. Involved in response to abiotic stressors and stress-related hormones.
<i>AT3G24982</i>	3.97E-02	9.01		Receptor Like Protein 40. Involved in signal transduction.
<i>AT3G25780</i>	3.65E-02	5.19		Allene Oxide Cyclase 3. Involved in the catalysis of an important step in the jasmonic acid biosynthetic pathway.
<i>AT3G26830</i>	1.01E-03	12.70		Phytoalexin Deficient 3. Involved in the camalexin biosynthetic process and defense response to fungus, including systemic acquired resistance.
<i>AT3G28540</i>	4.52E-03	4.29	*	P-Loop Containing Nucleoside Triphosphate Hydrolases Superfamily Protein.
<i>AT3G44720</i>	5.00E-03	2.37		Arogenate Dehydratase 4. Involved in the L-phenylalanine biosynthetic process.
<i>AT3G44860</i>	4.48E-07	20.51		Farnesoic Acid Carboxyl-O-Methyltransferase. Involved in DNA methylation.
<i>AT3G44990</i>	1.39E-03	-7.77		Xyloglucan Endotransglucosylase/Hydrolyse 31. Involved in cell wall biogenesis and organization.

Appendix H (continued). DEGs in response to AgNP at 80 nm treatment.

TAIR ID	FDR-corrected p-value	Fold Change	GO	Product Function
<i>AT3G45060</i>	3.31E-05	17.87		High Affinity Nitrate Transporter 2.6. Involved in nitrate assimilation and transport.
<i>AT3G45140</i>	2.53E-04	8.13		Lipoxygenase 2. Involved in jasmonic induced-defense response to wounding.
<i>AT3G46230</i>	6.02E-03	5.35		Heat Shock Protein 17.4. Involved in response to heat, ROS, and salt stress.
<i>AT3G46900</i>	1.53E-02	-8.97		Copper Transporter 2. Involved in copper homeostasis and transport.
<i>AT3G47480</i>	1.41E-03	3.92		Calcium binding EF-hand family protein.
<i>AT3G47960</i>	6.42E-03	3.03		Glucosinolate Transporter 1. Involved in glucosinolate transport to seeds.
<i>AT3G49120</i>	1.44E-04	6.50		Peroxidase CB/34. Involved in generating hydrogen peroxide in/around the cell wall as a defense response against pathogens.
<i>AT3G51450</i>	6.36E-07	8.86	*	Involved in the response to several stressors including stress hormones, fungal pathogens and wounding.
<i>AT3G51660</i>	4.47E-03	3.17	*	A MIF-superfamily protein.
<i>AT3G52340</i>	3.97E-02	-2.76		Sucrose-Phosphatase 2. Involved in sucrose biosynthetic process.
<i>AT3G54990</i>	3.57E-02	2.62		Schlafmutze. Involved in flowering repression and ethylene-activated signaling pathway.
<i>AT3G55970</i>	1.03E-06	12.20		Jasmonate-Induced Oxygenase 3. Part of the oxidation-reduction process.
<i>AT3G56240</i>	2.53E-04	-4.73		Copper Chaperone. Involved in copper ion homeostasis and transport.
<i>AT3G60140</i>	2.14E-02	-8.61		Beta Glucosidase 30/ Dark Inducible 2. Involved in aging and carbohydrate metabolism. Induced after 24-hour dark treatment.
<i>AT3G61280</i>	4.72E-03	5.65	*	O-glucosyltransferase rumi-like protein that is an integral component of the plasmid membrane.
<i>AT4G00050</i>	2.87E-02	2.89		Unfertilized Embryo Sac 10. Involved in double fertilization forming a zygote and endosperm.
<i>AT4G01070</i>	2.80E-02	3.83		UDP-Glucose-Dependent Glucosyltransferase 72 B1. Involved in the metabolism of xenobiotica.

Appendix H (continued). DEGs in response to AgNP at 80 nm treatment.

TAIR ID	FDR-corrected p-value	Fold Change	GO	Product Function
<i>AT4G01895</i>	1.15E-02	4.99		Encodes a protein that is a regulator of the systemic acquired resistance response.
<i>AT4G02380</i>	1.85E-02	-4.55		Late Embryogenesis Abundant 38. Involved in general defense response to abiotic and biotic stress.
<i>AT4G04840</i>	7.33E-04	6.92		Methionine Sulfoxide Reductase B6. Involved in the oxidation-reduction process.
<i>AT4G08870</i>	3.54E-03	6.09	*	Arginine Amidohydrolase 2. Encodes an arganise that is involved in fungal defense and ornithine metabolism. Gene expression is enhanced in response to jasmonate.
<i>AT4G12470</i>	3.54E-03	-5.32		Azelaic Acid Induced 1. Defense response. Priming of salicylic acid induction and systematic immunity triggered by pathogenic infection.
<i>AT4G13660</i>	1.50E-03	-7.17		Pinoresinol Reductase 2. Involved in lignan biosynthetic process.
<i>AT4G14365</i>	3.40E-02	2.73		XB3 Ortholog 4. Involved in protein ubiquitination.
<i>AT4G15630</i>	1.43E-02	2.55		Hypothetical Protein.
<i>AT4G16146</i>	2.02E-02	-4.00		cAMP-regulated phosphoprotein 19-related protein.
<i>AT4G16260</i>	3.66E-02	-3.50	*	Putative Beta-1,3-Endoglucanase. Involved in host defense against nematodes and fungi.
<i>AT4G17090</i>	3.97E-02	3.17		Beta-Amylase 3/8. Involved in maltose accumulation and biosynthesis, and response to cold.
<i>AT4G21830</i>	3.55E-07	72.59		Methionine Sulfoxide Reductase B7. Involved in the oxidation-reduction process.
<i>AT4G21850</i>	2.44E-02	6.52		Methionine Sulfoxide Reductase B9. Involved in the oxidation-reduction process.
<i>AT4G22490</i>	4.47E-03	-3.59	*	Bifunctional inhibitor/lipid-transfer protein/seed storage 2S albumin superfamily protein

Appendix H (continued). DEGs in response to AgNP at 80 nm treatment.

TAIR ID	FDR-corrected p-value	Fold Change	GO	Product Function
<i>AT4G22505</i>	2.79E-02	-7.15		Bifunctional inhibitor/lipid-transfer protein/seed storage 2S albumin superfamily protein
<i>AT4G22513</i>	7.73E-03	-3.73		Protease inhibitor/seed storage/LTP family protein.
<i>AT4G22517</i>	4.09E-03	-3.58		Protease inhibitor/seed storage/LTP family protein.
<i>AT4G22755</i>	2.51E-02	2.44		Methylsterol Monooxygenase 1-3.
<i>AT4G23210</i>	2.50E-05	5.61		Cysteine-Rich Receptor-Like Protein Kinase 13. Involved in hypersensitive cell death as a defense mechanism against pathogens by increasing salicylic acid.
<i>AT4G25100</i>	2.51E-02	-4.16		Iron(Fe) Superoxide Dismutase 1. Involved in the oxidation-reduction process, removal of ROS, and circadian rhythm.
<i>AT4G27860</i>	4.24E-03	3.84	*	Membrane of ER Body 1. Involved in manganese and iron transport and homeostasis.
<i>AT4G30670</i>	1.55E-04	-14.70		Putative Membrane Lipoprotein.
<i>AT4G31870</i>	2.44E-02	2.73		Glutathione Peroxidase 7. Involved in the degradation of hydrogen peroxide into water using glutathione as an electron donor.
<i>AT4G34230</i>	4.10E-02	3.35		Cinnamyl Alcohol Dehydrogenase 5. Involved in the oxidation-reduction process.
<i>AT4G36220</i>	1.01E-04	3.80		Ferulic Acid 5-Hydroxylase 1. Involved in lignan biosynthetic and oxidation-reduction process.
<i>AT5G01840</i>	3.97E-02	4.37		Ovate Family Protein 1. Functions as a transcriptional suppressor to suppress cell elongation.
<i>AT5G01900</i>	4.18E-02	17.39		WRKY DNA-Binding Protein 62. Involved in defense response to bacterium and response to salicylic acid signaling.
<i>AT5G02760</i>	3.66E-02	-22.11	*	Phosphatase functioning in sustaining leaf longevity and preventing early senescence.
<i>AT5G02940</i>	9.55E-04	2.63		Ion channel protein involved in potassium transport.

Appendix H (continued). DEGs in response to AgNP at 80 nm treatment.

TAIR ID	FDR-corrected p-value	Fold Change	GO	Product Function
<i>AT5G03350</i>	8.81E-05	8.28	*	Involved in systemic acquired resistance and response to salicylic acid.
<i>AT5G05340</i>	1.23E-02	6.38	*	Peroxidase 52. Involved in hydrogen peroxide catabolism and lignin biosynthesis.
<i>AT5G05600</i>	5.38E-03	2.87	*	Jasmonate-Induced Oxygenase 2. Part of the oxidation-reduction process.
<i>AT5G06870</i>	2.17E-05	6.00		Polygalacturonase Inhibiting Protein 2. Involved in plant defense response against fungal pathogens.
<i>AT5G10760</i>	2.81E-03	6.78	*	Apoplasmic/EDS1-Dependent 1. Involved in proteolysis and systemic acquired resistance.
<i>AT5G12420</i>	3.49E-03	3.65		WSD1-like family protein. Involved in triglyceride biosynthetic process and in maintaining plasmid membrane integrity.
<i>AT5G13220</i>	1.01E-03	5.90		Jasmonate-Zim-Domain Protein 10. Involved in defense response, response to jasmonic acid and wounding, and regulation of systemic acquired resistance.
<i>AT5G13330</i>	5.19E-02	-2.36		Related to AP2 6L. Ethylene Response Factor involved in ethylene signaling pathway.
<i>AT5G14780</i>	1.11E-03	-3.09		Formate Dehydrogenase. Involved in oxidation-reduction process and response to wounding.
<i>AT5G19110</i>	1.01E-03	24.75	*	Eukaryotic aspartyl protease family protein.
<i>AT5G20230</i>	3.52E-02	3.08		Blue Copper Binding Protein. Involved in response to aluminum and promotes lignin biosynthesis in response to cold.
<i>AT5G22570</i>	1.50E-02	22.84		WRKY DNA-Binding Protein 38. Involved in defense response to bacterium and response to salicylic acid signaling.
<i>AT5G23820</i>	3.95E-02	3.91	*	MD2-Related Lipid Recognition 3. Involved in defense response and regulated by stress hormones, including ethylene and jasmonate.
<i>AT5G24150</i>	2.19E-02	2.98		Squalene Monooxygenase 5. Involved in the oxidation-reduction process.
<i>AT5G24200</i>	4.87E-07	8.67		Alpha/Beta-Hydrolasas Family Protein.

Appendix H (continued). DEGs in response to AgNP at 80 nm treatment.

TAIR ID	FDR-corrected p-value	Fold Change	GO	Product Function
<i>AT5G24380</i>	4.24E-05	-7.24		Yellow Stripe-Like 2. Transports biomolecules across membranes.
<i>AT5G24570</i>	1.53E-03	-3.84		Hypothetical Protein.
<i>AT5G25260</i>	4.96E-02	3.75	*	Flotilin 2. Plasma membrane proteins involved in pathogenic interactions, water transport and intracellular trafficking.
<i>AT5G25350</i>	1.01E-02	-5.40		EIN3-Binding F Box Protein 2. Involved in ethylene-response pathway.
<i>AT5G25840</i>	3.97E-02	-2.78		DUF1677 Family Protein.
<i>AT5G26260</i>	2.90E-03	8.23	*	TRAF-like family protein.
<i>AT5G26270</i>	3.89E-03	3.36		Transmembrane Protein.
<i>AT5G38900</i>	3.72E-02	4.04	*	Protein Disulfide Isomerase. Involved in fungal defense response.
<i>AT5G39190</i>	5.25E-02	-5.18		Germin-Like Protein 2.
<i>AT5G39610</i>	5.84E-03	-14.52		NAC Domain Containing Protein. Involved in age-related cell death, senescence in leaves, and response to salt stress.
<i>AT5G44050</i>	3.66E-02	6.91		MATE Efflux Family Protein. Involved in drug transmembrane transport.
<i>AT5G44568</i>	5.06E-04	5.36		Transmembrane Protein.
<i>AT5G46350</i>	1.01E-03	5.77		WRKY DNA-Binding Protein 8. Involved in defense response to bacterium, fungus and virus.
<i>AT5G47330</i>	1.11E-02	7.81	*	Alpha/Beta-Hydrolasas Family Protein.
<i>AT5G47550</i>	2.51E-02	-4.06	*	Cysteine Proteinase Inhibitor 5. Involved in heat stress tolerance.
<i>AT5G47560</i>	2.02E-02	-3.79		Tonoplast Dicarboxylate Transporter. Involved in malate and sodium ion transport.
<i>AT5G50950</i>	4.22E-06	8.77		Fumarase 2. Involved in accumulation of fumarate which helps with nitrogen assimilation and cold acclimation.
<i>AT5G54160</i>	1.22E-02	2.70		Caffeate O-Methyltransferase 1. Involved in flavanol biosynthesis.
<i>AT5G55050</i>	1.88E-04	15.68	*	GDSL-motif esterase/acyltransferase/lipase. Involved in lipid and non-lipid catabolism.
<i>AT5G57480</i>	3.19E-02	5.10	*	Protein involved in ATP binding.
<i>AT5G57785</i>	6.98E-03	3.03		Hypothetical protein.

Appendix H (continued). DEGs in response to AgNP at 80 nm treatment.

TAIR ID	FDR-corrected p-value	Fold Change	GO	Product Function
<i>AT5G58670</i>	6.98E-03	5.46		Phospholipase C. Induced under abiotic stress and responds to abscisic acid signaling.
<i>AT5G60900</i>	3.17E-02	7.48		Receptor Like Protein Kinase 1. Involved in protein phosphorylation.
<i>AT5G61890</i>	6.98E-03	11.85	*	Ethylene Response Factor 114. Involved in response to ethylene and defense response to fungus.
<i>AT5G62130</i>	5.58E-05	6.26		PER1-like family protein.
<i>AT5G64100</i>	1.61E-04	-8.14	*	Peroxidase Superfamily Protein. Involved in hydrogen peroxide catabolism.
<i>AT5G65020</i>	3.89E-03	5.33		Annexin 2. Calcium binding proteins that are involved in response to abiotic stress and in polysaccharide transport.
<i>AT5G65280</i>	6.57E-03	7.97		GCR2-Like 1.
<i>AT5G65870</i>	3.19E-02	2.27		Phytosulfokine 5 Precursor. Encodes a plant peptide growth factor involved in cell differentiation.